



**AN *IN SILICO* APPROACH FOR SCREENING AND DISCOVERY OF DRUG  
LEADS TARGETING THE NON-CODING REGIONS OF ENTEROVIRUS A71  
RNA GENOME**

**OSATA SHAMIM WANJIKU**

**I56/12354/2018**

**Department of Biochemistry  
Faculty of Science and Technology  
University of Nairobi**

**A thesis submitted in partial fulfillment for an award of the degree of Master of  
Science in Bioinformatics of the University of Nairobi**

**©2023**

## DECLARATION

This thesis is my original work and has not been presented for a degree in any other university.



Signature:-----Date: 07.09.2023-----

OSATA SHAMIM WANJIKU  
I56/12354/2018

### Supervisor's approval

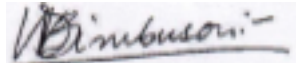
This thesis has been submitted for examination with our approval as university supervisors

Prof. Edward Muge  
Department of Biochemistry  
Faculty of Science and Technology  
University of Nairobi



Signature:-----Date: 07.09.2023-----

Prof. Wallace Bulimo  
Department of Epidemiology, Statistics and Informatics  
Kenya Medical Research Institute (KEMRI)



Signature:-----Date: 07.09.2023-----

## **DEDICATION**

I dedicate this thesis to the Osata family; Peter Osata, Shirin Osata, Shera Osata, James Martin Osata, Richard Osata, Esther Osata, Baraka Osata, Angeline Osata, and to Ruth Etyang, Georgina Wanjiru and Allan Omunyin, phenomenal stars in my universe. Thank you all for the enormous support accorded throughout this journey.

## **ACKNOWLEDGEMENTS**

First, I acknowledge God for granting me good health, knowledge, and wisdom to undertake this work. Secondly, I acknowledge the guidance and dedication accorded to this work by my supervisors, Prof. Wallace Bulimo and Prof. Edward Muge: I am utterly grateful for your prompt feedback, facilitation, and mentorship during this period. May God bless you. Thirdly, I acknowledge Accadius Lunayo for his continuous support and assistance that helped me understand difficult concepts concerning this work. Fourthly, I acknowledge my colleagues from the 2018 Bioinformatics class for their immense support and encouragement. Lastly, I acknowledge the University of Nairobi, the Department of Biochemistry, and the Center for Biotechnology and Bioinformatics, for providing me with the amazing opportunity to further my education.

## TABLE OF CONTENTS

|   |             |
|---|-------------|
| <b>DECLARATION</b> .....                                | <b>II</b>   |
| <b>DEDICATION</b> .....                                 | <b>III</b>  |
| <b>ACKNOWLEDGEMENTS</b> .....                           | <b>IV</b>   |
| <b>LIST OF TABLES</b> .....                             | <b>VII</b>  |
| <b>LIST OF FIGURES</b> .....                            | <b>VIII</b> |
| <b>LIST OF APPENDICES</b> .....                         | <b>XI</b>   |
| <b>LIST OF ABBREVIATIONS</b> .....                      | <b>XII</b>  |
| <b>ABSTRACT</b> .....                                   | <b>XIII</b> |
| <b>CHAPTER ONE: 1.0 INTRODUCTION</b> .....              | <b>1</b>    |
| 1.1 BACKGROUND OF THE STUDY .....                       | 1           |
| 1.2 PROBLEM STATEMENT .....                             | 2           |
| 1.3 JUSTIFICATION .....                                 | 2           |
| 1.4 RESEARCH QUESTIONS.....                             | 3           |
| 1.5 OBJECTIVES .....                                    | 4           |
| 1.5.1 <i>General objective</i> .....                    | 4           |
| 1.5.2 <i>Specific objectives</i> .....                  | 4           |
| <b>CHAPTER TWO: 2.0 LITERATURE REVIEW</b> .....         | <b>5</b>    |
| 2.1 ENTEROVIRUS A71 GENOME STRUCTURE .....              | 5           |
| 2.2 ENTEROVIRUS CLASSIFICATION .....                    | 6           |
| 2.3 UNTRANSLATED REGIONS OF ENTEROVIRUS A71 GENOME..... | 6           |
| 2.4 ENTEROVIRUS A71 REPLICATION .....                   | 8           |
| 2.5 CAP-DEPENDENT TRANSLATION.....                      | 9           |
| 2.6 ENTEROVIRUS A71 TRANSLATION .....                   | 10          |
| 2.7 EV-A71 PROTEINS.....                                | 11          |
| 2.7.1 <i>Structural proteins</i> .....                  | 11          |
| 2.7.2 <i>Non-structural proteins</i> .....              | 14          |
| 2.8 IRES CLASSIFICATION.....                            | 18          |
| 2.9 RIBONUCLEIC ACID .....                              | 20          |
| 2.10 GENERAL RNA SECONDARY STRUCTURE .....              | 21          |
| 2.11 RNA TERTIARY STRUCTURE .....                       | 26          |
| 2.12 RNA STRUCTURE MODELING APPROACHES.....             | 29          |
| 2.13 RNA AS A DRUG TARGET .....                         | 32          |
| 2.14 MOLECULAR DOCKING .....                            | 32          |
| <b>CHAPTER THREE: 3.0 MATERIALS AND METHODS</b> .....   | <b>34</b>   |
| 3.1 DATA RETRIEVAL AND PROCESSING.....                  | 34          |
| 3.2 SECONDARY STRUCTURE PREDICTION.....                 | 34          |

|  |           |
|--|-----------|
| 3.3 TERTIARY STRUCTURE MODELING .....                | 34        |
| 3.4 STRUCTURE EVALUATION .....                       | 35        |
| 3.5 VISUALIZATION AND STRUCTURE ANALYSIS .....       | 35        |
| 3.6 MOTIF IDENTIFICATION .....                       | 35        |
| 3.7 MOLECULAR DOCKING .....                          | 36        |
| <b>CHAPTER FOUR: 4.0 RESULTS .....</b>               | <b>37</b> |
| 4.1 SEQUENCE RETRIEVAL .....                         | 37        |
| 4.2 SECONDARY STRUCTURE MODELING.....                | 37        |
| 4.3 TERTIARY STRUCTURE MODELING .....                | 40        |
| 4.4: STRUCTURE EVALUATION .....                      | 44        |
| 4.5 MOTIF IDENTIFICATION .....                       | 44        |
| 4.6 MOLECULAR DOCKING .....                          | 47        |
| <b>CHAPTER FIVE: 5.0 DISCUSSION .....</b>            | <b>53</b> |
| 5.1 SEQUENCE RETRIEVAL .....                         | 53        |
| 5.2 SECONDARY STRUCTURE MODELING.....                | 54        |
| 5.3 TERTIARY STRUCTURE MODELING AND EVALUATION ..... | 56        |
| 5.4 MOTIF IDENTIFICATION.....                        | 57        |
| 5.5 MOLECULAR DOCKING STUDIES.....                   | 58        |
| <b>CHAPTER SIX: 6.0 CONCLUSION .....</b>             | <b>64</b> |
| 6.1 LIMITATIONS.....                                 | 64        |
| 6.2 RECOMMENDATIONS.....                             | 64        |
| <b>REFERENCES.....</b>                               | <b>65</b> |
| <b>APPENDICES .....</b>                              | <b>78</b> |

## LIST OF TABLES

|   |    |
|---|----|
| <b>Table 1:</b> WebRASP scoring of structure total energy based on distance-dependent pairwise atomic interaction. .... | 44 |
|---|----|

## LIST OF FIGURES

|   |    |
|---|----|
| <b>Figure 2.1:</b> Secondary structure depiction of EVA71 genome depicting the highly structural untranslated regions and the ORF that encodes for structural and non-structural proteins.....                        | 5  |
| <b>Figure 2.2:</b> A. Eukaryotic mRNA circularization via interactions between PABP1 and eIF4E. B. Circularization of the RNA genome in Poliovirus, which is crucial for RNA synthesis initiation.....                | 9  |
| <b>Figure 2.3:</b> A. A depiction of the eukaryotic translation process showing the involvement of IFs and circularization of mRNA. B) Translation in a cap-independent fashion. ....                                 | 11 |
| <b>Figure 2.4:</b> Different forms of enterovirus capsids formed at different stages of the virus life cycle.....   | 13 |
| <b>Figure 2.5:</b> 2B a viroporin predominantly co-located in the Golgi apparatus and endoplasmic reticulum, causing an efflux of calcium ions from the organelles and an increase in intracellular calcium ions..... | 15 |
| <b>Figure 2.6:</b> 3D polymerase from rhinovirus 16 (RV16) showing its human right-hand architecture with the thumb, palm, and fingers domains. ....  | 17 |
| <b>Figure 2.7:</b> Secondary structural representation of the four main IRES types showing the representative members, the AUG start codon of translation, and conserved motifs .....                                 | 19 |
| <b>Figure 2.8:</b> RNA phosphate backbone .....   | 20 |
| <b>Figure 2.9:</b> The hierarchical nature of RNA structure starting from the (a) primary structure, (b) secondary structure, and (c) tertiary structure. ....  | 22 |
| <b>Figure 2.10:</b> Showing Z-turns. U-turns and their variant conformations for the common tetraloop families GNRA, UNCG, and CUUG.....  | 24 |
| <b>Figure 2.11:</b> a) A representation of a k-turn; b) A crystal structure of a bulge loop on the hepatitis C virus IRES domain stabilized by magnesium (green) and manganese (purple) ions.....                     | 25 |
| <b>Figure 2.12:</b> RNA Secondary structures. ....  | 26 |
| <b>Figure 2.13:</b> A secondary (a) and NMR structure (b) of a kissing loop formed between two hairpin loops.....   | 27 |
| <b>Figure 2.14:</b> The secondary structures of B, M, I, and H-type pseudoknots .....   | 28 |



|   |    |
|---|----|
| <b>Figure 2.15:</b> A 2D (a) and 3D (b) structure of a 4-way junction.....  | 28 |
| <b>Figure 2.16:</b> a) An adenine base with three edges. b) The A-minor motifs types: 0, I, II, and III. c) shows a non-canonical WC/H a-minor motif.....   | 29 |
| <b>Figure 4.1:</b> Secondary Structure of the 3' UTR of EVA71 (100 nts long), containing two domains (X and Y) and a poly-A tail obtained using Forna. ....   | 37 |
| <b>Figure 4.2:</b> The secondary structure of the cloverleaf, domain I of the 5' UTR containing stem a and stem loops b-c obtained using Forna.....   | 38 |
| <b>Figure 4.3:</b> The 5' UTR of EVA71 containing six domains visualized using Forna. Domains II-VI form the IRES structure.....  | 39 |
| <b>Figure 4.4:</b> The 3' UTR 3D structure showing domains Y, Z, and the poly-A tail, obtained using RNAComposer and visualized by UCF Chimera. ....  | 40 |
| <b>Figure 4.5:</b> The tertiary structure of the 5' UTR of EVA71 with domains I (cloverleaf), II, and III obtained using RNAComposer and visualized by UCF Chimera, A. with labels, B. without labels. .... | 41 |
| <b>Figure 4.6:</b> The tertiary structure of the 5' UTR domains IV, V, and IV, obtained using RNAComposer and visualized by UCF Chimera, A. with labels, B. without labels.....                             | 43 |
| <b>Figure 4.7:</b> A summary of the five predicted 3' UTR motifs of EVA71. ....   | 45 |
| <b>Figure 4.8:</b> A summary of the twelve predicted motifs of the 5' UTR of EVA71. ....  | 46 |
| <b>Figure 4.9:</b> A summary of the first 20 docking scores, ACE, and transformations for ribavirin docked on the 3'UTR of EVA71.....   | 47 |
| <b>Figure 4.10:</b> Ribavirin bound to motif 1 of EVA71 3' UTR with an ACE of -251.84 kcal/mol. A. with labels showing docked position, B. without labels. ....   | 48 |
| <b>Figure 4.11:</b> Ribavirin and ursolic acid bound to the pocket formed on the 3'UTR of EVA71 with an ACE of -251.84 and -445.52 kcal/mol respectively.....   | 49 |
| <b>Figure 4.12:</b> A summary of the first 20 docking scores, ACE, and transformations for amantadine bound on the 5' UTR of EVA71.....   | 50 |
| <b>Figure 4.13:</b> Amantadine bound on motif 5, domain V of the IRES with an ACE of -226.51 kcal/mol. A. with labels showing docked position, B. without labels. ....                                      | 51 |
| <b>Figure 4.14:</b> A summary of the first 20 docking scores, ACE, and transformations of baicalin bound on the 5' UTR of EVA71. ....   | 51 |

**Figure 4.15:** Baicalin bound on motif 1 of domain II of the IRES with an ACE of -472.39 kcal/mol. A. with labels showing docked position, B. without labels. ....52

## LIST OF APPENDICES

|   |    |
|---|----|
| <b>Appendix A:</b> EV-A71 strain 306A UTR sequences.....  | 78 |
| <b>Appendix B:</b> Details of the MEME suite motif standard RNA alphabet format.....  | 79 |
| <b>Appendix C:</b> Details of the predicted 3' UTR motifs of EV-A71 showing the log-likelihood ratio, information content, relative entropy, Bayes threshold, and sites where the motif appears. ....                           | 80 |
| <b>Appendix D:</b> Details of the predicted 5' UTR motifs of EV-A71 showing the log-likelihood ratio, information content, relative entropy, Bayes threshold, and sites where the motif appears. ....                           | 82 |
| <b>Appendix E:</b> 3D structures of the 13 docked molecules in pdb format .....   | 86 |
| <b>Appendix F:</b> A summary of tables containing the top 20 docking scores, ACE, and transformations for molecules bound on the 5' UTR (dihydromyricetin, myricetin, morin hydrate, nobiletin, taxifolin, and diosmetin). .... | 89 |
| <b>Appendix G:</b> A summary of tables containing the top 20 docking scores, ACE, and transformations for molecules bound on the 3' UTR (formononetin, kaempferol, ursolic acid, 7-hydroxyisoflavone). ....                     | 92 |
| <b>Appendix H:</b> 3D docked complexes of the 5' UTR of EV-A71 with different molecules.....  | 94 |
| <b>Appendix I:</b> 3D docked complexes of the 3' UTR of EV-A71 with different molecules. ....   | 98 |

## LIST OF ABBREVIATIONS

|         |                                |
|---------|--------------------------------|
| 2D      | Two Dimensional                |
| 3D      | Three Dimensional              |
| EV-A71  | Enterovirus A71                |
| UTR     | Untranslated regions           |
| IRES    | Internal ribosome entry site   |
| HFMD    | Hand, foot and mouth disease   |
| RNA     | Ribonucleic Acid               |
| PCBP    | poly-C binding protein         |
| Vpg     | Virus genome-linked protein    |
| ROs     | Replication Organelles         |
| IF      | Initiation Factor              |
| ORF     | Open Reading Frame             |
| cryo-EM | Cryo electron microscopy       |
| WC      | Watson Crick                   |
| PDB     | Protein Data Bank              |
| NMR     | Nuclear magnetic resonance     |
| CRE     | cis-acting replication element |
| ACE     | Atomic contact energies        |
| RMSD    | root mean squared deviation    |
| ITAFs   | IRES trans-acting factors      |
| nts     | nucleotides                    |
| RNP     | Ribonucleoproteins             |
| mRNA    | messenger ribonucleic acid     |
| RdRp    | RNA-dependent RNA polymerase   |

## ABSTRACT

Enterovirus A71 (EV-A71) is the aetiological agent of Hand, Foot and Mouth Disease (HFMD) in underage children leading to neurological conditions including brain encephalitis and acute flaccid paralysis. HFMD is prevalent both in the Asia-Pacific and African regions with 13.7 million cases recorded from epidemics in China between 2008 and 2015 (Puenpa et al., 2019). No antiviral drugs against EV-A71 exists. Treatment rather relies on symptomatic management, which remains ineffective. Recent advances highlight the potential of non-coding RNA in therapeutics as they play an extensive role in controlling protein expression. The aim of this study was to determine the three-dimensional structure of the non-coding regions of EV-A71 and perform molecular docking targeting these region to identify potential drug leads. The study modelled the three-dimensional structure of the 3' UTR and 5'UTR of EV-A71 using a suite of webbased and standalone tools. Using MEME suite motif discovery, the study identified and provided the layout of significant motifs: five for the 5' UTR and one for the 3' UTR. Thirteen identified molecules; amantadine, ribavirin, baicalin, 7-hydroxy isoflavone, myricetin, kaempferol, taxifolin, diosmetin, dihydromyricetin, ursolic acid, baicalin, morin hydrate, and nobiletin with antiviral activity against enteroviruses were docked on the 3D structure of the 3' and 5' UTR via PatchDock, providing different docking positions and alternative potential drug targets. For the 5' UTR motif 1 (5'-AGCYAGUGGGUWG-3'), present in domain II that binds hnRNP that stimulates translation and motif 5 (5'-AGCYAGUGGGUWG-3'), eIF4G and eIF4A binding site for ribosomal assembly, were the most significant potential drug targets. The 3' UTR, which is crucial for replication, had one major motif (5'- UGGKSGURAAUKUG-3') that formed a binding pocket. Nobiletin, baicalin, ursolic acid, and diosmetin had the lowest atomic contact energies indicating higher affinity and specificity for EV-A71 UTRs (-496.03, -472.39, -445.52, and -394.16 kcal/mol, respectively). This work outlines the 3D structure of EV-A71 UTRs, the location of important motifs used in viral gene expression and translation, and potential drug target regions. Moreover, this work presents the potential compounds that can be used as combination therapy to drive fundamental research in therapeutics focusing on UTRs.

## CHAPTER ONE: 1.0 INTRODUCTION

### 1.1 Background of the study

Enterovirus A71 (EV-A71) is the leading cause of hand, foot, and mouth disease (HFMD). EV-A71 also causes neurological consequences such as brainstem encephalitis, acute flaccid paralysis, and aseptic meningitis, which can result in death (Chang et al., 2019). Also, EV-A71 can cause delayed neurological development and cognitive impairment (Yuan et al., 2018). Human enteroviruses are currently reclassified into four species: enterovirus A, B, C, D, and Rhinoviruses (Simmonds et al., 2020). Another study performed to identify the different genogroups circulating in West and Central Africa indicated that EV-A71 undergoes recombination forming new variants like the recently identified E and F genogroups in Africa and Madagascar (Fernandez-Garcia et al., 2018). Enterovirus A is responsible for above 90% of HFMD cases globally (Luchs et al., 2022). The virus spreads through contact with contaminated objects, surfaces, or persons. Diagnosis is through laboratory tests on the stool, mucus, and cerebrospinal fluid. Some common symptoms of EV-A71 infections include fever, sore throat, and a vesicular rash on the oral mucosa, hands, and feet (Luchs et al., 2022). Enterovirus treatment mainly targets symptoms, making it majorly supportive, hence the need to find novel drug targets (Li et al., 2019).

EV-A71 is associated with large-scale outbreaks of HFMD affecting infants and young children, causing multiple deaths worldwide. Asia-Pacific is the main region with a high prevalence of enterovirus infections, and numerous epidemics have been captured over the years. For instance, between 2008 and 2015, China recorded the highest number of outbreaks totaling approximately 13.7 million cases, with 123,261 severe cases and 3,322 deaths (Puenpa et al., 2019). Although enterovirus infections are predominantly concentrated in Asia-Pacific, new outbreaks have been reported in Brazil that exacerbate the importance of surveillance. In 2018, Brazil faced a countrywide enterovirus outbreak with a 71% positivity rate of the samples analyzed (Luchs et al., 2022). In 2021 during the COVID-19 pandemic, Brazil experienced another outbreak in Sao Paulo State (Carmona et al., 2022).

Similarly, enterovirus infections though poorly documented, are also rampant in sub-Saharan Africa. The first case of an enterovirus outbreak in Nairobi, Kenya, was in 2000, when 70 HIV-positive orphans between the ages of 4 and 11 were affected (Chakraborty et al., 2004). The epidemic spread further, impacting nearby orphanages (Chakraborty et al., 2004). A study was carried out to genotype Enteroviruses circulating the Kenyan population between 2008 and 2011. The study targeted sample isolates from patients aged two months to 7 years. The results indicated that the highest infection rate was with patients under three years of age with twenty-one human Enteroviruses identified, EV-A71 being detected at 6.5%, thus heightening the awareness that EV-A71 is an impending clinical burden that requires novel interventions (Opanda et al., 2016).

## **1.2 Problem statement**

Enterovirus A71 (EV-A71) is the causal organism of hand, foot, and mouth disease (HFMD) that affects children of five years. The viral infection neurodevelopment, resulting in decreased cognitive function, and is also capable of causing neurological issues which are severe and can lead to death. Unfortunately, there are no medications specifically designed for EV-A71 treatment. Developing remedies for EV-A71 infections using traditional methods which involve target discovery and validation, followed by assay development, high throughput screening, hit identification, lead optimization, and eventually the selection of a candidate drug for clinical development has been unsuccessful due to their laborious and expensive nature and time constraints (Hughes et al., 2011). The untranslated regions (UTRs) of EV-A71 are essential in the virus life cycle and can be potential drug targets, but there are no 3D structures available to perform *in silico* drug targeting. The development and implementation of rational and comprehensive strategies to treat viral infections are of paramount concern.

## **1.3 Justification**

Enterovirus A71, an important aetiological agent causing severe neurological disease, resulting in high morbidity and mortality in children. Currently, the treatment of EV-A71 is majorly supportive, with no effective antivirals. Three inactivated vaccines for severe HFMD have received approval from China's Food and Drug Administration

(FDA); however, they are not included in the government immunization program and their worldwide accessibility is yet to be established (Li et al., 2019). The nature of the EVA71 and the lack of effective antivirals warrant the development of novel drug targets. The lack of experimentally determined RNA structures warrants using computational approaches for 3D structural modeling (Rother et al., 2011). Notably, computational biology introduces a fast and improved technique for recognizing potential drug targets and drug leads. Moreover, the absence of EV-A71 UTR's structure necessitates its determination to offer improved knowledge of the structure of the virus and offer potential alternative drug targets. EV-A71 3' UTR and 5' UTR are essential in replication and translation processes, respectively; therefore, determining their structures will provide an understanding of their diverse function in EV-A71's life cycle and as a potential drug target.

#### **1.4 Research questions**

1. What are the distinct motifs at the 5' and 3' UTRs that are potential small molecule drug targets?
2. Among the small molecules in the PubChem database, are there any that can bind with high specificities and affinities to the 5' and 3' UTRs, hence serving as possible anti-EV-A71 therapeutics?



## **1.5 Objectives**

### **1.5.1 General objective**

To determine the 3D structure of the 3' and 5' UTR regions of EV-A71 and evaluate their potential as drug targets.

### **1.5.2 Specific objectives**

1. To determine the secondary and tertiary structures of the 3' and 5' UTRs of EV-A71 RNA genome using *de novo* computational modeling.
2. To identify unique motifs in the 3' UTR and 5' UTR of EV-A71 that could serve as potential small-molecule drug targets through fold recognition algorithms.
3. To conduct screening of the Pub-Chem structure database for possible EV-A71 drug leads utilizing structure-based molecular docking and the detected motifs in the 3-D structures.

## CHAPTER TWO: 2.0 LITERATURE REVIEW

### 2.1 Enterovirus A71 genome structure

EV-A71 is a positive-sense single-stranded RNA virus spanning about 7500 nucleotides. The virus has one ORF, characterized by highly structured untranslated 5' and 3' regions (Yuan et al., 2018). The genome encodes one polyprotein with approximately 2100 amino acids that is hydrolyzed into three precursors, P1, P2, and P3. The P1 precursor protein encodes the structural proteins VP1, VP2, VP3, and VP4 (Figure 2.1).

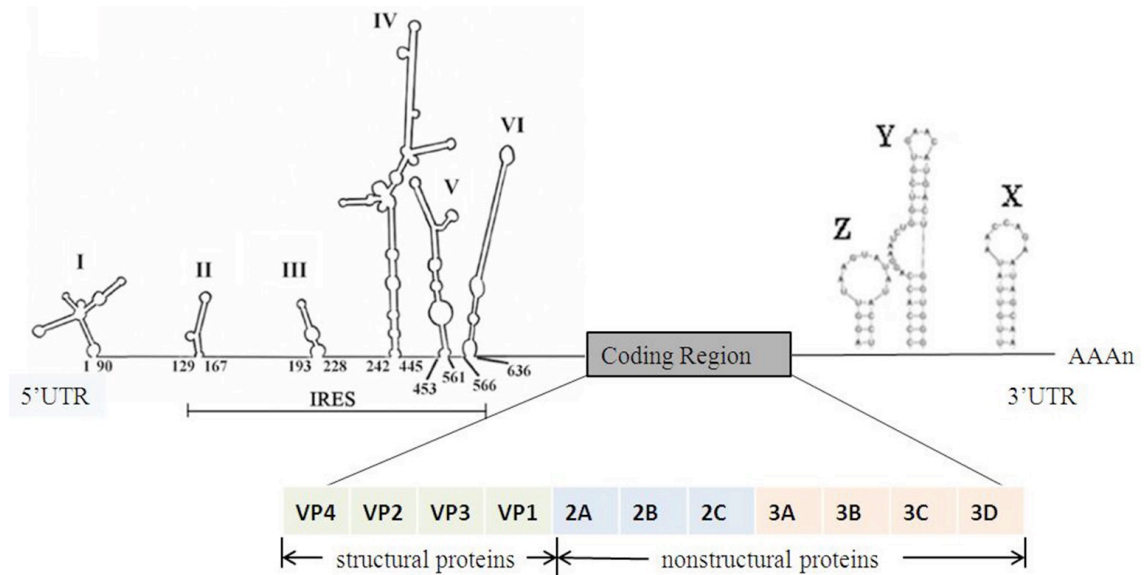


**Figure 2.1:** Secondary structure depiction of EVA71 genome depicting the highly structural untranslated regions and the ORF that encodes for structural and non-structural proteins (Yuan et al., 2018).

P2 and P3 encode for non-structural proteins. For P2, the proteins are 2A, 2B, and 2C while P3 encodes 3A, 3B, 3C and 3D (Chen et al., 2022). The 5' UTR is required for translation and replication. The 5' UTR contains an IRES region, which consists of five stem-loop structures (II to VI) that promote a cap-independent translation and stem-loop I essential for RNA synthesis (Barton et al., 2001). The 3' UTR contains three putative stem-loop structures, X, Y, and Z, and a poly A tail, all required for viral replication. Based on sequence analysis between sub-genotypes, the structures are highly conserved, starting with X, Y then Z (Yuan et al., 2018).

## **2.2 Enterovirus classification**

Classification of Enteroviruses was traditionally based on antigenic identity via serum neutralization assays. The approach involves the identification of antigenic characteristics through neutralization using serum containing standardized type-specific reagent antisera. The traditional method is time-consuming, labor intensive, and requires abundant antisera for different serotype identification (WHO & CDCP, 2015). Additionally, it is sensitive to antigenic variation and virus aggregation. Enterovirus serotypes are not associated with specific diseases but share in causing several symptoms. The advent of gene sequencing shows the use of the VP1 gene in identifying a prototype strain sequence. Generic RT-PCR primers are available to amplify all enterovirus serotypes (WHO & CDCP, 2015). Amplification of the VP1 gene aids in the discrimination of the prototype strains of enterovirus, including untypeable enterovirus isolates. The advanced approach that utilizes adaptations of generic primers improves assay sensitivity allowing quick surveillance of enterovirus isolates even on clinical specimens.

Initially, Enteroviruses classification recognized four groups: polioviruses, coxsackievirus A, coxsackievirus B, and echoviruses (Oberste et al., 1999). The classification was based on pathogenesis, the structure of the virus, or its growth capabilities on tissue culture. The current classification approach utilizes the genomic properties of the virus. Human enteroviruses are currently re-classified into four species: enterovirus A, B, C, D, and Rhinoviruses (Simmonds et al., 2020). Viruses exhibit mutations and recombination, resulting in continual evolution and the formation of hybrids from recombination of viruses within the same species, posing a categorization challenge (WHO & CDCP, 2015).

## **2.3 Untranslated regions of Enterovirus A71 genome**

Untranslated regions (UTRs) are segments in the 3' and 5' regions of RNA that do not encode proteins and are not part of the open reading frame. They perform critical functions in the cell, such as translation control. Untranslated or non-coding areas of EV-A71 are crucial to the virus's life cycle. The complex secondary and tertiary

structures of EV-A71 UTRs are essential for translation and replication processes (Yuan et al., 2018). The area of the 3' UTR is approximately 100 nucleotides long and comprises three stem-loops, namely X, Y, and Z, with a genetically encoded poly (A) tail (Yuan et al., 2018). The domains in X and Y interact, forming tertiary structures previously termed the "kissing interaction" but recently referred to as the "Kissing-like pseudoknot" (Dutkiewicz et al., 2016). In the cell cytoplasm, replication occurs after the RNA genome enters the cell due to conformational changes in the capsid structure during attachment to the cell receptor. The positive strand of RNA undergoes translation to produce proteins required for RNA strand synthesis and the formation of new virions (Lai et al., 2020). Synthesis of the negative strand depends on the circularization of the genome. Circularization occurs due to a RNP complex that forms on the cloverleaf structure, which interacts with a PABP attached to the 3' poly (A) tail (Herold & Andino, 2001). The main structures that ensure only viral RNA is copied are the cloverleaf motif at the 5' end, a CRE, and a pseudoknot on the 3' end. UTRs of EV-A71 interact during vital functions of the virus life cycle.

A study done by Svitkin and Sonenberg (2007) showed the importance of the length of the 3' bound poly (A) tail in Hepatitis C RNA genomes in the binding of the polymerase such that a shortened poly (A) tail inhibited the replication process. The 5'UTR also consists of critical structural elements vital for the life cycle of EVA71. It has six domains, domains II to VI are significant in translation, and domain I is essential for RNA genome replication. Domain I is the cloverleaf structure, while domain II to IV forms the IRES important for cap-independent translation (Yang & Wang, 2019). The cloverleaf structure on the 5' end is critical in the uridylylation of the viral genome-linked protein (Vpg), which then binds to the 3' end, acting as the priming step of replication (Dutkiewicz et al., 2016).

The 5' UTR is as important in viral genome translation as the 3' UTR is in virus replication. The internal ribosome entry site (IRES), which promotes the internal binding of the ribosome's 40S subunit, is one of the secondary structures flanking the 5' UTR (Jang et al., 1989; Su et al., 2018). The direct recruitment of ribosomal subunits via the

IRES results in the utilization of fewer initiation factors compared to the cap-dependent eukaryotic translation process. Because of their roles in regulating translation and replication processes, there has been a significant shift in research in recent years toward untranslated regions of RNA genomes. Translation is essential to the virus life cycle as it codes for structural and non-structural proteins vital for viral infections (Liu et al., 2005).

## **2.4 Enterovirus A71 Replication**

Replication begins after the translation of the RNA genome. The replication process is mediated by non-structural proteins, which include protein 3D and the RdRp. VPg uridylylation by 3D polymerase and a CRE on protein 2C mark the replication start (van der Linden et al., 2015). 3D polymerase elongates the uridylylated protein primer forming a negative strand used as a template for the positive strand synthesis. EV-A71 replication is facilitated by the formation of intracellular membranous structures known as virus factories, which contain replication organelles (ROs), virus replication complexes, and sites for virus particle assembly (Sachse et al., 2019). ROs play significant roles in viral replication, including enzyme activity regulation and innate immunity evasion. The RO structures vary across the viral infection cycle, appearing as single-membrane tubules at the beginning of infection and evolving into multilamellar vesicles in later stages (Li et al., 2020).

The enterovirus genome contains three critical RNA structures for replication: the oriL, oriR, the origin of replication present on the 3' UTR, and oril, the CRE, a template for VPg uridylylation (Zoll et al., 2009). Before elongation of the VPg-pUpU primer for RNA strand synthesis, the RNP complex formed at the oriL 5' UTR interacts with the PABP bound on the poly-A tail 3' UTR end, causing circularization, which is essential for replication to begin, as depicted in Figure 2.2 (Herold & Andino, 2001). Positive-stranded RNA that is newly synthesized either undergoes translation and replication or is packaged to form new viral particles that are released to infect new cells (van der Linden et al., 2015).

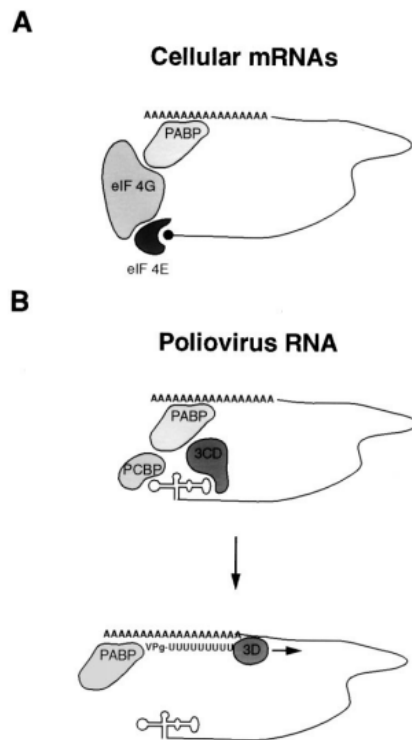


**Figure 1.2:** **A.** Eukaryotic mRNA circularization via interactions between PABP1 and eIF4E. **B.** Circularization of the RNA genome in Poliovirus, which is crucial for RNA synthesis initiation. (Herold & Andino, 2001).

## 2.5 Cap-dependent translation

Eukaryotic translation begins with messenger RNA (mRNA), a key stage of gene expression carried out by ribosomal complexes. The process is cap-dependent, with the cap being a 7-methyl guanylate structure at the 5' end of the mRNA. Translation occurs in four stages: initiation, elongation, termination, and ribosome recycling (Hao et al., 2020). Initiation involves the formation of the eIF2•GTP•Met-tRNA<sup>iMet</sup> ternary complex followed by its assembly with eIF1, eIF1A, eIF3, and eIF5 initiation factors and the 40S subunit forming the 43S pre-initiation complex which scans the 5' UTR (Hao et al., 2020; Jackson et al., 2010). The 48S preinitiation complex forms after the scanning of the mRNA in the 5' to 3' direction by the 43S complex and recognition of the start codon (Hao et al., 2020). The irreversible hydrolysis of GTP bound to eIF2 causes the 60S ribosomal subunit to join the 40S subunit to form the 80S elongation complex.

The elongation complex carries out the elongation of the translated protein by adding an amino acid for each codon on the mRNA. Additionally, during initiation, the 5' UTR and 3' UTR interact via poly (A) binding protein (PABP) bound at the 3' end and the eIF4G complex bound at the 5' end, causing circularization of the mRNA (Komar & Hatzoglou, 2011). The termination phase begins once a stop codon enters the A site of the ribosome mediated by the release factors eRF1 and eRF3 (Hellen, 2018). Ribosome recycling, the final step, involves disassociating ribosomal subunits, deacylation of tRNA, and releasing mRNA (Kapp & Lorsch, 2004).

## **2.6 Enterovirus A71 translation**

Translation takes place cap-independently and involves the Internal Ribosome Entry Site. EV-A71 genome is flanked with a highly structural 5' UTR that is important in recruiting the ribosome for translation. Although EV-A71 utilizes the IRES for translation, it still requires canonical initiation factors, including eIF1, eIF1A, eIF2, eIF3, eIF4A, eIF4B, and the central domain of eIF4G (Lai et al., 2020). The shortened initiation factor eIF4G binds to domain V of the IRES, in turn recruiting eIF4A, which causes conformational changes downstream towards the 3' borders of the IRES to form the 43S pre-initiation complex as portrayed in Figure 2.3 (Su et al., 2018).

Aside from canonical factors, IRES-mediated translation involves a range of RNA-binding proteins known as ITAFs. One of the most common ITAFs that promote IRES activity is the heterogeneous nuclear ribonucleoprotein A1 (hnRNP A1) (Kim et al., 2017). Other ITAFs that stimulate EV-A71 IRES activity include polypyrimidine tract-binding protein 1 (PTB1) and poly (rC)-binding proteins 1 and 2 (PCBP1/2), to mention a few (Lai et al., 2020). Furthermore, EVA71 and other Picornaviruses alter host factors to improve the viral translation, such as cleavage of the initiation factor eIF4G and poly-A binding protein (PABP) by protein 2C (Hung et al., 2016; Lloyd, 2016).

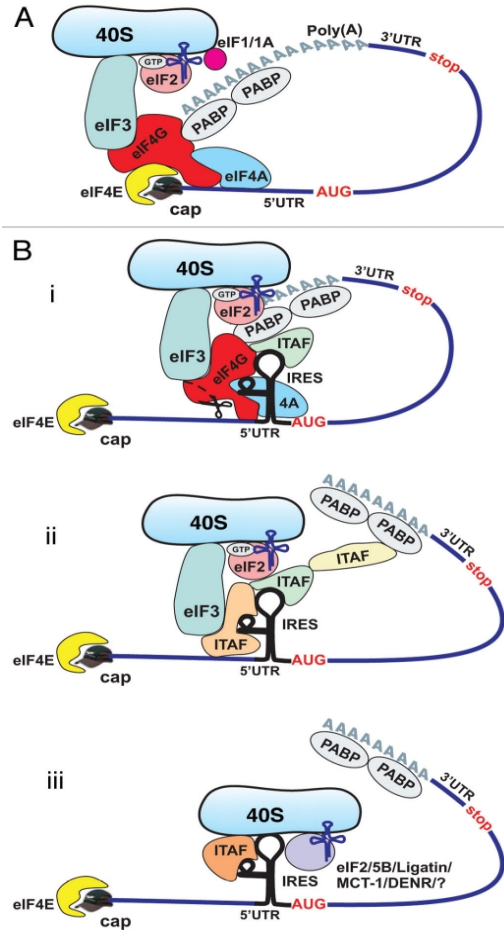


**Figure 2.2:** A. A depiction of the eukaryotic translation process showing the involvement of IFs and circularization of mRNA. B) Translation in a cap-independent fashion (Komar & Hatzoglou, 2011).

## 2.7 EV-A71 proteins

EV-A71 encodes 11 proteins, each essential for a specific function to promote translation, replication, and virulence. The proteins are VP1, VP2, VP3, VP4, 2A, 2B, 2C, 3A, 3B, 3C and 3D. VP1-VP4 are the structural proteins that form the icosahedral capsid, which encloses the positive sense single-strand RNA.

### 2.7.1 Structural proteins

Polyprotein 1 (P1) yields VP0, VP1, and VP3 after cleavage to form structural proteins. VP0 is then broken down into VP2 and VP4. EV-A71's asymmetrical T=pseudo3 icosahedral capsid contains the four proteins, VP1 to VP4, arranged in 60 protomers (He



et al., 2021). VP1, VP2, and VP3 form the outer surface, with VP4 found within the interior of the capsid. Throughout the virus life cycle, virion assembly produces varying intermediates of the capsid with distinct characteristics as shown in Figure 2.4. Recent studies show various forms of enterovirus capsids viewed via cryo-electron microscopy: empty particles (80S), 'A-particles' (intermediates of uncoating, 135S), the expanded one particle (transitioning to 'A particles'), and the mature virion (160S) as shown in Figure 7 (Shingler et al., 2013).

VP1 consists of 294 amino acids and forms the most external part of EV-A71 (Yuan et al., 2018). The capsid has five, three, and two-fold axes. The five-fold axis forms a depression known as the 'canyon' (Yuan et al., 2018). The 'pocket factor' stabilizing the virion is hydrophobic and displayed on the canyon's surface (Plevka et al., 2012). When a cell is infected, VP1 binds to specific receptors such as P-selectin glycoprotein ligand-1 (PSGL-1) and scavenger receptor class B2 (SCARB2), with an antibody-like fold in the canyon that results in the forceful release of the 'pocket factor' from the 'canyon,' destabilizing EV-A71 and allowing the RNA genome to be released (Yuan et al., 2018).

The 'pocket factor' of EV-A71 is accessible to solvents (Plevka et al., 2012). The VP1 gene 3' end contains the BC-loop, a specific neutralization site for antigens used for EV-genotyping (Opanda et al., 2016). A study on Coxsackievirus B4 shows the significance of VP1's BC loop in identifying serotype specificity (Reimann et al., 1991). The amino acid variations on VP1's BC loop and the b-B region are attributed to antigenic differences (Norder et al., 2003). VP1 is a significant structural protein in genotyping enteroviruses and viral entry (Bessaud et al., 2014).

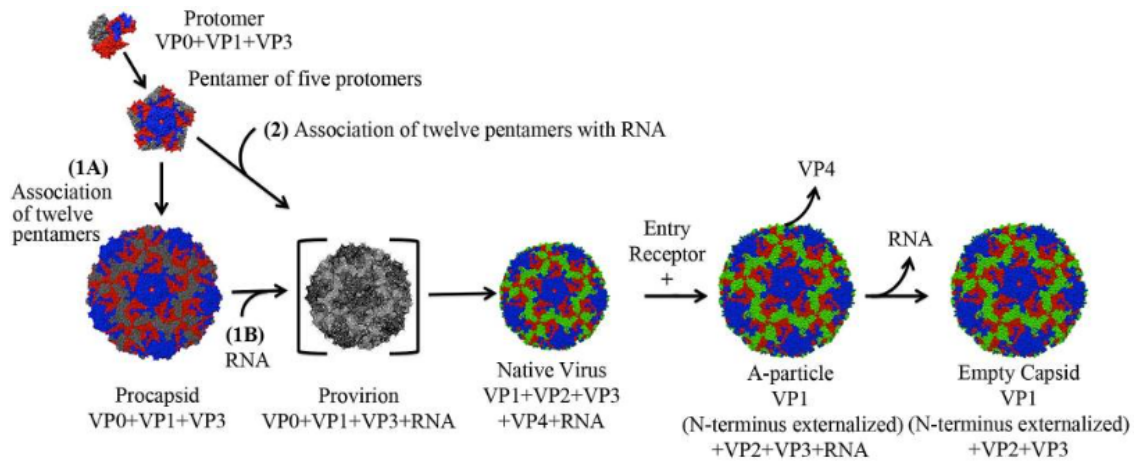


**Figure 2.3:** Different forms of enterovirus capsids formed at different stages of the virus life cycle (Shingler et al., 2013).

The twofold axes of EV-A71 capsid contain adjacent VP2 and VP3 protomers. VP2 contains 254 amino acids with a highly variable surface loop and highly conserved linear epitope from residues 136-150 (Yuan et al., 2018). The "puff" is the most significant surface loop that forms the canyon's "southern rim" (Plevka et al., 2012). VP3 has 245 amino acids with highly conserved regions across sub-genogroups spanning 59-67. The "Knob" is VP3's important surface protrusion and a conserved epitope. In some picornaviruses, the puff and knob are significant in binding to non-antibody-like receptors (Plevka et al., 2012).

The last structural protein VP4 contains 69 amino acids and is present inside the virion. VP4 contains a covalently attached myristoyl group offering the capsid stability (Smyth & Martin, 2002). Due to the fact that VP4 is more conserved than VP1, VP2, and VP3, numerous studies are focusing on discovering linear neutralizing epitopes for vaccine targeting (Yuan et al., 2018). VP4 protein's most significant role is the "A particle" formation during uncoating, which involves the release and insertion of VP4 into the membrane, resulting in a channel for viral RNA entry into the host cell (Shingler et al., 2013; Yuan et al., 2018).

### 2.7.2 Non-structural proteins

Protein 2Apro is a 150-amino acid cysteine protease. The protein has a chymotrypsin-like fold with an active site containing the catalytic triads C110A, H21, and D39. Protein 2A has a cl-to-el2 loop present at the N-terminal domain. The C-terminus contains two motifs: a hydrophobic "LLWL" and an acid "DEE" motif (Mu et al., 2013). The folding of the hydrophobic motif is required to position the acidic motif in viral replication. 2Apro is a significant structural protein in replication, pathogenesis, and apoptosis (Feng et al., 2014). Additionally, catalysis of the peptide bond from the polyprotein is performed by 2Apro to yield VP1, the C-terminal, and P2, the N-terminal.

Protein 2B is a type II viroporin, a small hydrophobic protein that promotes virus release by modifying cellular membranes. Viroporins are common viral proteins containing 50 to 120 amino acids with a hydrophobic domain that forms an amphipathic alpha-helical structure that eventually forms hydrophilic pores on the transmembrane (Li et al., 2019). The hydrophobic regions are known as HR1 and HR2, with a short hydrophilic turn in between them (Martinez-Gil et al., 2011). Enteroviral viroporins comprise 97 to 99 amino acids forming homomultimers on membranes and plasma, increasing calcium ions conductance channel activity, depicted in Figure 2.5 (Supasorn et al., 2020). In host cells, 2B plays three major roles: regulating apoptosis and autophagy, interfering with membrane permeability, and modulating host cell immune response (Li et al., 2019). Additionally, viroporins promote the completion of the viral life cycle by interfering with normal physiological functions (Ao et al., 2014). Change in calcium ion concentration is the main underlying mechanism used by 2B to exert its functions (de-Jong et al., 2008).

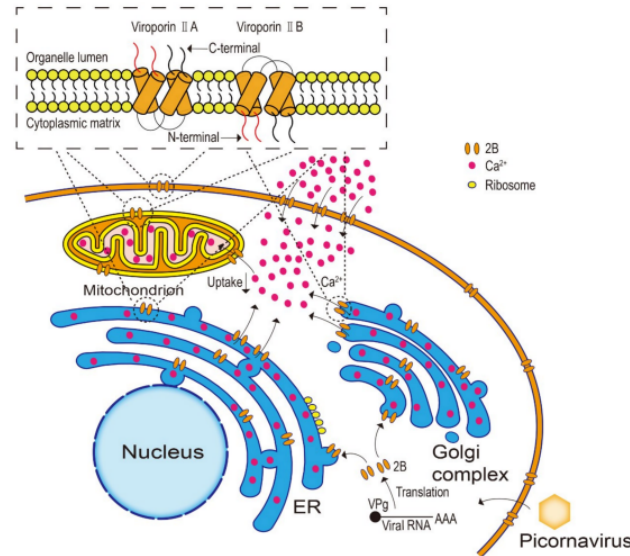


**Figure 2.4:** 2B a viroporin predominantly co-located in the Golgi apparatus and endoplasmic reticulum, causing an efflux of calcium ions from the organelles and an increase in intracellular calcium ions (Li et al., 2019).

Protein 2C is highly conserved and multifunctional. According to Wang et al. (2020), 2C has been linked to RNA replication, virus uncoating, binding of RNA, host membrane rearrangement, encapsidation, morphogenesis, and ATPase activity. Additionally, protein 2C is implicated in immune evasion mediated by recruiting protein phosphatase 1 (PP1), which cascades into the inactivation of the TNF- $\alpha$ -mediated NF- $\kappa$ B signaling pathway (Li et al., 2016). 2C is classified as a superfamily 3 (SF3) helicase based on its ATPase associated with diverse cellular Activities (AAA+ ATPase) (Bauer et al., 2020). AAA+ ATPases have pleiotropic functions essential to the cell's physiology, such as DNA replication, membrane fusion, ribosomal RNA processing, and remodeling (Shorter & Houry, 2018).

Studies show that protein 2C contains a binding motif on the N-terminal membrane, a C-rich motif, an ATPase binding domain, and RNA binding sites (Guan et al., 2017). 2C's role as an ATPase and in viral replication is attributed to the amphipathic helix that promotes self-oligomerization (Wang et al., 2020). The role of protein 2C in viral replication is due to a structural element known as the CRE, which is within a small hairpin and contains a conserved GXXXAAAXXXXXXA sequence (Xi et al., 2021).

The CRE participates in VPg uridylylation (Cordey et al., 2008). Although protein 2C has not been extensively explored, its pleiotropic nature makes it a key nonstructural protein vital in the EVA71 life cycle.

Protein 3A is also highly conserved among enteroviruses. It is significant in membrane remodeling through interactions with Golgi Brefeldin A resistant guanine nucleotide exchange factor 1 (GBF1) and ADP-ribosylation factor 1 (ARF1) (Lu et al., 2021; Pascal et al., 2020; Xiao et al., 2017). A study shows protein 3A implicated in viral replication through PI4KB-ACBD3 interaction (Xiao et al., 2017). Furthermore, the recruitment of PI4KIII increases the production of phosphatidylinositol-4-phosphate (PI4P), which recruits virus polymerase and other proteins that can alter membrane properties (Pascal et al., 2020).

Protein 3B is the VPg, made of approximately 22 amino acids. VPg is a crucial protein in the replication of EV-A71. During replication initiation, uridylylation of the VPg is a core step performed by two copies of 3C protease and the RdRp (Chen et al., 2013). For uridylylation to occur, VPg has to be bound to 3D polymerase displaying an extended V-shaped conformation at the polymerase's bottom of the palm domain (Chen et al., 2013). The uridylylated form of 3B functions as an RNA replication primer. (Pascal et al., 2020).

Protein 3C is key in the segmentation of precursor proteins of EVA71. It is a 184 amino acid cysteine protease with a chymotrypsin-like fold (Yuan et al., 2018). 3C has two major roles in the viral cycle of EV-A71: precursor cleavage and RNA binding (Xie et al., 2018). 3C cleaves itself from the P3 precursor protein, followed by P2 and P3. Studies show that protein 3C has RNA binding activity (Shih et al., 2004). Additionally, 3C inhibits host innate immunity by downregulating mir-526a, inhibiting interferon production in a cascade of events (Li et al., 2021). The protein has the  $\beta$ -ribbon, a surface loop with two residues, glycine 123 and histamine 133 which are significant for 3C's proteolytic role (Yuan et al., 2018).

3D polymerase is the enterovirus RdRp, a 52 kDa protein containing a shared common fold with three other polymerases called the “right hand” (Pascal et al., 2020). The polymerase is designed as a human right hand and contains three domains: a thumb, palm, and fingers, as depicted in Figure 2.6 (Liu et al., 2016). The largest additional secondary structural component is a three-turn helix above the beta-sheet and connects the palm to the thumb area to the right (Pascal et al., 2020). 3D polymerase plays several distinct roles in EV-A71’s life cycle, the most important being RNA synthesis and uridylylation of VPg (Yuan et al., 2018). 3D employs VPg for RNA strand synthesis as a primer (Jiang et al., 2011). Additional roles include activation of inflammatory responses and immune evasion.

Covalently linked 3C protease, and 3D polymerase which forms 3CD also influence the viral life cycle. According to Jing et al. (2017), 3CD contributes to the virulence and temperature sensitivity of EV-A71. Additionally, 3CD increases host protein growth arrest and DNA damage-inducible protein 34 (GADD34) expression to promote viral replication (Li et al., 2022). Furthermore, 3CD can inhibit IFN- activation by targeting the cytosolic receptor retinoid acid-inducible gene I, promoting EV-A71 pathogenesis (Lei et al., 2010).

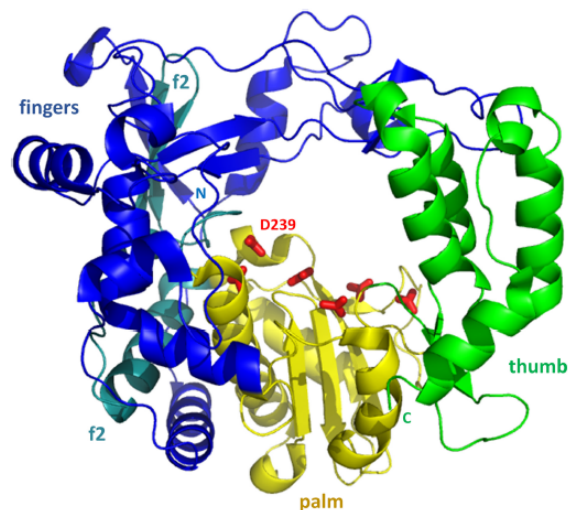


**Figure 2.5:** 3D polymerase from rhinovirus 16 (RV16) showing its human right-hand architecture with the thumb, palm, and fingers domains (Pascal et al., 2020).

## 2.8 IRES Classification

The IRES is the most significant section of the 5' UTR of EV-A71 involved in viral translation. Several common traits distinguish the various types of IRESs that have been identified. IRES types are categorized into four: type I IRES, common in enteroviruses; type II IRES present in cardioviruses and aphthoviruses; type III IRES and type IV IRES, portrayed in Figure 2.7 (Cathcart et al., 2014). All IRESs have a unique scanning mechanism for initiating translation. Moreover, all IRESs do not share structural elements, and the sequences are not homologous (Nikonov et al., 2017). Type I IRES present in picornaviruses has a length of about 450 nucleotides (nts) and contains five domains. It also contains the motif Y<sub>n</sub> X<sub>m</sub> AUG (Y- pyrimidine sequence n=8-10 nts, X-linker, m=18-20 nts) at the three-prime terminus of the 5' UTR, the region for ribosome binding (Sweeney et al., 2014). The motif is separated by a non-conserved region of fewer than 30 nts in rhinoviruses and greater than 150 nts in polioviruses (Nikonov et al., 2017). Conserved regions in domains two, four, and five are functionally important (Lai et al., 2020). After binding eIF4G and eIF4A, the 43S complex binds to the IRES. Type I IRESs fold into dense structures containing three pseudoknots (PKI, PKII, and PKIII) that engage with the ribosome's 40S subunit, indicating that they can initiate translation without additional ITAFs (Yang & Wang, 2019).

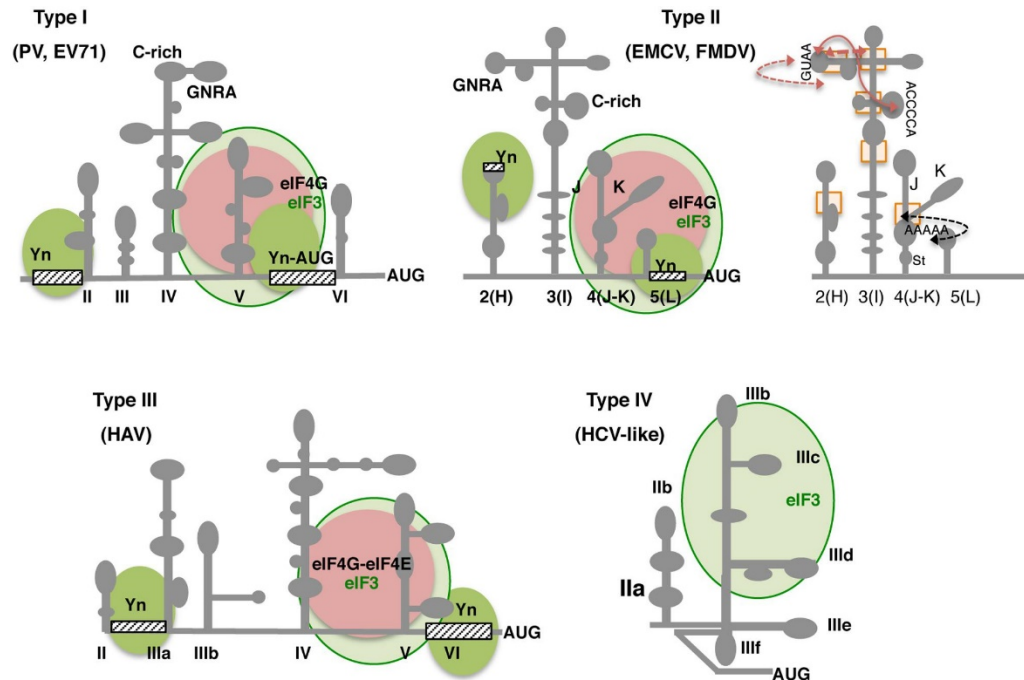


**Figure 2.6:** Secondary structural representation of the four main IRES types showing the representative members, the AUG start codon of translation, and conserved motifs (Martinez-Salas et al., 2018).

Type II IRES has five domains and a Yn Xm AUG motif at the 3' terminal (Yu et al., 2011). Except for domain four, which contains a C-rich and GNRA, type II IRES domains differ from type I IRES. (N-any of the four nucleotides and R is a purine) tetra loop (Figure 2) (Martinez-Salas et al., 2015). The initiation of translation requires eIF4G and eIF4A binding on domains J and K (Chamond et al., 2014; Yu et al., 2011). Type II IRESs do not require translation initiation factors and hence lack ITAFs, unlike type I IRES. However, as demonstrated in some cases, type I IRESs need the cellular RNA binding protein (RBP), pyrimidine-binding protein (PTB) (Kafasla et al., 2009).

Type III IRES is approximately 410 nts long and is only found in the hepatitis A virus (McKnight & Lemon, 2018). It has distinct sequences and structural elements. Hepatitis A IRES, unlike the other IRES types, requires eIF4E to initiate translation (Nikonov et al., 2017). Type IV IRES is approximately 330 nts long and does not form the pre-initiator complex. They form the 48S initiation complex by directly binding to eIF3 and 40S subunit. Type V IRES is a hybrid consisting homologous domains with type I and



type II IRES. It also contains the motif Yn Xm AUG present in the hairpin of domain L. Initiation of translation involves PTB, several canonical factors, and an ATP-dependent RNA helicase DHX29 (Nikonov et al., 2017). ITAFs and canonical initiation factors are required to bind to the ribosomal subunit for Type III and V IRES (Yang & Wang, 2019).

## 2.9 Ribonucleic Acid

The primary structure of RNA is a chain of ribonucleotide monomer units. The ribonucleotide contains a nucleic base (purine, A, G or pyrimidine U, C) covalently bonded to a ribose sugar attached to a phosphate molecule via an N-glycosidic bond (Leontis & Westhof, 2001). The connection of an O-glycosidic bond between two succeeding ribonucleotides, oxygen, and phosphate atoms forms the RNA phosphate backbone, as depicted in Figure 2.8 (Grover, 2022).

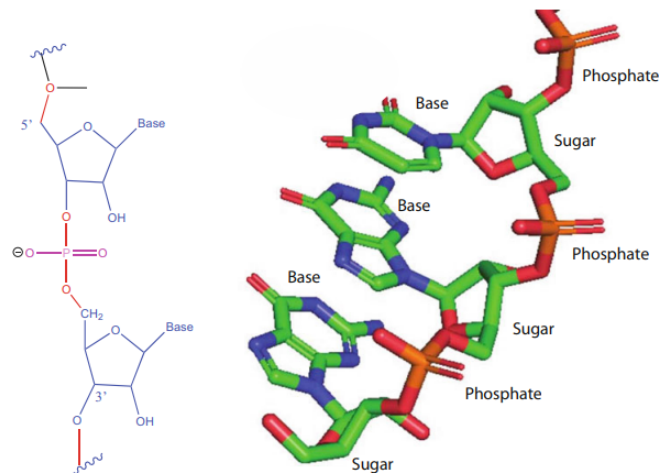


**Figure 2.8:** RNA phosphate backbone (Grover, 2022)

The nucleobases interact with one another by forming a minimum of two hydrogen bonds, resulting in base pairs. Three possible hydrogen bond interactions exist between nucleobase edges: the Watson-Crick (WC) edge, the Hoogsteen edge, and the Sugar edge (Gruyter, 2013). In addition to the three bonds, base pairs can form with other bases, one per edge. Pseudo-base pairs can also be created via single bonds between a base and a sugar or two base residues.

According to Leontis and Westhof. (2001), base-pair types are classified into twelve families. Base-pair families are identified based on base-sugar glycosidic bonds (cis or trans) orientation and their interacting edges. A cis configuration has both glycosidic bonds on one side of the reference plane perpendicular to the line connecting the base ring system's centroid; otherwise, the configuration is trans.

The WC base pairs include A-U and G-C (Fallmann et al., 2017). Non-WC base pairs are the non-standard interactions that occur via the sugar and Hoogsteen edges, forming base triples. Even though they are referred to as mismatches, noncanonical base pairs are an essential component of RNA tertiary structure. The wobble base pair (G-U) is a highly common non-WC base pairing, followed by the sheared base pair (G-A), the reverse Hoogsteen base pair (A-U), and the imino base pair (G-A) (Chen & Varani, 2001).

## **2.10 General RNA secondary structure**

The secondary structure of RNA consists of paired and unpaired regions. It is also hierarchical as it is sequential, starting from a primary structure to the secondary, tertiary, then quaternary structure, as indicated in Figure 2.9 (Mathews, 2019). Compared to tertiary structures, which are dominated by weak non-canonical base pairs, the secondary structure is dominated by WC base pairing, resulting in greater thermodynamic stability. The higher stability of RNA secondary structure confers the advantage that it can be accurately predicted via phylogeny and algorithms that compute the thermodynamic calculations of the free energies for the formation of each base pair (Chen & Varani, 2001). The most common RNA secondary structure motifs are hairpins, bulges, and internal loops (Figure 2.12).

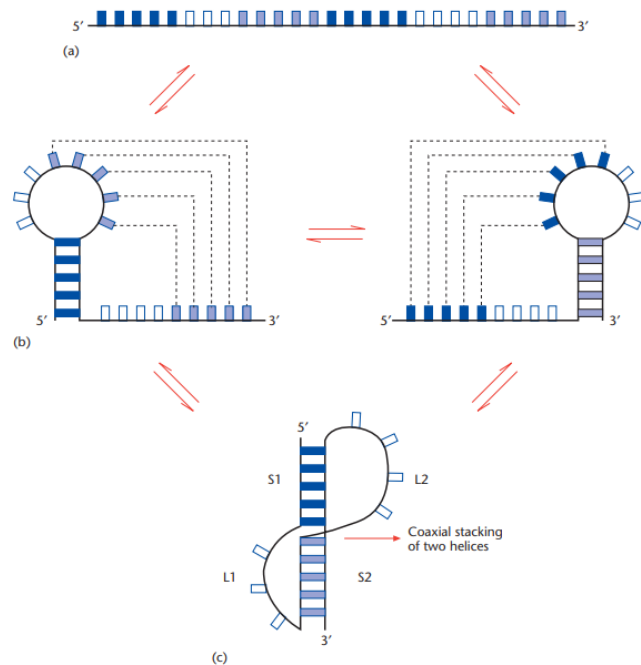


**Figure 2.9:**The hierarchical nature of RNA structure starting from the (a) primary structure, (b) secondary structure, and (c) tertiary structure (Chen & Varani, 2001).

### Hairpin (stem-loops)

The formation of a double helical tract known as a stem results from folding back the phosphodiester backbone on itself, leaving a single-stranded region of unpaired nucleotides known as the loop (Kiliszek et al., 2017). They participate in long-distance interactions essential for RNA folding and stability (Grover, 2022). Hairpins are crucial secondary RNA structures that play significant roles, such as guiding RNA folding, protecting RNA from breakdown, influencing interactions, and acting as recognition motifs for RBPs (Svoboda & Cara, 2006).

Owing to their diverse structures and functions, RNA hairpins have many applications, including as aptamers in medicine and as biosensors in food and the environment (Kiliszek et al., 2017). Additionally, RNA hairpins have been extensively used in RNAi technology (Ge et al., 2010; Moore et al., 2013; Sliva & Schnierle, 2010). Hairpins can be of various sizes containing three (triloop), four (tetraloop), or more nucleotides in their loops.

### **Triloops**

Triloops are RNA stem-loops that contain three nucleotides. They are common structural motifs that are highly significant in RNA tertiary structure. Triloops are present in 7% of bacterial loops and 16% of eukaryotes (Thulasi et al., 2010). They are crucial in biological processes such as virus replication and synthesis (Lisi & Major, 2007; Olsthoorn & Bol, 2002).

### **Tetraloops**

Tetraloops account for over 50% of hairpins (Sheeshy et al., 2010). Hairpins with four nucleotides are unusually common in RNA structures, and they are classified into three families: UNCG, GNRA, and CUUG. UNCG and GNRA tetraloops take different conformations known as Z-turns and U-turns, which promote tertiary interactions, as illustrated in Figure 2.10 (D'Ascenzo et al., 2018). Tetraloop families are distinguished by the fact that the loop's first and last nucleotides form noncanonical interactions to close the loop, leaving only two unpaired nucleotides (Chen & Varani, 2001).

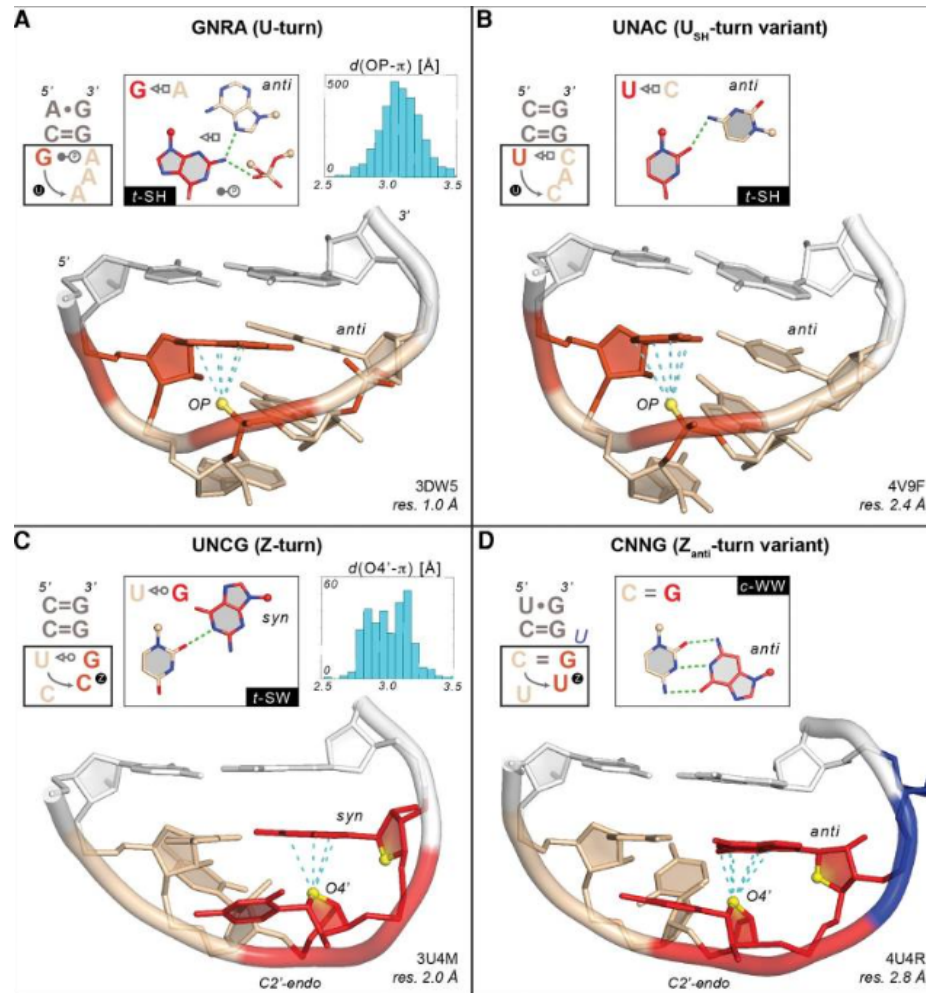


**Figure 2.10:** Showing Z-turns, U-turns and their variant conformations for the common tetraloop families GNRA, UNCG, and CUUG (D’Ascenzo et al., 2017).

### Internal loops and bulges

Internal loops are classified into two types: symmetrical and asymmetrical. Two common asymmetrical internal loops are the kink turn (k-turn) motif and the E-loop (S-loop) (Klein et al., 2021; Réblová et al., 2003). K-turns serve as mediators for tertiary interactions and act as ligand binding sites, especially proteins from the L7Ae family, which are RBPs, as shown in Figure 2.11 (Huang & Lilley, 2016). The first E-loop was identified in *E. coli*'s 5S ribosomal RNA (Grover, 2022). Loop E motifs are crucial in organizing multi-helix junctions and serve as interaction recognition sites (Owens & Baumstark, 2007).

Internal loops and bulges reduce the thermodynamic stability of an RNA structure; however, they are very significant as unpaired nucleotides are readily available for interactions with proteins and other ligands (Chen & Varani, 2001). Stacking the bulge loop nucleotides within the helix makes the RNA flexible (Grover, 2022). Bulges are essential in biological processes such as intron splicing, feedback regulation, protein binding, and tertiary folding of RNA (Crowther et al., 2017). Internal loops and bulges cause bending in an RNA molecule, which influences ligand binding. Internal loops and bulges provide ideal locations for conformational switches, which can result in structural changes (Chen & Varani, 2001). Moreover, the presence of bulge loops alters the dimensions of the RNA grooves, marking them as recognition sites for ligand binding (Grover, 2022).

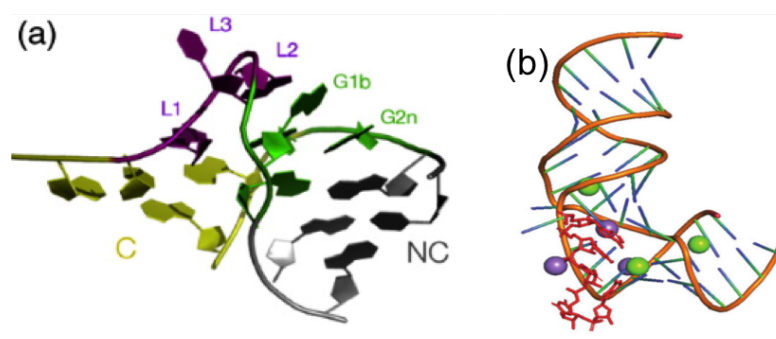


**Figure 2.11:** a) A representation of a k-turn; b) A crystal structure of a bulge loop on the hepatitis C virus IRES domain stabilized by magnesium (green) and manganese (purple) ions (Grover, 2022).

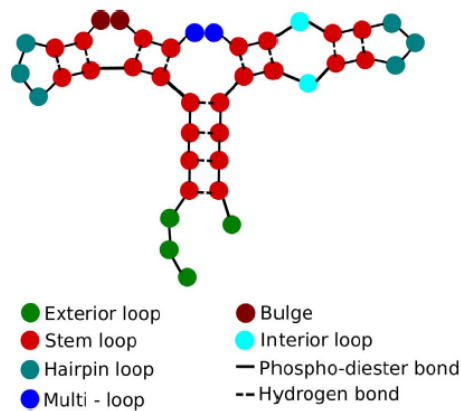


**Figure 2.12:** RNA Secondary structures (Fallman et al., 2017).

### 2.11 RNA tertiary structure

These alignment of separate RNA stacks along a common axis is known as coaxial stacking. RNA's tertiary structure is formed by connecting secondary structure elements via coaxial stacking and long-range interactions. Adenosine platforms, base triples, kissing loops, and pseudoknots are common coaxial stacking motifs (Chen &Varani, 2001; Gruyter, 2013). Adenosine platforms, also known as the A-A platform motif, are helical adenosine strands with side-by-side configurations resulting in a pseudo base pair (Cate et al., 1996). They are essential in mediating long-range interactions.

Base triples are hydrogen bond edge-to-edge interactions of three RNA nucleobases occurring as repeated clusters (Almakarem et al., 2012). Base triples enable tertiary structure assembly by facilitating critical long-range interactions such as a helical region base pair docking (Firdaus-Raih et al., 2011). They can also result from the formation of pseudoknots that create room for further tertiary interactions, which stabilize the RNA structure (Gruyter, 2013).

Tertiary structures of RNA have important contacts between unpaired regions that play crucial biological roles known as loop-loop interactions, such as kissing loops and pseudoknots. Kissing loops arise from interactions of two terminal hairpin loops (Chen &Varani, 2001). Kissing loops are essential tertiary elements as they are vital in gene expression regulation for prokaryotes and eukaryotes and stabilizing riboswitches

structures (Blouin & Lafontaine, 2007; Garst et al., 2011; Grutyer, 2013). Additionally, kissing loops are used in antisense recognition, ribosomal frameshifting, and translation initiation (Bouchard & Legault, 2014). Kissing loop interactions have been studied extensively in retroviral genomes, such as the HIV-I RNA dimerization initiation site, as illustrated in Figure 2.13 (Ennifar et al., 2001). Moreover, kissing loops also stabilize the complex architecture of RNA structures such as RNA-RNA dimers (Cao & Chen, 2011; Li et al., 2006).

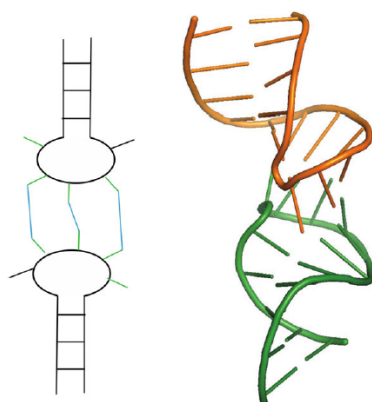


**Figure 2.13:** A secondary (a) and NMR structure (b) of a kissing loop formed between two hairpin loops (Grover, 2022)

Pseudoknots, conversely, are formed via WC base-pairing interactions of a complementary sequence of loops and an unpaired region. Pseudoknots are common motifs in RNA structures primarily present in viruses' three-prime end (Li et al., 2014). Pseudoknots influence viral gene expression by causing ribosomal frame shifts (Chen & Varani, 2001). The simplest pseudoknots are the H-type, forming when a single-stranded region outside a loop bond paired bases in a hairpin loop, portrayed in Figure 2.14 (Peselis & Serganov, 2014). H-type pseudoknots are essential in viral IRES and telomerase RNA (Sperschneider et al., 2011). Other types of pseudoknots are B, M, and I, although the nomenclature is limitedly employed, and most pseudoknots are generally known as H-type (Brierley et al., 2007).



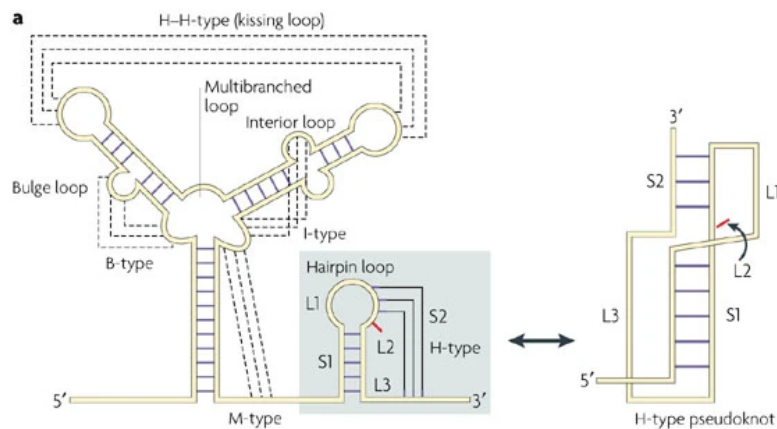


**Figure 2.14:** The secondary structures of B, M, I, and H-type pseudoknots (Brierley et al., 2007).

RNA junctions are another example of coaxial stacking. They are hubs that form when multiple helices come together. The three-way junction is the most common, forming a Y shape. RNA can form other junctions of higher order, such as a 4-way or 5-way junction (Figure 2.15). Junctions give the RNA structure flexibility by allowing it to change conformation due to a small molecule or protein binding (Chen & Varani, 2001).

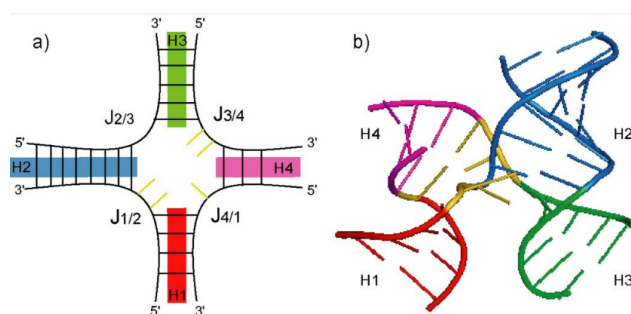


**Figure 2.15:** A 2D (a) and 3D (b) structure of a 4-way junction (Laing & Schlick, 2009).

The A-minor motif is significant in the stabilization of RNA tertiary and quaternary structure (Figure 2.16). It entails extensive contact between unpaired adenosines extended from one secondary structural element and a receptor helix's minor groove, resulting in a minor groove base triple interaction (Chen & Varani, 2001). They are classified into four types: type 0, type I, type II, and type III (Baulin, 2021). The position

of the adenosine 2'OH relative to the 2'OH groups of the receptor base pair is used to classify A-minor interactions.

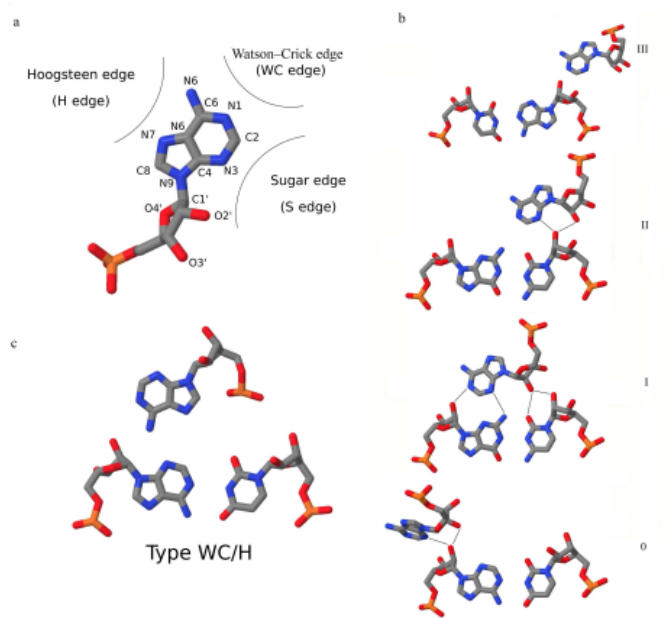


**Figure 2.16:** a) An adenine base with three edges. b) The A-minor motifs types: 0, I, II, and III. c) shows a non-canonical WC/H a-minor motif. (Baulin, 2021)

Ribose zippers involve hydrogen bonding between different regions of an RNA chain or between RNA chains. Most ribose zippers form antiparallel interactions between chains, and almost all link stems with loop segments such as junctions (Tamura & Holbrook, 2002). Due to the formation of hydrogen bonds, ribose zippers are critical tertiary interactions that stabilize RNA structures (Grover, 2022).

## 2.12 RNA structure modeling approaches

RNA plays a crucial role in carrying genetic material that is translated into proteins. Besides, it is instrumental in regulating genetic information, thereby making it a significant drug target for treating several human diseases (Sheridan, C. (2021). Knowledge of RNA folding, energetics, and kinetics is vital to understanding the varying functional states of RNA (Magnus et al., 2019). The increase in the availability of metagenomic sequences due to the development of whole genome sequencing techniques has resulted in identifying more RNA families and accumulating knowledge on RNA sequences. RNA structure can be determined experimentally using different

approaches such as X-ray crystallography, NMR, and cryo-EM (Fu et al., 2022). By 2018, approximately 1345 RNA structures and 2284 RNA complexes determined via cryo-EM, NMR spectroscopy, X-ray crystallography, and other methods were deposited in the PDB (Ponce-Salvatierra et al., 2019).

Despite increased deposits in the Rfam database, by 2020, only about 99 RNA families had been experimentally determined and were available in the PDB (Li et al., 2020). The laborious, time-consuming, and expensive nature of RNA experimental structure determination warrants using novel approaches. Therefore, numerous advances have utilized computational approaches to predict secondary and tertiary RNA structures to complement experimental efforts. Computational methods employ biophysical and biochemical data obtained from techniques such as chemical probing of RNA secondary structure (Ponce-Salvatierra et al., 2019). Thermodynamic models are widely used to model RNA structures, and they incorporate selective 2'-OH acylation by primer extension (SHAPE)-informed free energies, yielding highly accurate RNA structures (Schlick & Pyle, 2017).

There are three 3D modeling approaches; *de novo*, fragment assembly, and comparative modeling. *De novo* modeling is 3D structures prediction in the absence of a template. Instead, *De novo* modeling relies on force-field simulations to find the optimal structure via sampling the conformational space (Li et al., 2020). Comparative modeling, also known as homology modeling, entails using the structure of a homologous molecule as a template to model the query structure. This approach is established on the observation that RNA 3D structures are highly conserved even with divergent sequences (Rother et al., 2011). Fragment assembly involves predicting RNA 3D structure using fragments of experimentally determined structures (Chojnowski et al., 2021).

Secondary structure prediction entails base pairing of complementary regions and hydrogen bonding between side chains, forming a range of significant folds for RNA function. Computational characterizations of significantly large-sized RNA molecules demand special routines such as a scanning analysis window to perform accurate RNA

folding predictions. One of the tools for secondary structure prediction is the ScanFold web server, which combines several thermodynamic and statistical methods to generate 2D models. ScanFold has been previously used to characterize HIV-1 and Zika virus (ZIKV). Additionally, it has been used to generate SARS-CoV-2 RNA structure (Andrews et al., 2020). The ScanFold method highlights regions that are highly significant functional structures and generates unique 2D models.

The server's full pipeline embodies two subroutines executed from different servers: ScanFold-Scan and ScanFold-Fold (Andrews et al., 2020). ScanFold-Scan performs an analysis of the input sequence that creates a scanning window. ScanFold-Fold utilizes results from the scanning window to identify low z-score windows. ScanFold-Scan subroutine employs several metrics, including P-value, Z-score, Minimum Free Energy (MFE), and Ensemble Diversity.

RNA structure is hierarchical and sequential, which ascertains the accuracy of computational modeling. Tertiary structure modeling is based on the correct prediction of 2D structure, which is majorly dominated by WC-base pairs (Westhof et al., 2011). RNA 2D structure prediction can be performed by different tools using a common approach that employs free energy minimization, which is key to RNA structure, to search for thermodynamically stable states (Fu et al., 2022; Schroeder, 2018; Westhof et al., 2011). Some of the tools used for 3D modelling of RNA include modeRNA, and RNAcomposer. ModeRNA utilizes templates to model tertiary structures of RNA while RNAcomposer uses 3D RNA fragments to identify the one that best fits the provided secondary structure, followed by refinement of the assembled structure via the CHARMM force field (Biesiada et al., 2016; Rother et al., 2011). Notwithstanding the advances in RNA modeling, the field faces numerous challenges, including analysis of RNA motifs, updating RNA structure databases, and structure quality (Schlick & Pyle, 2017).

### **2.13 RNA as a drug target**

RNA is an important drug target for different bacterial and viral infections, cardiovascular diseases, and cancers. RNA's importance in transcription regulation, translation, protein function, protein transport, and catalysis places it at the center of therapeutic models, especially in cases where compounds have failed (Chordia & Kumar, 2019).

RNA tertiary structure is the starting point for therapeutic design; therefore, computational structure prediction is critical to RNA drug targeting. RNA motifs can be used as a small molecule target. For instance, Oxazolidinones, a group of antibiotics active against a spectrum of Gram-positive bacteria, is an example of compounds that target ribosomal RNA inhibiting protein synthesis (Drysdale et al., 2002). However, most small-molecule therapeutic interventions target proteins, leaving out 70% of the human genome that is druggable non-coding RNA. (Warner et al., 2018).

Advancements are underway to shift focus on non-coding RNA as small molecule drug targets (Matsui & Corey, 2017). According to Hermann. (2016), several drug-like small molecules that target viral replication in human immunodeficiency virus (HIV), HCV, influenza A, and severe respiratory syndrome coronavirus (SARS CoV) were identified. Although non-coding RNA presents novel therapeutic opportunities, significant hurdles must be overcome for the research to translate into clinical development. One of the crippling challenges is the specificity and selectivity of the target (Hermann, 2016; Winkle et al., 2021).

### **2.14 Molecular docking**

Molecular docking is a computer technique that aids in the study of molecular interactions, particularly those involving ligands (small molecules) and target biomolecules such as proteins or nucleic acids such as RNA. There are two main steps involved in molecular docking, which include prediction of the pose or orientation of the ligand, followed by assessment of binding affinity. In the prediction phase, complex algorithms and mathematical models take into account characteristics such as molecule

shape, electrostatic interactions, and hydrophobicity. An array of methods such as point complementarity, Monte Carlo technique, and distance geometry are used to improve accuracy of pose prediction (Adelusi et al., 2022). The subsequent step assesses the strength of the ligand-target molecule interaction. Affinity is an important factor in determining the likelihood and stability of binding. Some of the common tools used for molecular docking include Autodock Vina, Patchdock, GOLD, FITTED, DOCK 6, MORDOR and rDOCK (Zhou et al., 2022).

Two approaches are involved in the docking process of RNA and small molecules; blind and local docking. Blind docking entails docking of a small molecule on a receptor without any knowledge of the binding location while local docking is the vice versa (Zhou et al., 2022). The choice of docking approach relies on the knowledge of the binding site. While molecular docking has made significant advances, it still faces hurdles such as the complexities of RNA structural variety and the need for appropriate docking techniques to capture the complexities of RNA-protein or RNA-ligand interactions. As the field of molecular docking evolves, studies reveal advances in RNA structure prediction and the growing relevance of RNA in therapeutic applications, necessitating a more nuanced knowledge of RNA-ligand interactions via computational approaches.

## CHAPTER THREE: 3.0 MATERIALS AND METHODS

### 3.1 Data retrieval and processing

The Enterovirus A71 sequence was obtained from the Virus Pathogen Resource (ViPR) (<https://www.bv-brc.org/>). Selection of the Enterovirus A71 sequence was based on the completeness of the sequence (approximately 7,420 nucleotides), host (Human), a poly A tail, and a recent collection date. Additionally, since certain Enterovirus A71 strains are avirulent, the virulence was also taken into account to only focus on pathogenic variants. The fasta file was retrieved from the NCBI GenBank database (<https://www.ncbi.nlm.nih.gov/genbank/>). The obtained EVA71 sequence was stored in two separate fasta files containing the 3' UTR and the 5' UTR. Further processing entailed identifying the 5' and the 3'UTRs obtained from the GenBank file format. BLASTn was performed to query the sequence and identify a template for structural modeling. Coxsackievirus B3 complete genome was the sole discovered sequence with an experimentally confirmed secondary structure; thus, it was obtained from the NCBI GenBank database and used to validate the predicted structure of KJ746493.1.

### 3.2 Secondary structure prediction

Secondary sequence prediction was performed using the ScanFold web server (<https://mosslabtools.bb.iastate.edu/>). The two separate files containing sequences of EV-A71 3' and 5' UTRs were uploaded on the ScanFold web server full pipeline, with the window size set to 90 and the parameters such as step size, temperature and randomizations used in their default setting. The outputs were two dot-bracket notation files for the 3' and 5' UTRs which were utilized to model the tertiary structure of the UTRs.

### 3.3 Tertiary structure modeling

RNAComposer (<https://rnacomposer.cs.put.poznan.pl/>) was utilized for determining the tertiary structure of the UTRs. The 3' UTR contained 100 nts and was uploaded separately on RNAComposer for tertiary structure modeling. The tertiary structure of the 5' UTR was modeled via RNAComposer in two parts, each containing three domains: domains I, II, III (containing 240 nts) and domains IV, V, VI (containing 397 nts), stored

in separate files. The files were then uploaded to the RNAComposer server, which predicted the tertiary structures. The outputs of this step were three pdb files containing 3-D structures of EVA71 UTRs. Two files were for the 5' UTRs, file one containing domains I, II, and III, and file two containing domains IV, V, and VI. The third file contained the 3-D structure of the 3' UTRs. These files were then used to validate the predicted structures and further used for molecular docking.

### **3.4 Structure evaluation**

The 3D structures were searched against the WebRASP server (<http://melolab.org/webrasp/home.php>). The server uses RASP to compute energy scores to evaluate the RNA structures' stability. RASP performs an all-atom knowledge-based potential assessment calculation for scoring RNA 3D structures built on atomic interactions that are pairwise distance-dependent (Norambuena et al., 2013). The inputs are pdb files of the RNA structures containing atomic coordinates. WebRASP server calculates the RNA molecule's energy profile and general energy score. The PDB files of EVA71, the 5' UTR domain I, II, III, domain IV, V, VI, and the 3' UTR search results are recorded in Table 5.

### **3.5 Visualization and structure analysis**

The secondary structures obtained in dot bracket notation from ScanFold webserver were visualized and manipulated on Varna (v3-92) (<https://varna.lri.fr/>) and Forna (<http://rna.tbi.univie.ac.at/forna/>). The 3D structure and molecular docking complexes were visualized and edited using UCSF Chimera (version 1.15) (<https://www.cgl.ucsf.edu/chimera/>).

### **3.6 Motif identification**

Maximum Expectation maximization for Motif Elicitations for (MEME) Suite (version 5.4.1, <https://meme-suite.org/meme/>) is a webserver that performs motif-based sequence analysis for DNA, RNA, and proteins using the MEME algorithm (Bailey et al., 2015). The fasta files of the 3' and 5' UTRs were uploaded on the MEME suite motif discovery tool, which discovered novel, ungapped motifs (Bailey & Elkan, 1994). The motif mode



selected was classic, which is the original MEME objective function for motif discovery, the site of distribution was selected as any number of repetitions to identify the different positions containing the same motif, and the number of motifs to be found was entered as five for the 3' UTR and twelve for the 5' UTR.

### **3.7 Molecular docking**

This technique determines the interaction between a ligand and a receptor. Patchdock server (version Beta 1.3, <http://bioinfo3d.cs.tau.ac.il/PatchDock/>) is a molecular docking algorithm that finds transformations that result in good molecular shape complementarity (Schneidman-Duhovny et al., 2005). The compounds obtained from literature demonstrated the potential to inhibit the enterovirus translation or replication (Badshah et al., 2021; Benschop et al., 2015; Chiang et al., 2005; Lalani & Poh, 2020; Li et al., 2015; Wang et al., 2013). The docking compounds were 13, including 7-hydroxy isoflavone, amantadine, baicalin, dihydromyricetin, diosmetin, formononetin, kaempferol, morin hydrate, myricetin, nobiletin, ribavirin, taxifolin, and ursolic acid (Appendice E). The 2D structure of these compounds was downloaded from PubChem (<https://pubchem.ncbi.nlm.nih.gov/>); then, using Open Babel (version 2.3.1) (<https://openbabel.org/wiki/OpenBabelGUI>), they were converted to pdb format. The pdb files of the receptor (5' and 3' UTRs obtained in section 3.1.3) and ligands (from Open Babel) were then uploaded to the Patchdock server with the complex type selected as protein-small ligand and the clustering RMSD set at 2.0 (Schneidman-Duhovny et al., 2005). The server yielded results for geometric shape complementarity score (GSC score), approximate area interface, and atomic contact energy (ACE) (Yadav et al., 2017).

## CHAPTER FOUR: 4.0 RESULTS

### 4.1 Sequence retrieval

The sequence KJ746493.1 Enterovirus A71 strain 306A was selected from the Virus Pathogen Database (ViPR). A blast was performed on the NCBI GenBank database to ascertain the sequence is enterovirus A71 and to identify the template sequence. The Blast confirmed this sequence from Enterovirus A71 and identified similar sequences, including those of Coxsackievirus B3. From the genome annotations, it was determined that the 5' and 3' UTRs of KJ746493.1 had 742 and 101 nucleotides, respectively.

### 4.2 Secondary structure modeling

The secondary structures of the 5' and 3' UTRs of Enterovirus A71 were predicted *de novo* and separately using the ScanFold webserver pipeline. VARNA and Forna were used to visualize the 2D structure of EVA71.

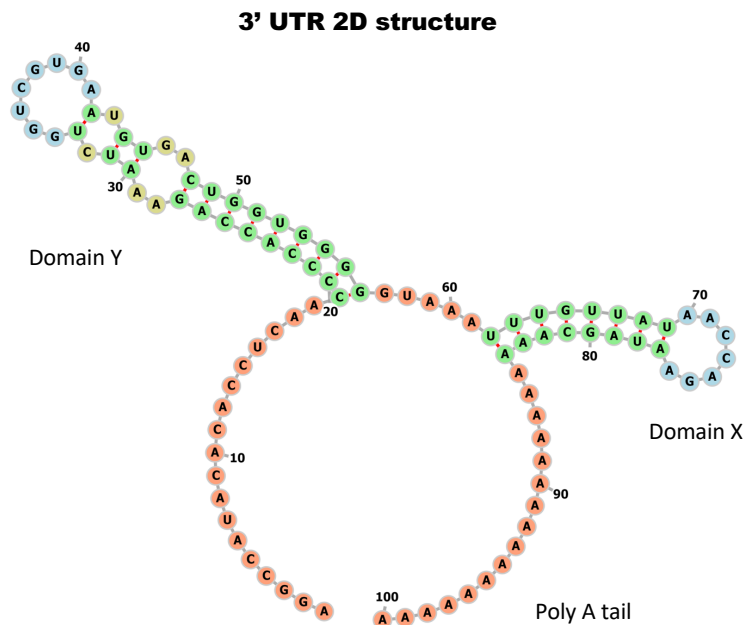


**Figure 4.1:** Secondary Structure of the 3' UTR of EVA71 (100 nts long), containing two domains (X and Y) and a poly-A tail obtained using Forna.



# 5' UTR

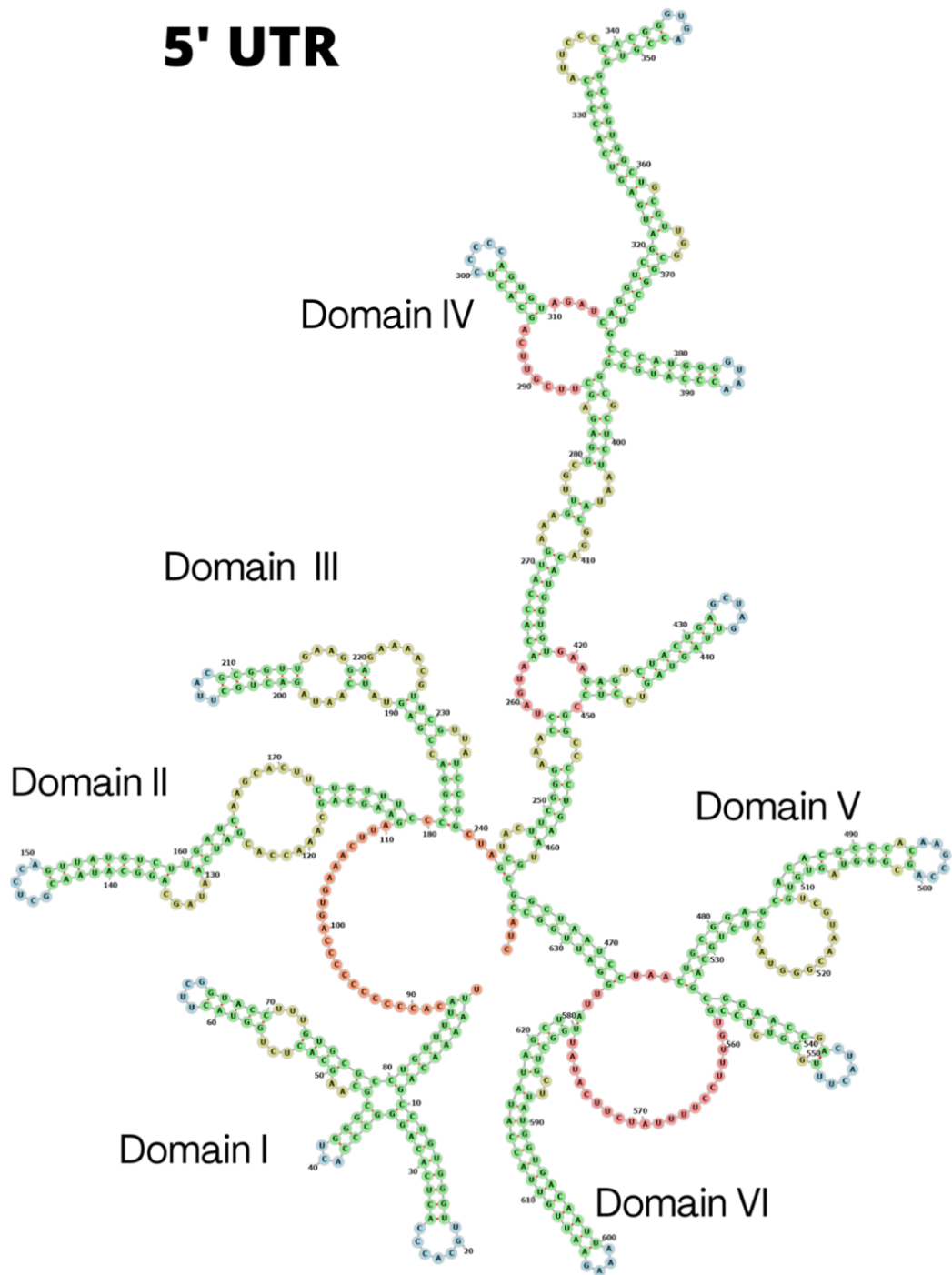


**Figure 4.3:** The 5' UTR of EVA71 containing six domains visualized using Forna. Domains II-VI form the IRES structure.

### 4.3 Tertiary structure modeling

The tertiary structure was modeled using the RNAComposer webserver (. The modeling was performed using domains from the secondary structure predicted by the ScanFold webserver pipeline. Since the maximum sequence length is limited to 500 residues in RNAComposer, domains 1, 2, and 3 were modeled together, while domains 4.5 and 6 were modeled together. UCSF Chimera was used to visualize the 3D structures of the 5' and 3' UTR of EVA71.

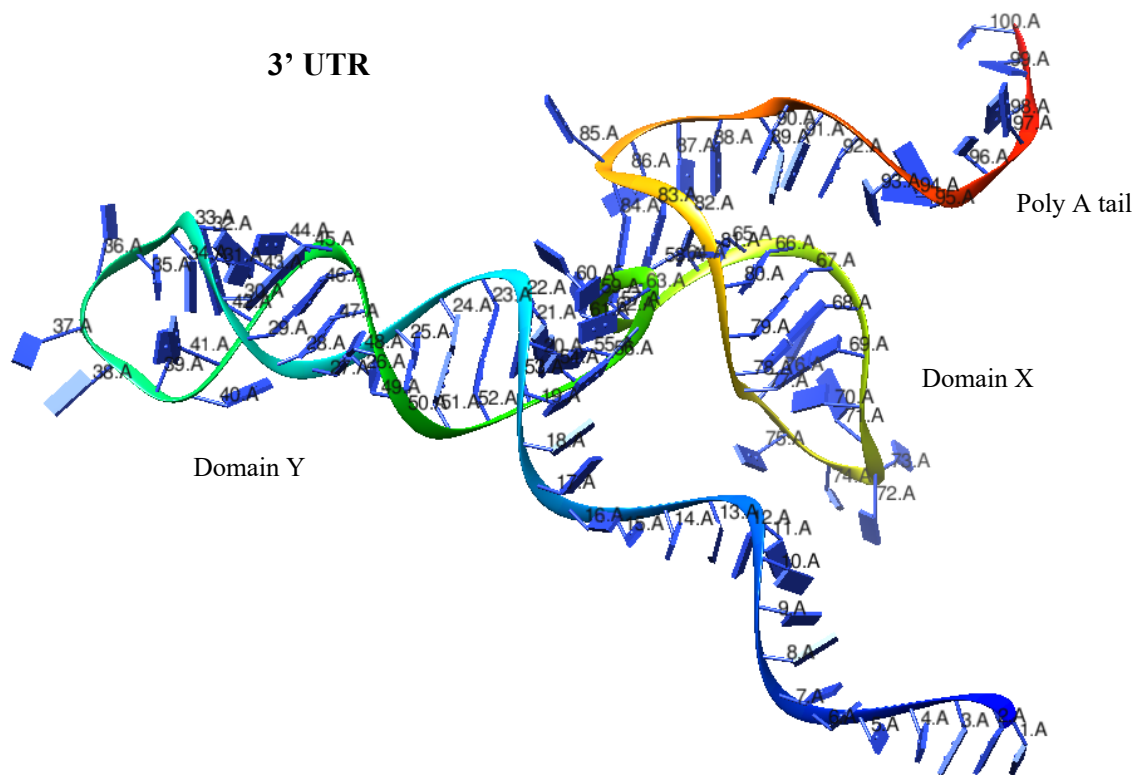


**Figure 4.4:** The 3' UTR 3D structure showing domains Y, Z, and the poly-A tail, obtained using RNAComposer and visualized by UCF Chimera.

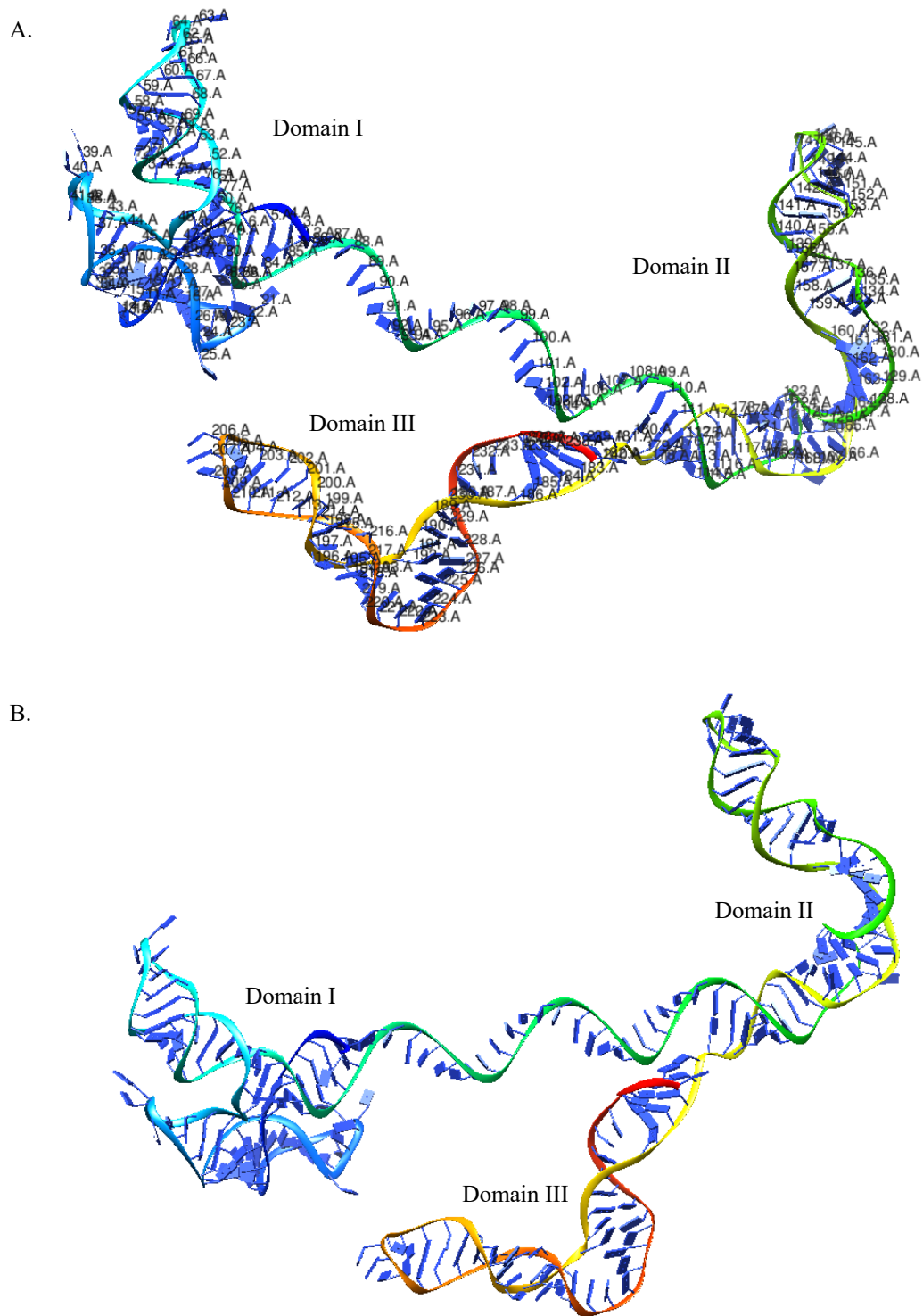
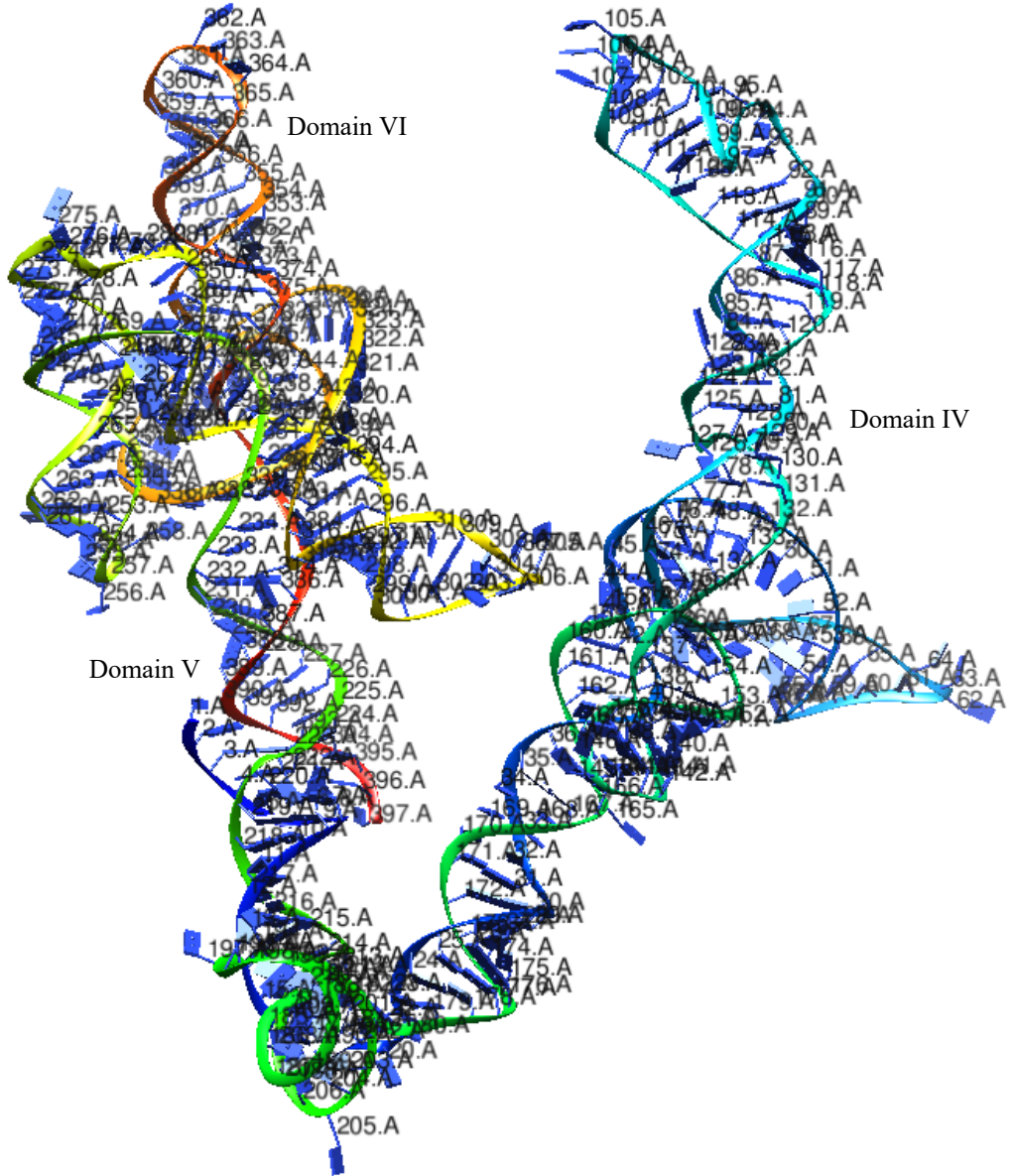


**Figure 4.5:** The tertiary structure of the 5' UTR of EVA71 with domains I (cloverleaf), II, and III obtained using RNAComposer and visualized by UCF Chimera, A. with labels, B. without labels.

A.



B.

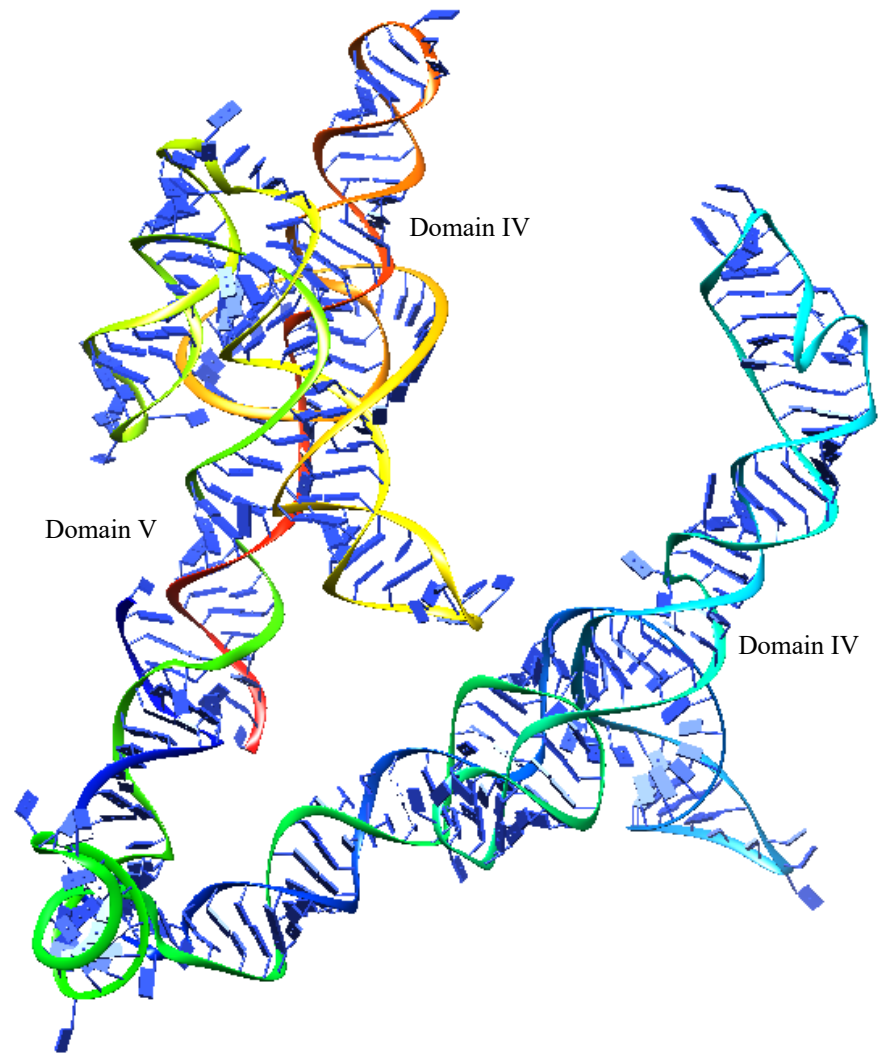


**Figure 4.6:** The tertiary structure of the 5' UTR domains IV, V, and IV, obtained using RNAComposer and visualized by UCF Chimera, A. with labels, B. without labels.



#### 4.4: Structure evaluation

The structure total energies for all the domains obtained for the 5' and 3' UTRs were large negative values (Table 1).

**Table 1:** WebRASP scoring of structure total energy based on distance-dependent pairwise atomic interaction.

| EVA71                                     | 5' Domains I, II, III | 5' Domains IV, V, VI | 3' UTR     |
|---|-----------------------|----------------------|------------|
| Number of residues per region             | 240 nts               | 397 nts              | 100 nts    |
| Structure total energy (kcal/mol/contact) | -109,778.00           | -171,402.00          | -41,401.60 |
| Number of contacts                        | 1,042,556             | 2,216,127            | 405,756    |

#### 4.5 Motif Identification

Motifs were identified using MEME suite. Five motifs were predicted for the 3' UTR and 12 motifs for the 5' UTR. Four of the 12 motifs on the 5'UTR were also identified from literature (Davila-Calderon et al., 2020; Lai et al., 2020; Tolbert et al., 2017). The predicted 3' UTR motifs were motif 1: UGGKSGURAAUKUG, motif 2: CMCACC, motif 3: KWAUARC, motif 4: RGMMAU, and motif 5: AAAAAA which is the poly-A tail (Figure 4.7; Appendice B).

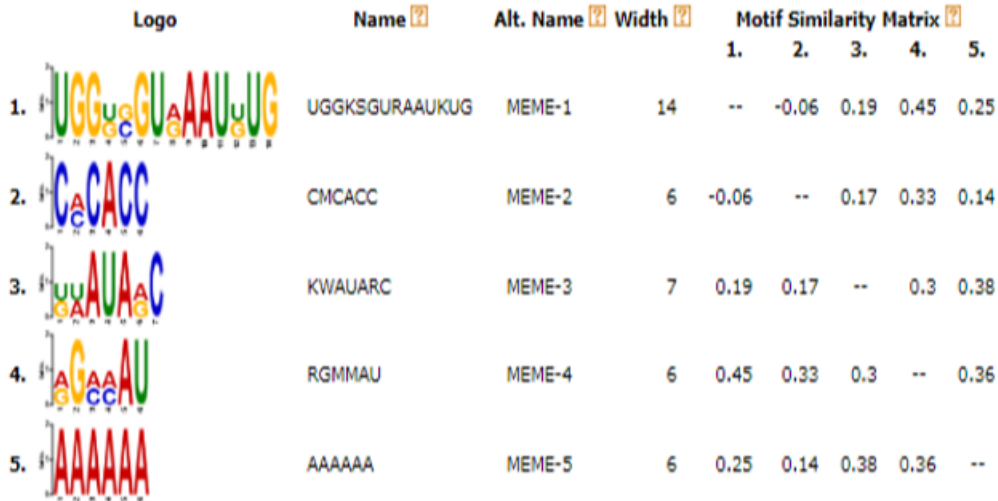


**Figure 4.7:** A summary of the five predicted 3' UTR motifs of EVA71.

The predicted 5' UTR motifs were motif 1: GAAACYUAGWARCA, motif 2: AUCAAUAG, motif 3: UUAAA, motif 4: UACUUYGG, motif 5: AGCYAGUGGGUWG, motif 6: AAGCACU, motif 7: AWG WGAMAA, motif 8: UAAU, motif 9: GGGUAA, motif 10: GAWGAGU, motif 11: UUWURUCUUSAU, and motif 12: UGAA (Figure 4.8; Appendice B)

Motifs with a pale red background are very similar to other earlier specified motifs and may be biasing the results. It is recommended that you re-run MAST and request it to remove redundant motifs.

| Logo | Name           | Alt. Name | Width | Motif Similarity Matrix |      |      |      |      |      |      |      |      |      |      |      |
|------|----------------|-----------|-------|-------------------------|------|------|------|------|------|------|------|------|------|------|------|
|      |                |           |       | 1.                      | 2.   | 3.   | 4.   | 5.   | 6.   | 7.   | 8.   | 9.   | 10.  | 11.  | 12.  |
|      | GAAACYUAGWARCA | MEME-1    | 14    | --                      | 0.34 | 0.57 | 0.39 | 0.35 | 0.59 | 0.35 | 0.56 | 0.44 | 0.33 | 0.19 | 0.75 |
|      | AUCAUAG        | MEME-2    | 8     | 0.34                    | --   | 0.47 | 0.21 | 0.39 | 0.48 | 0.28 | 0.67 | 0.22 | 0.42 | 0.25 | 0.67 |
|      | UUAAA          | MEME-3    | 5     | 0.57                    | 0.47 | --   | 0.27 | 0.36 | 0.4  | 0.57 | 0.67 | 0.53 | 0.25 | 0.57 | 0.67 |
|      | UACUUYGG       | MEME-4    | 8     | 0.39                    | 0.21 | 0.27 | --   | 0.4  | 0.38 | 0.2  | 0.67 | 0.33 | 0.19 | 0.34 | 0.3  |
|      | AGCYAGUGGGUWG  | MEME-5    | 13    | 0.35                    | 0.39 | 0.36 | 0.4  | --   | 0.33 | 0.17 | 0.62 | 0.54 | 0.33 | 0.23 | 0.58 |
|      | AAGCACU        | MEME-6    | 7     | 0.59                    | 0.48 | 0.4  | 0.38 | 0.33 | --   | 0.31 | 0.42 | 0.33 | 0.23 | 0.14 | 0.5  |
|      | AWGGWGAMAA     | MEME-7    | 10    | 0.35                    | 0.28 | 0.57 | 0.2  | 0.17 | 0.31 | --   | 0.39 | 0.45 | 0.39 | 0.21 | 0.79 |
|      | UAAU           | MEME-8    | 4     | 0.56                    | 0.67 | 0.67 | 0.67 | 0.62 | 0.42 | 0.39 | --   | 0.75 | 0.33 | 0.61 | 0.42 |
|      | GGGUAA         | MEME-9    | 6     | 0.44                    | 0.22 | 0.53 | 0.33 | 0.54 | 0.33 | 0.45 | 0.75 | --   | 0.44 | 0.21 | 0.42 |
|      | GAWGAGU        | MEME-10   | 7     | 0.33                    | 0.42 | 0.25 | 0.19 | 0.33 | 0.23 | 0.39 | 0.33 | 0.44 | --   | 0.31 | 0.65 |
|      | UUWURUCUUSAU   | MEME-11   | 12    | 0.19                    | 0.25 | 0.57 | 0.34 | 0.23 | 0.14 | 0.21 | 0.61 | 0.21 | 0.31 | --   | 0.56 |
|      | UGAA           | MEME-12   | 4     | 0.75                    | 0.67 | 0.67 | 0.3  | 0.58 | 0.5  | 0.79 | 0.42 | 0.42 | 0.65 | 0.56 | --   |

Figure 4.8: A summary of the twelve predicted motifs of the 5' UTR of EVA71.

## 4.6 Molecular docking

The 13 small molecules that have been shown to inhibit replication or translation of Enterovirus E71 were selected for docking, included 7-hydroxy isoflavone, amantadine, baicalin, dihydromyricetin, diosmetin, formononetin, kaempferol, morin hydrate, myricetin, nobiletin, ribavirin, taxifolin and ursolic acid (Badshah et al., 2021; Benschop et al., 2015; Chiang et al., 2005; Lalani & Poh, 2020; Li et al., 2015; Wang et al., 2013).

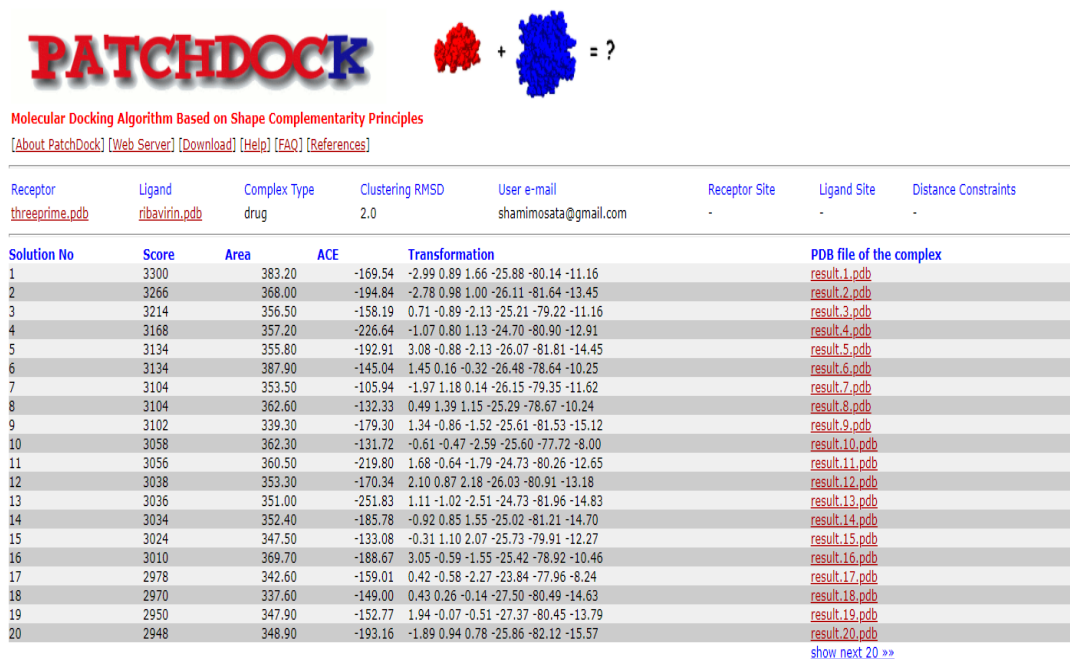
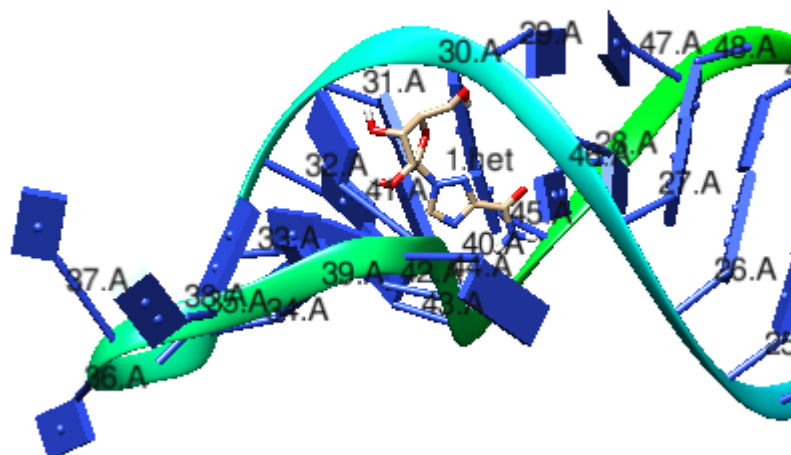


**Figure 4.9:** A summary of the first 20 docking scores, ACE, and transformations for ribavirin docked on the 3'UTR of EVA71.

A.



B.

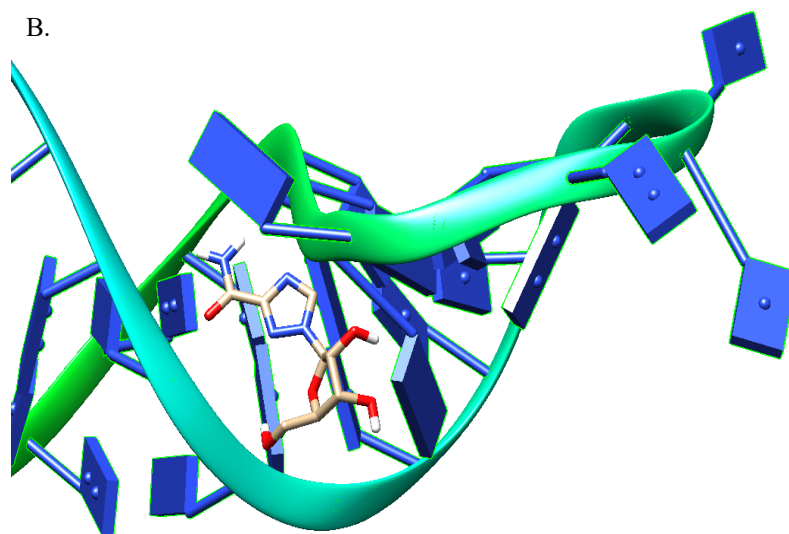


**Figure 4.10:** Ribavirin bound to motif 1 of EVA71 3' UTR with an ACE of -251.84 kcal/mol. A. with labels showing docked position, B. without labels.

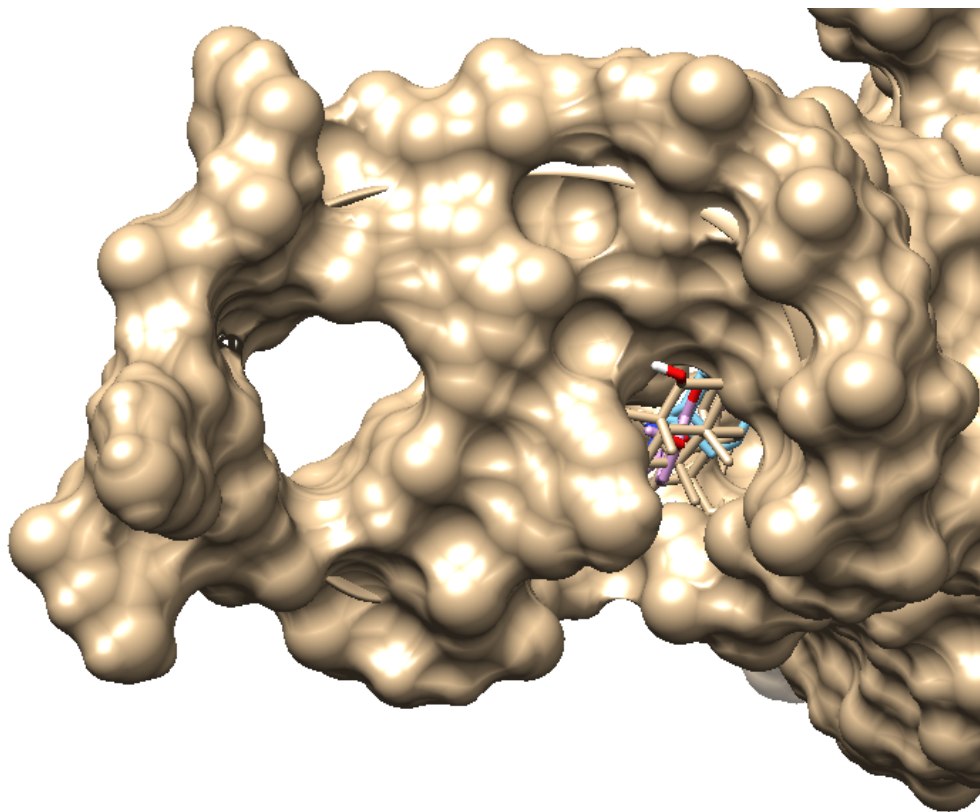


**Figure 4.11:** Ribavirin and ursolic acid bound to the pocket formed on the 3'UTR of EVA71 with an ACE of -251.84 and -445.52 kcal/mol respectively.



Molecular Docking Algorithm Based on Shape Complementarity Principles

[\[About PatchDock\]](#) [\[Web Server\]](#) [\[Download\]](#) [\[Help\]](#) [\[FAQ\]](#) [\[References\]](#)

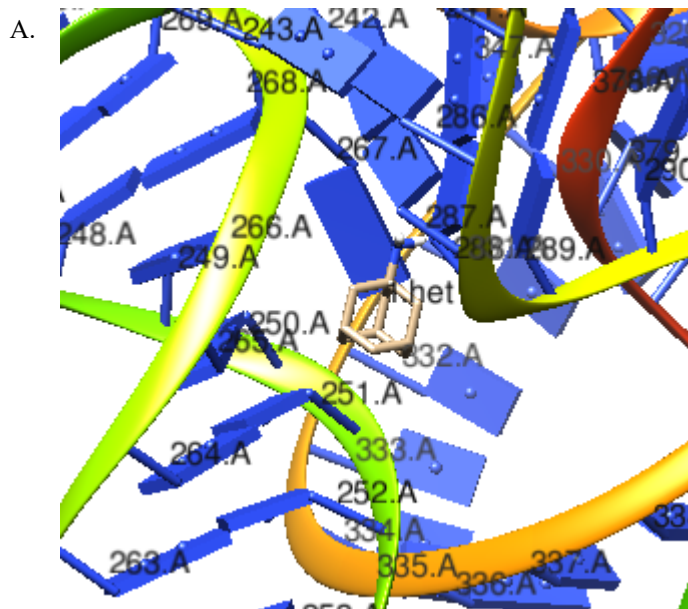
| Receptor                   | Ligand                         | Complex Type | Clustering RMSD | User e-mail           | Receptor Site | Ligand Site | Distance Constraints |
|----------------------------|--------------------------------|--------------|-----------------|-----------------------|---------------|-------------|----------------------|
| <a href="#">dom4fs.pdb</a> | <a href="#">amantadine.pdb</a> | drug         | 2.0             | shamimosata@gmail.com | -             | -           | -                    |

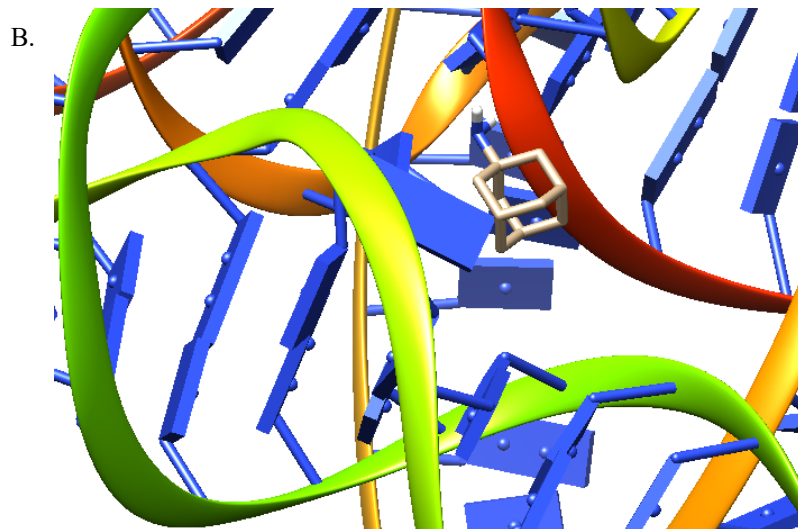
  

| Solution No | Score | Area   | ACE     | Transformation                        | PDB file of the complex       |
|-------------|-------|--------|---------|---------------------------------------|-------------------------------|
| 1           | 3010  | 331.40 | -186.42 | -3.14 0.26 2.34 -27.75 49.33 -56.16   | <a href="#">result.1.pdb</a>  |
| 2           | 2994  | 330.80 | -203.98 | 1.38 0.09 2.43 -27.43 50.03 -55.84    | <a href="#">result.2.pdb</a>  |
| 3           | 2988  | 327.30 | -180.88 | 1.04 -0.58 -1.91 -27.11 48.72 -56.19  | <a href="#">result.3.pdb</a>  |
| 4           | 2966  | 338.60 | -175.76 | -2.41 -0.72 -1.63 -27.61 49.23 -55.91 | <a href="#">result.4.pdb</a>  |
| 5           | 2958  | 322.90 | -195.19 | -0.94 0.52 1.85 -27.02 49.80 -55.69   | <a href="#">result.5.pdb</a>  |
| 6           | 2956  | 326.40 | -188.19 | 2.70 -0.04 -0.07 -27.22 49.37 -56.02  | <a href="#">result.6.pdb</a>  |
| 7           | 2932  | 328.10 | -188.37 | -0.79 0.67 -0.61 -27.23 49.47 -55.57  | <a href="#">result.7.pdb</a>  |
| 8           | 2852  | 335.70 | -174.29 | 2.91 0.81 -2.49 -27.32 49.33 -55.41   | <a href="#">result.8.pdb</a>  |
| 9           | 2844  | 321.20 | -181.09 | -1.59 -0.27 -3.10 -27.84 49.25 -56.16 | <a href="#">result.9.pdb</a>  |
| 10          | 2822  | 322.60 | -187.99 | -0.32 -0.80 -1.46 -26.43 48.90 -55.82 | <a href="#">result.10.pdb</a> |
| 11          | 2784  | 328.40 | -174.63 | 0.57 -0.25 0.33 -27.73 49.47 -55.66   | <a href="#">result.11.pdb</a> |
| 12          | 2758  | 325.60 | -174.27 | 0.09 0.49 -2.50 -28.02 49.16 -55.94   | <a href="#">result.12.pdb</a> |
| 13          | 2742  | 321.70 | -221.47 | -1.25 0.39 -0.95 2.76 35.43 17.73     | <a href="#">result.13.pdb</a> |
| 14          | 2736  | 318.20 | -225.75 | 0.46 -0.15 1.45 3.10 35.92 17.58      | <a href="#">result.14.pdb</a> |
| 15          | 2718  | 307.70 | -182.28 | -2.00 -0.04 -1.07 -26.38 48.18 -56.15 | <a href="#">result.15.pdb</a> |
| 16          | 2718  | 290.00 | -186.84 | -1.70 0.92 -0.72 -13.41 53.61 13.09   | <a href="#">result.16.pdb</a> |
| 17          | 2716  | 322.50 | -226.51 | -1.58 -0.23 1.50 2.94 35.80 17.55     | <a href="#">result.17.pdb</a> |
| 18          | 2696  | 317.90 | -223.78 | 0.31 0.52 -0.67 2.84 35.80 17.64      | <a href="#">result.18.pdb</a> |
| 19          | 2692  | 286.10 | -179.65 | -0.94 -0.90 -1.12 -13.42 53.55 12.89  | <a href="#">result.19.pdb</a> |
| 20          | 2682  | 274.60 | -211.32 | -2.19 -1.32 2.56 -0.75 -26.41 -33.85  | <a href="#">result.20.pdb</a> |

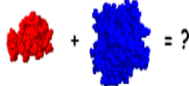
[show next 20 >>](#)

**Figure 4.12:** A summary of the first 20 docking scores, ACE, and transformations for amantadine bound on the 5' UTR of EVA71.





**Figure 4.13:** Amantadine bound on motif 5, domain V of the IRES with an ACE of -226.51 kcal/mol. A. with labels showing docked position, B. without labels.

**PATCHDOCK** 

Molecular Docking Algorithm Based on Shape Complementarity Principles  
[\[About PatchDock\]](#) [\[Web Server\]](#) [\[Download\]](#) [\[Help\]](#) [\[FAQ\]](#) [\[References\]](#)

| Receptor                   | Ligand                       | Complex Type | Clustering RMSD | User e-mail           | Receptor Site | Ligand Site | Distance Constraints |
|----------------------------|------------------------------|--------------|-----------------|-----------------------|---------------|-------------|----------------------|
| <a href="#">dom4fs.pdb</a> | <a href="#">baicalin.pdb</a> | drug         | 2.0             | shamimosata@gmail.com | -             | -           | -                    |

| Solution No | Score | Area   | ACE     | Transformation                       | PDB file of the complex       |
|-------------|-------|--------|---------|--------------------------------------|-------------------------------|
| 1           | 5866  | 664.60 | -391.69 | 0.99 0.56 -0.66 -24.23 46.13 -53.71  | <a href="#">result_1.pdb</a>  |
| 2           | 5458  | 652.40 | -379.97 | 2.09 -0.20 2.68 -26.02 47.78 -54.77  | <a href="#">result_2.pdb</a>  |
| 3           | 5310  | 603.20 | -386.25 | -1.51 0.94 2.56 -29.60 21.40 -47.94  | <a href="#">result_3.pdb</a>  |
| 4           | 5258  | 598.80 | -397.48 | -2.82 1.00 0.15 -24.27 45.06 -55.13  | <a href="#">result_4.pdb</a>  |
| 5           | 5232  | 637.90 | -369.95 | 2.69 -0.36 2.83 -24.59 48.09 -54.17  | <a href="#">result_5.pdb</a>  |
| 6           | 5212  | 600.80 | -306.40 | 0.41 0.81 -0.35 -23.37 46.47 -52.21  | <a href="#">result_6.pdb</a>  |
| 7           | 5188  | 579.90 | -335.38 | 0.91 1.11 -0.01 -24.21 48.48 -51.96  | <a href="#">result_7.pdb</a>  |
| 8           | 5154  | 623.30 | -472.39 | -2.54 0.09 -1.45 -24.82 44.32 -55.11 | <a href="#">result_8.pdb</a>  |
| 9           | 5154  | 566.20 | -375.12 | 0.38 0.34 -0.10 -27.45 20.64 -44.47  | <a href="#">result_9.pdb</a>  |
| 10          | 5148  | 558.70 | -265.69 | 1.64 -0.99 -1.55 -3.07 21.97 20.62   | <a href="#">result_10.pdb</a> |
| 11          | 5134  | 591.90 | -394.18 | 2.36 1.15 1.85 -13.08 52.72 14.27    | <a href="#">result_11.pdb</a> |
| 12          | 5130  | 562.90 | -361.75 | 2.53 0.77 0.66 -23.95 45.31 -54.10   | <a href="#">result_12.pdb</a> |
| 13          | 5120  | 598.40 | -340.65 | -2.45 0.15 1.43 -1.51 46.97 17.77    | <a href="#">result_13.pdb</a> |
| 14          | 5108  | 584.60 | -341.78 | 1.84 -1.17 -1.95 -2.90 22.60 22.17   | <a href="#">result_14.pdb</a> |
| 15          | 5100  | 549.40 | -344.51 | 2.98 1.50 0.10 -28.08 20.30 -49.93   | <a href="#">result_15.pdb</a> |
| 16          | 5098  | 566.90 | -365.90 | 2.74 -1.34 -2.85 -12.95 52.78 10.53  | <a href="#">result_16.pdb</a> |
| 17          | 5092  | 605.10 | -354.10 | 2.84 -1.22 -2.02 -14.56 53.55 11.63  | <a href="#">result_17.pdb</a> |
| 18          | 5068  | 561.00 | -319.55 | 1.08 0.68 -0.09 -26.63 20.16 -44.14  | <a href="#">result_18.pdb</a> |
| 19          | 5048  | 640.30 | -349.02 | 2.00 -0.04 -0.72 -26.58 46.97 -54.31 | <a href="#">result_19.pdb</a> |
| 20          | 5046  | 555.40 | -303.02 | 3.11 -1.07 -1.74 -22.76 46.01 -50.78 | <a href="#">result_20.pdb</a> |

[show next 20 >>](#)

**Figure 4.14:** A summary of the first 20 docking scores, ACE, and transformations of baicalin bound on the 5' UTR of EVA71.



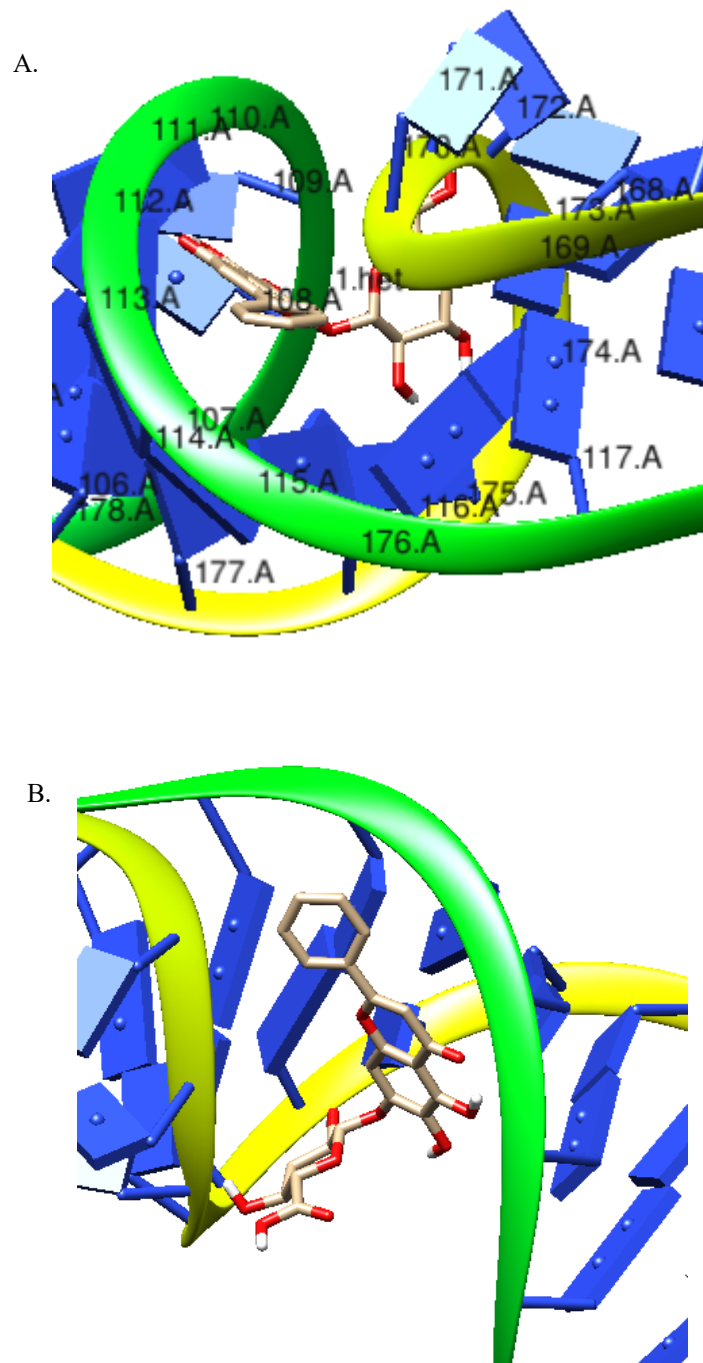


**Figure 4.15:** Baicalin bound on motif 1 of domain II of the IRES with an ACE of -472.39 kcal/mol. A. with labels showing docked position, B. without labels.

## CHAPTER FIVE: 5.0 DISCUSSION

Experimental methods are instrumental in determining RNA structure, which is essential to its function. However, experimental determination of RNA structures is technically difficult, laborious, and expensive resulting in the insignificant characterization of RNA structures (Ponce-Salvatierra et al., 2019). Computational techniques rapidly and affordably address the issue by giving the means to characterize RNA structures using RNA folding algorithms that consider the physical basis of RNA folding. Evolutionary information, such as conserved functional motifs from related RNA sequences, improves the accuracy of structural prediction or modeling of other RNA structures. Folding algorithms employ a similar principle that depends on the Turner nearest-neighbor energy parameters to generate the most stable and closest resemblance to the native RNA secondary structure with up to approximately 70% accuracy in sequences less than 700 nts (Andrews et al., 2018).

Additionally, the great stability of RNA secondary structure permits successful structure prediction from sequence using phylogeny and thermodynamic algorithms, which compute free energies (Chen & Varani, 2001). RNA structures' hierarchical and sequential nature dictates the interdependence in accurately modeling the different structural levels. The 3D structure modeled in this work demonstrates further the significance of utilizing *de novo* computational approaches in understanding and characterizing RNA structural elements. It also shows the precise location of important motifs and potential molecules for EV-A71 drug development.

### 5.1 Sequence retrieval

The retrieved sequence from the ViPR database was obtained from throat swabs of HFMD infected patients, submitted in 2014, with a length of 7424 nts (Appendice A). Throat swabs are the most significant specimens for patients with EVA71 (Ooi et al., 2007). The blast revealed an 88.71% similarity of EV-A71 with Coxsackievirus B3 (AY752946.1), which had an experimentally determined IRES secondary structure on IRESite that verified the predicted secondary structure of the 5' UTR of EV-A71 (KJ746493.1).

## 5.2 Secondary structure modeling

Six domains were predicted for the 5' UTR of EV-A71. Domains III and VI are more variable, while IV and V are relatively conserved (Lai et al., 2020). Domain I is the cloverleaf structure, which contains 90 nts consisting of a stem with three stem-loops, one of which contains two internal loops. Due to the importance of the cloverleaf structure in replication, it is highly conserved in enteroviruses (Sharma et al., 2009). According to Pascal et al. (2020), a recent NMR/small-angle X-ray scattering (NMR/SAXS) determined the cloverleaf structure of rhinovirus, shows the established structural features of stem-loops b, c, d, and stem a similar to the features in the predicted structure in our results (Figure 4.2). Two of the most conserved elements, the three-string cytidine-rich region on stem-loop b and the three-pyrimidine mismatch in stem-loop d, are also conserved in the predicted structure of EV-A71 in this study (Pascal et al., 2020).

The cytidine-rich region of stem-loop b interacts with the heterogeneous nuclear ribonucleoprotein E (hnRNP E), also known as the cellular PCBP, an essential step in the formation of a complex that is crucial for circularization of the EV-A71 RNA genome during negative-strand synthesis (Dutkiewicz et al., 2016). Stem-loop d has a UUCG tetraloop, essential in stabilizing the loop structure and conferring conformational flexibility (Chen & Varani, 2001). According to Du et al. (2004), the consensus uUACGg tetraloop from different Enteroviruses results in structural rearrangements that yield features that work synergistically to enhance the binding affinity of the virus to nonstructural proteins 3C or 3CD. Additionally, stem-loop d interacts with 3CD precursor protein, interactions that are crucial for viral replication (Spear et al., 2015). Lastly, the specific sequence A-U pairs present on stem a are required to effectively synthesize plus strand RNA (Vogt & Andino, 2010). Downstream of domain I is a ten nucleotide C-rich region recognized by PCBP2 and essential for genome replication regulation (Mahmud et al., 2019). Overall, domain I is crucial for the replication of EVA71.

Domains II, IV, and V harbor important motifs crucial for the virus's life cycle. Domain II comprises a single hairpin loop with two internal loops, one asymmetrical and two symmetrical. It contains 68 nts spanning positions 111-179 of the EV-A71 genome. This study established the presence of a bulge with five nucleotides and a 5'-RY (U/A) CCA-3' conserved hairpin loop (Figure 4.3). Previous studies confirm that the NMR-determined structure of domain II of the EV-A71 genome has this five-nucleotide bulge as a structural motif that binds hnRNP A1 and AU-rich element RNA-binding factor 1 (AUF1) cellular proteins (Davila-Calderon et al., 2020; Tolbert et al., 2017). The hnRNP A1 protein also interacts with the hairpin conserved 5'-RY (U/A) CCA-3' loop to stimulate translation (Levengood et al., 2013). On the other hand, AUF1 counteracts the stimulatory activity of hnRNP A1 to ensure that translation meets replication needs of EV-A71 (Davila-Calderon et al., 2020). In this study, an additional internal loop was predicted in domain II that is not found in other Enterovirus domains. The significance of this extra internal loop remains undetermined. Domain III consists of 58 nts beginning at position 181-240 and consists of a stem-loop with three internal loops and a capping hairpin tetraloop (Figure 4.3). Domain III's functional relevance is uncertain.

In this study's model, domain IV is a complicated stem-loop with four hairpin loops and 220 nts of internal loops spanning positions 243-463 (Figure 4.3). According to Mahmud et al. (2019), domain IV of Enteroviruses is richly endowed with specific interaction sites for host ITAFs, which are vital for viral functional activities. Interaction of the polypyrimidine tract binding protein (PTB) with IRES's domain IV was demonstrated in a study on the regulation of EVA71 translation via PTB, a member of the hnRNP family (Xi et al., 2019). Domain IV includes two important motifs, a GNRA apical tetraloop and an internal C-rich loop (Martinez-Salas et al., 2018). In our model, the internal C-rich loop is at positions 336-338, and the GNRA apical tetraloop spans positions 344-347 (Figure 4.3). This study shows domain V as a hairpin loop with a bulge and two internal loops of 57 nts from 476-533. An additional hairpin loop with an internal loop and a bulge made of 24 nts from 534-558 was predicted close to domain V and, from previous models, could be considered as part of domain V (Yuan et al., 2018). Domain V contains a hairpin with an internal loop, the binding site for the initiation

factor eIF4G (de Breyne et al., 2009). In cap dependent translation, eukaryotic initiation factor 4F (eIF4F), which contains eIF4E (cap binding protein), eIF4G (scaffolding protein), and eIF4A (ATP dependent RNA helicase), binds to the cap to start the initiation process (Komar & Hatzoglou, 2011). In cap independent translation, the IRES's domain V is eIF4G's binding site, which recruits eIF4A to modify the IRES' conformation downstream toward its 3' borders (Su et al., 2018). Domain V has significant roles in virulence, canonical factor binding, and ribosome binding, therefore presenting as a potential therapeutic target (Mahmud et al., 2019).

Domain VI is one stem-loop with an internal loop containing 43 nts from position 580-623 (Figure 4.3). The single-stranded area between IRES domain V and VI harbors the Yn-Xm-AUG (Ym-pyrimidine rich, Xm- 15-25 nucleotide spacer followed by AUG) motif (Lai et al., 2020). The motif is an intrinsically disordered RNA region that can bind multiple proteins and is marked as important for ribosomal binding (Mahmud et al., 2019). In the model in this study, the non-functional AUG triplet is located at position 589-591 of domain VI.

The secondary structure prediction for EV-A71 3' UTR shows two conserved stem-loops, X and Y (Figure 4.1). The three putative stem-loop structures are significant in replication (Lai et al., 2020). Domain Z is only present in the enterovirus B-like subgroup (Merkle et al., 2002). Stem loops X and Y are highly conserved and consist of 8 and 12 base pairs, respectively, as predicted in this study (Zoll et al., 2009). Stem-loop X and Y base pair to form a kissing interaction essential for ligand recognition. Stem-loop X and Y regulate the synthesis of the negative RNA strand and are, therefore, vital for the EV-A71's life cycle (Merkle et al., 2002).

### **5.3 Tertiary structure modeling and evaluation**

The tertiary structure of EV-A71 5' UTR contains four-way and three-way junctions on domain I and IV, respectively. Domain one forms a four-way junction with stem a and stem loops b, c, and d. Several interactions occur within a four-way junction, including long-range, helix packing, base stacking, and internal base pair interactions (Laing &

Schlick, 2009). The NMR structure of rhinovirus 5' UTR depicts an A-form geometry for stem-loop d that reveals a highly accessible major groove (Pascal et al., 2020) which is also evident in the predicted EV-A71 structure. In this study's model, the major groove is found on stem-loop d (Figure 4.5). The three-way junction on domain IV is a hub for all the functional activities occurring in the domain as it contains the C-rich pyrimidine loop, the GNRA apical loop, and a bulge (Mahmud et al., 2019).

Junctions confer conformational and functional flexibility to the RNA (Chen & Varani, 2001). A predicted pseudoknot was observed in the IRES's ribosome-landing pad (RLP) in polioviruses as depicted in figure 4.6 (Le et al., 1992). This conserved tertiary structural element is formed because of base pairings between the highly conserved 17 to 21 single stranded nucleotide sequences on the 3' end of the IRES. Our model depicts the pseudoknot formed between domain V and domain VI (Figure 4.4). The 3' UTR also exhibits a pseudoknot-like tertiary structure between the loops of domains X and Y (Mirmomeni et al., 1997). This structure is crucial in amplifying viral RNA in infected cells (Jacobson et al., 1993). Additionally, the tertiary intramolecular kissing interaction that forms the Kissing domain (K domain) is crucial for ligand recognition and negative strand synthesis initiation (Merkle et al., 2002). WebRASP energy scores for the 3' and 5' UTRs are significantly low, with many contacts representing the atomic interactions, indicating structural stability as portrayed in table 1 (Norambuena et al., 2013).

#### **5.4 Motif identification**

The *de novo* prediction of motifs by the motif discovery algorithm on MEME suite resulted in five motifs for the 3' UTR and 12 for the 5' UTR. From the results obtained, motif 1 (GAAACYUAGWARCA), motif 2 (AUCAAUAG), motif 5 (AGCYAG UGGGUWG), motif 7 (AWGGWGAMAA), and motif 11 (UUWURUCUUSAU) are considered viable motifs based on the e-value (Appendice B). MEME suite's main motif attribute is the e-value which gives the statistical significance of a motif and is based on the log-likelihood ratio, width, sites, relative entropy, and information content. Additionally, the predicted motifs are highly conserved. Of the selected viable motifs predicted by MEME suite for the 5' UTR, two of the five motifs outlined in literature

were among the predicted motifs; the short stem-loop AUAGC motif on domain II which was predicted as motif 2 in position 127-134, and motif 5 which is present on domain V nucleotides as a hairpin with an internal loop in position 496-508 and interacts with translation initiation factors eIF4G and eIF4A for 48 ribosomal assembly (Lai et al., 2020). The GNRA motif on domain IV that comes after a C-rich internal loop was not predicted; however, it is present at positions 344-347.

Lastly, the predicted motif 7 on domain VI from positions 589-598 follows the Yn-Xm-AUG motif documented in literature, which starts from nucleotide 561-591 in this study's 5' UTR secondary structure. The Yn-Xm-AUG is presented as the entry site of the ribosome but not for translation 5' UTR (Lai et al., 2020). Motif 2 was also predicted to be present on an internal loop on domain III positions 192-199. The 3' UTR motif 1 (UGGKSGURAAUKUG) was the most significant motif. Motif 1 of the 3' UTR was predicted in two start positions, 33 and 52 is significant for forming a kissing domain crucial for EVA71 replication (Merkle et al., 2002). Polioviruses and group C human enteroviruses have a pyrimidine tandem base pair motif in the stem of domain Y. In contrast, other human enteroviruses' stem of domain Y comprises WC and G-U base pairs (Zoll et al., 2009). This is because the conservation of the stem loops' overall structures is only seen within enterovirus subgroups.

## **5.5 Molecular docking studies**

The PatchDock algorithm is geometry-based and explores docking transformation (Schneidman-Duhovny et al., 2005). The RMSD clustering employed serves to discard redundant solutions. ACE is the desolvation free energy required to move atoms from water to a protein interior (Zhang et al., 1997). To accomplish the transformation, ACE utilizes an adaptation method coined by Miyazawa and Jernigan, which provides estimates of observed contact energies of replacing residue-water with residue-residue interaction in a protein crystal structure database (Zhang et al., 1997). ACE is measured in kcal/mol (Raj et al., 2019). The lower the ACE value, the better the desolvation energy (Guo et al., 2012), hence the ease of insertion of a ligand small molecule at the docking site of the receptor molecule. This would represent the most stable and hence

favorable pose at the ligand site. In this study, the docked complexes with the lowest ACE were selected from a list of 20 top scores (Appendice F & G). The docking of the compounds on various motifs and regions of the 3' and 5' UTRs suggests their potential as drug leads.

Amantadine was one of the most significantly docked molecules, which belongs to the adamantane class of drugs. The US Food and Drug Administration (FDA) approved it in 1976 as a prophylactic agent for influenza A virus (Araujo et al., 2020). As an ion channel blocker, amantadine blocks the early stages of viral replication by inhibiting the M2 protein, preventing viral uncoating, and the assembly of progeny virions. Through chance, amantadine is currently used to treat Parkinson's disease by blocking dopamine reuptake into presynaptic neurons causing direct stimulation of postsynaptic receptors (Nisar et al., 2019). The pleiotropic nature of amantadine's mechanism of action also shows activity against IRES-mediated translation in Hepatitis A virus (Benschop et al., 2015). Chen et al. (2008) identified amantadine as an IRES inhibitor using a transfection assay targeting distinctively identifying compounds inhibiting cap independent translation mechanism. In this study, amantadine docked on domain V of the IRES position 507 of the 5'UTR with an ACE of -226.51 kcal/mol proposing a different mode of action (Figure 4.13). The position where amantadine docked was predicted as motif 5, a key motif in translation (Lai et al., 2020). Additionally, amantadine has been shown to inhibit replication in Echovirus-5, Echovirus-18, and EVA71 (Benschop et al., 2015). This study corroborates the activity of amantadine against EVA71. It suggests inhibition of translation as the mechanism of antiviral action against this virus due to binding to the virus's domain V 5' untranslated region (UTR). Amantadine also docked on the 3'UTR at motif 1, which starts at 33 to 46, indicating its potential to inhibit replication.

The molecule ribavirin was discovered to dock tightly onto the 3' UTR of EVA71, which was a curious and fortuitous discovery. Ribavirin is a synthetic guanosine analog with varying mechanisms of action. It is clinically used in the treatment of Hepatitis C virus (HCV), Respiratory syncytial virus (RSV), and several hemorrhagic fever viruses (Beaucourt & Vignuzzi, 2014). There are five proposed modes of action for ribavirin



that entail direct or indirect effects on the virus. The proposed indirect mechanisms include the inhibition of inosine monophosphate dehydrogenase, which decreases intracellular guanosine triphosphate, and the immunomodulatory effect of unphosphorylated ribavirin, which results in enhanced type 1 T-helper cells. The direct mechanism of action includes interfering with RNA capping by mimicking 7-methyl guanosine, mutagenizing the genome by misincorporating ribavirin, and inhibiting the RdRp. Previous studies have shown that ribavirin can inhibit replication in EV-A71 (Benschop et al., 2015). In this study, ribavirin docked on the 3' UTR region motif 1, which forms a binding pocket with an ACE of -251.84 kcal/mol, confirming its potential activity at inhibiting replication in EV-A71 (Figure 4.10).

In this study, several flavonoids were shown to dock with high affinities to the 3' and 5' UTR domains of EV-A71. Flavonoids are natural polyphenolic secondary metabolites with proven antiviral properties (Panche et al., 2016; Ullah et al., 2020). Antioxidant, anticancer, antimicrobial, immunomodulatory, and antioxidant activities are common flavonoid properties. Flavonoids demonstrate the ability to disrupt viral replication and translation processes (Lalani & Poh, 2020). The antiviral activity of the flavonoids baicalin, ursolic acid, dihydromyricetin, 7-hydroxy isoflavone, diosmetin, formononetin, kaempferol, morin hydrate, myricetin, nobiletin, and taxifolin was investigated in the current study. According to previous reports (Badshah et al., 2021; Chiang et al., 2005; Li et al., 2015; Tsai et al., 2011; Li et al., 2017; Wang et al., 2013; Wang et al., 2015), four of the eleven selected flavonoids, namely baicalin, formononetin, kaempferol, and hydroxysioflavones and their derivatives, target EV-A71 via known mechanisms of action. This study confirms the potential use of these and other flavonoids as drugs through a mechanism that targets the untranslated regions of the EV-A71 genome and is discussed below.

Baicalin docked on domain II of the IRES at motif 1 (AGCYAGUGGGUWG), position 113 to 116, with an ACE of -472.39 kcal/mol (Figure 4.15). Baicalin is 5,6-dihydroxy-7-O-glucuronide flavone glycoside obtained from the skullcap plants belonging to the genus *Scutellaria*. Baicalin exhibits antiviral, antibacterial, anti-inflammatory, and

immunomodulatory activities. Several studies show the inhibitive action of baicalin on the influenza A virus, human immunodeficiency virus (HIV), dengue virus, and hepatitis B virus (HBV) (Li et al., 2021; Li et al., 2015). The proposed mode of action of baicalin on EV-A71 is through inhibition of the 3D polymerase and interference with the Fas/FasL apoptosis regulation signaling pathways (Li et al., 2015). According to Badshah et al. (2021), baicalin also inhibits protein translation in enteroviruses. In addition, this study has shown that baicalin docked on domain II of the IRES at motif 1 with high affinity, demonstrating a different mechanism of action against these viruses. Domain II of the IRES contains structural motifs that bind proteins in the cell, such as hnRNP A1 and AUF1, which are crucial for translation (Davila-Calderon et al., 2020; Tolbert et al., 2017). The binding of baicalin on motif 1 of domain II shows its potential to inhibit translation.

Formononetin showed the potential of inhibiting the 5' UTR by binding on domain II position 124 of the IRES with high affinity. Formononetin is an O-methylated isoflavone with anti-inflammatory, antitumor, and antioxidant properties. Several studies show the antiviral properties of formononetin (Li et al., 2017). Wang et al. (2015) conducted a study that explored the mechanism of action of formononetin against EVA71. In the study, the researchers proved that formononetin could inhibit EV-A71-induced cytopathic effect by suppressing the activation of extracellular signal-regulated kinase (ERK), p38, and c-Jun N-terminal kinase (JNK) signal pathways (Wang et al., 2015). However, in this study, formononetin showed the potential of inhibiting the 5' UTR by binding on domain II position 124 of the IRES with an ACE of -273.30 kcal/mol, suggesting a different mode of action and its potential in inactivating translation (Appendice H).

Kaempferol bound with high affinity to the stem-loop motif 1 of the 3' UTR. Kaempferol is a natural flavonol found in plants such as broccoli and kale. Kaempferol interferes with viral replication and inhibits IRES activity of the 5' UTR of EVA71 (Badshah et al., 2021). Tsai et al. (2011) noted the antiviral activity of kaempferol using rhabdomyosarcoma cells infected with EV-A71, which exhibited up to 80% cell survival

hence inhibition of viral infection. The postulated mechanism of action was that Kaempferol interfered with the IRES transacting factors hnRNP and far upstream element binding (FUBP) proteins which then affected viral cap independent translation (Tsai et al., 2011). Kaempferol binds on the stem-loop motif 1 of the 3' UTR with an ACE of -294.26 kcal/mol, proposing that it can directly interrupt viral replication (Appendice I).

7-hydroxy isoflavone bound with high affinity to motif 1 of the 3'UTR of EV-A71. 7-hydroxy isoflavone is an isoflavone with a hydroxyl group at position seven and has *in vitro* antiviral activity against EV-A71. Wang et al. (2013) demonstrated 7-hydroxyisoflavones' activity against EV-A71. Although the study did not elaborate on the exact mechanism, the suggested mechanism of action is the inhibition of early stages of replication (Wang et al., 2013). In this study, 7-hydroxy isoflavone binds at motif 1 of the 3'UTR of EV-A71 with an ACE of -266.51 kcal/mol, potentially inhibiting viral replication (Appendice I).

Similarly to 7-hydroxy isoflavone, ursolic acid docked at motif 1 of the 3' UTR of EV-A71 but with a significantly higher affinity. Ursolic acid is a pentacyclic triterpene found in various fruits and vegetables. According to Chiang et al. (2005), ursolic acid exhibited strong antiviral activity against EV-A71, herpes simplex virus 1 (HSV-1), and Coxsackievirus B1 (CVB1). It was found that the action of ursolic acid on CVB1 and EV-A71 was during the replication phase and infection process (Chiang et al., 2005). Similar to 7-hydroxy isoflavone, ursolic acid also docked at motif 1 of the 3' UTR of EV-A71 but with a lower ACE of -445.52 kcal/mol (Figure 4.11).

Little evidence has been presented on the antiviral activities of diosmetin, morin hydrate, dihydromyricetin, myricetin, nobiletin, and taxifolin against EV-A71. However, this study presents the potential use of the flavonoids mentioned above as drug targets for EV-A71. Morin hydrate and myricetin bound to motif 5 (AGCYAGUGGGUWG) position 507 of domain V with ACE of -339.64 kcal/mol and -362.84 kcal/mol, respectively (Appendice H). Dihydromyricetin is a flavonol, while taxifolin, also known

as dihydroquercetin, is a flavanone with anti-inflammatory and antiviral properties. In this study, compounds bound to the pocket with motif 1 on domain II of the IRES (positions 113-116 and 171-173) recorded ACE of -313.37 kcal/mol and -263.92 kcal/mol, respectively indicating its potential at inhibiting viral replication (Appendice H).

Nobiletin and diosmetin bound to domain IV of the IRES between positions 181 and 211 with the ACE -496.03 kcal/mol and -394.16 kcal/mol, respectively (Appendice H). The docking of these compounds presents an alternative mode of action for antiviruses and highlights the potential drug targets. Motif 1 and 5 are significant potential drug targets for the 5' UTR while motif 1 is the main potential drug target for the 3' UTR of EV-A71. As elucidated by the results, domains II, IV, and V of the IRES, 5' UTR, and domain Y of the 3' UTR are the most potential drug targets. The compounds that registered the lowest ACE values, namely ursolic acid, nobiletin, diosmetin, and baicalin, show potential for further experimental validation.

## CHAPTER SIX: 6.0 CONCLUSION

This study's findings have allowed for the formulation of the following conclusions:

- 1) UTRs are essential for the life cycle of EV-A71 therefore determination of the 3D RNA structure of the 3' and 5' UTRs of EV-A71 UTRs enabled the identification of potential drug targets.
- 2) The 3' and 5' UTR identified motifs play vital roles in driving the viral cycle of EV-A71, and can therefore serve as potential drug targets.
- 3) The identified compounds (ursolic acid, nobiletin, diosmetin, and baicalin) with the lowest ACE that docked on the 3' and 5' UTRs can be used as potential drug targets during the development of EVA71-targeting drugs.

### 6.1 LIMITATIONS

This study had one major limitation;

- 1) The identification of supporting literature to demonstrate the potential of identified regulatory motifs for the 3' UTR as drug targets proved challenging.

### 6.2 RECOMMENDATIONS

The current study recommends the following:

- 1) Additional research should be conducted on the structural features of UTRs to facilitate the identification of novel drug targets.
- 2) It is necessary to perform *in vivo* experimental validation of identified motifs to confirm their potential as novel EV-A71 drug targets.
- 3) Molecular dynamics simulations should be utilized to validate the docked molecules.

## REFERENCES

- Adelusi, T. I., Oyedele, A.-Q. K., Boyenle, I. D., Ogunlana, A. T., Adeyemi, R. O., Ukachi, C. D., Idris, M. O., Olaoba, O. T., Adedotun, I. O., Kolawole, O. E., Xiaoxing, Y., & Abdul-Hammed, M. (2022). Molecular modeling in drug discovery. *Informatics in Medicine Unlocked*, 29, 100880. doi:10.1016/j.imu.2022.100880
- Almakarem, A., Petrov, A., Stombaugh, J., Zirbel, C., & Leontis, N. (2012). A comprehensive survey and geometric classification of base triples in RNA structures. *Nucleic acids research*, 40(4), 1407-1423. doi:10.1093/nar/gkr810
- Andrews, R., Peterson, J., Haniff, H., Chen, J., Williams, C., Grefe, M., . . . Moss, W. (2020). An in silico map of the SARS-CoV-2 RNA Structurome. *BioRxiv*, 1. doi:10.1101/2020.04.17.045161
- Andrews, R., Roche, J., & Moss, W. (2018). ScanFold: an approach for genome-wide discovery of local RNA structural elements—applications to Zika virus and HIV. *PeerJ*. doi:10.7717/peerj.6136
- Ao, D., Sun, S.-Q., & Guo, H.-C. (2014). Topology and biological function of enterovirus non-structural protein 2B as a member of the viroporin family. *Veterinary Research*, 1, 1-9. doi:10.1186/s13567-014-0087-6
- Araújo, R., Aranda-Martínez, J., & Aranda-Abreuc, G. (2020). Amantadine Treatment for People with COVID-19. *Archives of Medical Research*, 51(7), 739-740. doi:10.1016/j.arcmed.2020.06.009
- Badshah, S., Faisal, S., Muhammad, A., Poulson, B., Emwas, A., & Jaremko, M. (2021). Antiviral activities of flavonoids. *Biomedicine & Pharmacotherapy*, 140. doi:10.1016/j.biopha.2021.111596
- Bailey, T., & Elkan, C. (1994). Fitting a mixture model by expectation maximization to discover motifs in biopolymers. *Proceedings of the Second International Conference on Intelligent Systems for Molecular Biology* (pp. 28-36). Menlo Park, California: AAAI Press.
- Bailey, T. L., Johnson, J., Grant, C. E., & Noble, W. S. (2015). The MEME Suite. *Nucleic Acids Research*, 43(W1), W39–W49. https://doi.org/10.1093/nar/gkv416
- Barton, D., Donnell, B., & Flanagan, J. (2001). 5' Cloverleaf in poliovirus RNA is a cis-acting replication element required for negative-strand synthesis. *EMBO Journal*, 20(6), 1439–1448. doi:10.1093/emboj/20.6.1439
- Bauer, L., Manganaro, R., Zonsics, B., Hurdiss, D., Zwaagstra, M., Donselaar, T., & van Kuppeveld, F. (2020). Rational design of highly potent broad-spectrum enterovirus inhibitors targeting the nonstructural protein 2C. *PLoS biology*, 18(11), e3000904. doi:10.1371/journal.pbio.3000904
- Baulin, E. (2021). Features and Functions of the A-Minor Motif, the Most Common Motif in RNA Structure. *Biochemistry (Moscow)*, 86(8), 952-961. doi:10.1134/S000629792108006X
- Beaucourt, S., & Vignuzzi, M. (2014). Ribavirin: a drug active against many viruses with multiple effects on virus replication and propagation. Molecular basis of ribavirin resistance. *Current Opinion in Virology*, 8, 10-15. doi:10.1016/j.coviro.2014.04.011
- Benschop, K., Avoort, H., Duizer, E., & Koopmans, M. (2015). Antivirals against enteroviruses: a critical review from a public health perspective. *Antiviral Therapy*, 20(2), 121-130. doi:10.3851/IMP2939

- Bessaud, M., Razafindratsimandresy, R., Nougairède, A., Joffret, M.-L., Deshpande, J., Dubot-Pères, A., & Bailly, J.-L. (2014). Molecular Comparison and Evolutionary Analyses of VP1 Nucleotide Sequences of New African Human Enterovirus 71 Isolates Reveal a Wide Genetic Diversity. *Plos One*, *9*(3), e90624. doi:10.1371/journal.pone.0090624
- Biesiada, M., Purzycka, K., Szachniuk, M., Blazewicz, J., & Adamiak, R. (2016). Automated RNA 3D Structure Prediction with RNAComposer. *Methods in Molecular Biology*, 199-215. doi:10.1007/978-1-4939-6433-8\_13
- Blouin, S., & Lafontaine, D. (2007). A loop-loop interaction and a K-turn motif located in the lysine aptamer domain are important for the riboswitch gene regulation control. *RNA*, *13*(8), 1256–1267. doi:10.1261/rna.560307
- Bouchard, P., & Legault, P. (2014). A remarkably stable kissing-loop interaction defines substrate recognition by the *Neurospora* Varkud Satellite ribozyme. *RNA*, *20*(9), 1451–1464. doi:10.1261/rna.046144.114
- Brierley, I., Pennell, S., & Gilbert, R. (2007). Viral RNA pseudoknots: versatile motifs in gene expression and replication. *Nature Reviews Microbiology*, *5*(8), 598-610. doi:10.1038/nrmicro1704
- Cao, S., & Chen, S.-J. (2011). Structure and stability of RNA/RNA kissing complex: with application to HIV dimerization initiation signal. *RNA*, *17*(12), 2130–2143. doi:10.1261/rna.026658.111
- Carmona, R., Machado, B., Reis, F., Jorge, A., Cilli, A., Dias, A., & Timenetsky, M. (2022). Hand, foot, and mouth disease outbreak by Coxsackievirus A6 during COVID-19 pandemic in 2021, São Paulo, Brazil. *Journal of Clinical Virology*, *154*, 105245. doi:10.1016/j.jcv.2022.105245
- Cate, J., Gooding, A., Podell, E., Zhou, K., Golden, B., Szewczak, A., & Doudna, J. (1996). RNA tertiary structure mediation by adenosine platforms. *Science*, *273*(5282), 1696-1699. doi:10.1126/science.273.5282.1696.
- Cathcart, A., Baggs, E., & Semler, B. (2014). Picornaviruses: Pathogenesis and Molecular Biology. *Reference Module in Biomedical Research*, *3*, 1-11. doi:http://dx.doi.org/10.1016/B978-0-12-801238-3.00272-5
- Chamond, N., Deforges, J., Ulryck, N., & Sargueil, B. (2014). 40S recruitment in the absence of eIF4G/4A by EMCV IRES refines the model for translation initiation on the archetype of Type II IRESs. *Nucleic Acids Research*, *42*(16), 10373–10384. doi:10.1093/nar/gku720
- Chang, C.-S., Liao, C.-C., Liou, A.-T., Chang, Y.-S., Chang, Y.-T., Tzeng, B.-H., . . . Shih, C. (2019). Enterovirus 71 targets the cardiopulmonary system in a robust oral infection mouse model. *Scientific Reports*, *9*(1), 1-15. doi:10.1038/s41598-019-47455-3
- Chen, Y., & Varani, G. (2001). RNA Structure. *Encyclopedia of Life Sciences*, 1-9. doi:10.1002/9780470015902.a0001339.pub2
- Chen, C., Wang, Y., Shan, C., Sun, Y., Xu, P., Zhou, H., & Lou, Z. (2013). Crystal Structure of Enterovirus 71 RNA-Dependent RNA Polymerase Complexed with Its Protein Primer VPg: Implication for a trans Mechanism of VPg Uridylylation. *Journal of Virology*, *87*(10), 5755–5768. doi:10.1128/JVI.02733-12
- Chen, J.-H., Zhang, R.-H., Lin, S.-L., Li, P.-F., Lan, J.-J., Song, S.-S., & Jiang, S.-J. (2018). The Functional Role of the 3' Untranslated Region and Poly(A) Tail of Duck Hepatitis A Virus Type 1 in Viral Replication and Regulation of IRES-

- Mediated Translation. *Frontiers in Microbiology*, 2250. doi:10.3389/fmicb.2018.02250
- Chen, T., Grauffel, C., Yang, W.-Z., Chen, Y.-P., Yuan, H., & Lim, C. (2022). Efficient Strategy to Design Protease Inhibitors: Application to Enterovirus 71 2A Protease. *ACS Bio & Med Chem Au*, 1-13. doi:10.1021/acsbiochemau.2c00001
- Chen, Y.-j., Zeng, S.-j., Hsu, J., Horng, J.-t., Yang, H.-m., Shih, S.-r., & Wu, T.-y. (2008). Amantadine as a regulator of internal ribosome entry site. *Acta Pharmacologica Sinica*, 29(11), 1327-1333. doi:10.1111/j.1745-7254.2008.00876.x
- Chakraborty, R., Iturriza-Gómara, M., Musoke, R., Palakudy, T., D'Agostino, A., & Gray, J. (2004). An epidemic of enterovirus 71 infection among HIV-1-infected orphans in Nairobi. *Aids*, 18(14), 1968-1970.
- Chiang, L.-C., Ng, L.-T., Cheng, P.-W., Chiang, W., & Lin, C.-C. (2005). Antiviral Activities Of Extracts And Selected Pure Constituents of Ocimum Basilicum. *Clinical and Experimental Pharmacology and Physiology*, 32, 811-816. doi:10.1111/j.1440-1681.2005.04270.x
- Chojnowski, G., Zaborowski, R., Magnus, M., & Bujnicki, J. (2021). RNA fragment assembly with experimental restraints. *bioRxiv*. doi:10.1101/2021.02.08.430198
- Chordia, N., & Kumar, A. (2019). RNA as a Drug Target and its Tools and Databases. *Journal of Biotechnology and Biomedicine*, 2, 009-014.
- Cordey, S., Gerlach, D., Junier, T., Zdobnov, E., Kaiser, L., & Tapparel, C. (2008). The cis-acting replication elements define human enterovirus and rhinovirus species. *RNA*, 14(8), 1568-1578. doi:10.1261/rna.1031408
- Crowther, C., Jones, L., Morelli, J., Mastrogiacomo, E., Porterfield, C., Kent, J., & Serra, M. (2017). Influence of two bulge loops on the stability of RNA duplexes. *RNA*, 23(2), 217-228. doi:10.1261/rna.056168.116
- D'Ascenzo, L., Vicens, Q., & Auffinger, P. (2018). Identification of receptors for UNCG and GNRA Z-turns and their occurrence in rRNA. *Nucleic Acids Research*, 46(15), 7989-7997. doi:10.1093/nar/gky578
- D'Ascenzo, L., Leonarski, F., Vicens, Q., & Auffinger, P. (2017). Revisiting GNRA and UNCG folds: U-turns versus Z-turns in RNA hairpin loops. *RNA*, 23(3), 259-269. doi:10.1261/rna.059097.116
- Davila-Calderon, J., Patwardhan, N., Chiu, L.-Y., Sugarman, A., Cai, Z., Penutmutchu, S., & Tolbert, B. (2020). IRES-targeting small molecule inhibits enterovirus 71 replication via allosteric stabilization of a ternary complex. *Nature communications*, 11(1), 1-13. doi:10.1038/s41467-020-18594-3
- de Breyne, S., Yu, Y., Unbehaun, A., Pestova, T., & Hellen, C. (2009). Direct functional interaction of initiation factor eIF4G with type 1 internal ribosomal entry sites. *Proceedings of the National Academy of Sciences*, 106(23), 9197-9202. doi:10.1073/pnas.090015310
- Drysdale, M., Lentzen, G., Matassova, N., Murchie, A., Aboul-Ela, F., & Afshar, M. (2002). 2 RNA as a Drug Target. *Progress in medicinal chemistry*, 39, 73-119. doi:10.1016/s0079-6468(08)70069-9
- Du, Z., Yu, J., Ulyanov, N., Andino, R., & James, T. (2004). Solution Structure of a Consensus Stem-Loop D RNA Domain that Plays Important Roles in Regulating



- Translation and Replication in Enteroviruses and Rhinoviruses. *Biochemistry*, *43*, 11959-11972. doi:10.1021/bi048973p
- Dutkiewicz, M., Stachowiak, A., Swiatkowska, A., & Ciesiołka, J. (2016). Structure and function of RNA elements present in enteroviral genomes. *Acta Biochimica Polonica*, *63*(4), 623-630. doi:10.18388/abp.2016\_1337
- Ennifar, E., Walter, P., Ehresmann, B., Ehresmann, C., & Dumas, P. (2001). Crystal structures of coaxially stacked kissing complexes of the HIV-1 RNA dimerization initiation site. *Nature Structural Biology*, *8*, 1064-1068. doi:10.1038/nsb727
- Fallmann, J., Will, S., Engelhardt, J., Grüning, B., Backofen, R., & Stadler, P. F. (2017). Recent advances in RNA folding. *Journal of Biotechnology*, *261*, 97-104. doi:10.1016/j.jbiotec.2017.07.007
- Feng, Q., Langereis, M., Lork, M., Nguyen, M., Hato, S., Lanke, K., & van Kuppeveld, F. (2014). Enterovirus 2Apro Targets MDA5 and MAVS in Infected Cells. *Journal of Virology*, *88*(6), 3369–3378. doi:10.1128/JVI.02712-13
- Fernandez-Garcia, M., Volle, R., Joffret, M.-L., Sadeuh-Mba, S., Gouandjika-Vasilache, I., Kebe, O., & Bessaud, M. (2018). Genetic Characterization of Enterovirus A71 Circulating in Africa. *Emerging infectious diseases*, *24*(4), 754-757. doi:10.3201/eid2404.171783
- Firdaus-Raih, M., Harrison, A.-M., Willett, P., & Artymiuk, P. (2011). Novel base triples in RNA structures revealed by graph theoretical searching methods. *BMC Bioinformatics*, *12*(S2). doi:10.1186/1471-2105-12-S13-S2
- Fu, L., Cao, Y., Wu, J., Peng, Q., Nie, Q., & Xie, X. (2022). Ufold: fast and accurate RNA secondary structure prediction with deep learning. *Nucleic Acids Research*, *50*(3), e14. doi:10.1093/nar/gkab1074
- Garst, A., Edwards, A., & Batey, R. (2011). Riboswitches: Structures and Mechanisms. *Cold Spring Harbour Perspectives in Biology*, *3*(6), a003533. doi:10.1101/cshperspect.a003533
- Ge, Q., Ilves, H., Dallas, A., Kumar, P., Shorestein, J., Kazakov, S., & Johnston, B. (2010). Minimal-length short hairpin RNAs: The relationship of structure and RNAi activity. *RNA*, *16*(1), 106–117. doi:10.1261/rna.1894510
- Grover, N. (Ed.). (2022). *Fundamentals of RNA Structure and Function*. Colorado, USA.
- Gruyter, D. (2013). *RNA Structure and Folding: Biophysical Techniques and Prediction Methods*. (D. Klostermeier, & C. Hammann, Eds.) Germany: Hubert & Co. GmbH & Co. KG, Göttingen. doi:10.1515/9783110284959
- Guan, H., Tian, J., Qin, B., Wojdyla, J., Wang, B., Zhao, Z., & Cui, S. (2017). Crystal structure of 2C helicase from enterovirus 71. *Science advances*, *3*(4), e1602573. doi:10.1126/sciadv.1602573
- Guo, F., Li, S., Wang, L., & Zhu, D. (2012). Protein-protein binding site identification by enumerating the configurations. *BMC Bioinformatics*, *13*, 158. doi:10.1186/1471-2105-13-158
- Hao, P., Yu, J., Ward, R., Liu, Y., Hao, Q., An, S., & Xu, T. (2020). Eukaryotic translation initiation factors as promising targets in cancer therapy targets in cancer therapy. *Cell Communication and Signaling*, *18*(1), 1-20. doi:10.1186/s12964-020-00607-9

- He, X., Zhang, M., Zhao, C., Zheng, P., Zhang, X., & Xu, J. (2021). From Monovalent to Multivalent Vaccines, the Exploration for Potential Preventive Strategies Against Hand, Foot, and Mouth Disease (HFMD). *Virologica Sinica*, 36(2), 167-175. doi:10.1007/s12250-020-00294-3
- Hellen, C. (2018). Translation Termination and Ribosome Recycling in Eukaryotes. *Cold Spring Harbor Perspectives in Biology*, 10(10), a032656. doi:10.1101/cshperspect.a032656
- Hermann, T. (2016). Small molecules targeting viral RNA. *Wiley Interdisciplinary Reviews: RNA*, 7(6), 726-743. doi:10.1002/wrna.1373
- Herold, J., & Andino, R. (2001). Poliovirus RNA replication requires genome circularization through a protein-protein bridge. *Molecular cell*, 7(3), 589-591. doi:10.1016/s1097-2765(01)00205-2
- Huang, L., & Lilley, D. (2016). The Kink Turn, a Key Architectural Element in RNA Structure. *Journal of Molecular Biology*, 428(5Part A), 790–801. doi:10.1016/j.jmb.2015.09.026
- Hughes, J., Rees, S., Kalindjian, S., & Philpott, K. (2011). Principles of early drug discovery: Principles of early drug discovery. *British Journal of Pharmacology*, 162(6), 1239–1249. <https://doi.org/10.1111/j.1476-5381.2010.01127.x>
- Hung, C.-T., Kung, Y.-A., Li, M.-L., Brewer, G., Lee, K.-M., Liu, S.-T., & Shih, S.-R. (2016). Additive Promotion of Viral Internal Ribosome Entry Site-Mediated Translation by Far Upstream Element-Binding Protein 1 and an Enterovirus 71-Induced Cleavage Product. *PLoS pathogens*, 12(10), e1005959.
- Jackson, R., Hellen, C., & Pestova, T. (2010). The mechanism of eukaryotic translation initiation and principles of its regulation. *Nature Reviews Molecular cell biology*, 11(2), 113-127.
- Jackson, T., & Belsham, G. (2021). Picornaviruses: A View from 3A. *Viruses*, 13(3), 456. doi:10.3390/v13030456
- Jacobson, S., Konings, D., & Sarnow, P. (1993). Biochemical and genetic evidence for a pseudoknot structure at the 3' terminus of the poliovirus RNA genome and its role in viral RNA amplification. *Journal of Virology*, 67(6), 2961-2971. doi:10.1128/JVI.67.6.2961-2971.1993
- Jiang, H., Weng, L., Zhang, N., Arita, M., Li, R., Chen, L., & Toyoda, T. (2011). Biochemical characterization of enterovirus 71 3D RNA polymerase. *Biochimica et Biophysica Acta (BBA)-Gene Regulatory Mechanisms*, 1809(3), 211-219. doi:10.1016/j.bbagr.2011.01.001
- Jing, L., Feng, G., Bin, H., Dong, C., Qiang, Z., Bin, L., & Ling, W. (2017). Contribution of 3CD Region to the Virulence of Enterovirus 71. *Biomedical and Environmental Sciences*, 30(10), 767-771. doi:10.3967/bes2017.103
- Kafasla, P., Morgner, N., Pöyry, T., Curry, S., Robinson, C., & Jackson, R. (2009). Polypyrimidine Tract Binding Protein Stabilizes the Encephalomyocarditis Virus IRES Structure via Binding Multiple Sites in a Unique Orientation. *Molecular Cell*, 34(5), 556-568. doi:10.1016/j.molcel.2009.04.015
- Kapp, L., & Lorsch, J. (2004). The molecular mechanics of eukaryotic translation. *Annual review of biochemistry*, 73, 657-704. doi:10.1146/annurev.biochem.73.030403.080419

- Kiliszek, A., Błaszczyk, L., Kierzek, R., & Rypniewski, W. (2017). Stabilization of RNA hairpins using non-nucleotide linkers and circularization. *Nucleic Acids Research*, *45*(10), e92. doi:10.1093/nar/gkx122
- Kim, H.-J., Lee, H.-R., Seo, J.-Y., Ryu, H., Lee, K.-H., Kim, D.-Y., & Kim, K.-T. (2017). Heterogeneous nuclear ribonucleoprotein A1 regulates rhythmic synthesis of mouse Nfil3 protein via IRES-mediated translation. *Scientific Reports*, *7*(1), 1-15. doi: 10.1038/srep42882
- Klein, D., Schmeing, T., Moore, P., & Steitz, T. (2001). The kink-turn: a new RNA secondary structure motif. *The EMBO journal*, *20*(15), 4214-4221. doi:10.1093/emboj/20.15.4214
- Komar, A., & Hatzoglou, M. (2011). Cellular IRES-mediated translation: the war of ITAFs in pathophysiological states. *Cell cycle*, *10*(2), 229-240. doi:10.4161/cc.10.2.14472
- Lai, M.-C., Chen, H.-H., Xu, P., & Wang, R. (2020). Translation control of Enterovirus A71 gene expression. *Journal of Biomedical Science*, *27*(1), 1-9. doi:10.1186/s12929-019-0607-9
- Laing, C., & Schlick, T. (2009). Analysis of four-way junctions in RNA structures. *Journal of Molecular Biology*, *390*(3), 547–559. doi:10.1016/j.jmb.2009.04.084
- Lalani, S., & Poh, C. (2020). Flavonoids as Antiviral Agents for Enterovirus A71 (EV-A71). *Viruses*, *12*(2), 184. doi:10.3390/v12020184
- Le, S.-Y., Chen, J.-H., Sonenberg, N., & Maizel, J. (1992). Conserved tertiary structure elements in the 5' untranslated region of human enteroviruses and rhinoviruses. *Virology*, *191*(2), 858-866. doi:10.1016/0042-6822(92)90261-M
- Lei, X., Liu, X., Ma, Y., Sun, Z., Yang, Y., Jin, Q., & Wang, J. (2010). The 3C Protein of Enterovirus 71 Inhibits Retinoid Acid-Inducible Gene I-Mediated Interferon Regulatory Factor 3 Activation and Type I Interferon Responses. *Journal of Virology*, *84*(16), 8051-8061. doi:10.1128/JVI.02491-09
- Leontis, N., & Westhof, E. (2001). Geometric nomenclature and classification of RNA base pairs. *RNA*, *7*(4), 499-512.
- Levengood, J., Tolbert, M., Li, M.-L., & Tolbert, B. (2013). High-affinity interaction of hnRNP A1 with conserved RNA structural elements is required for translation and replication of enterovirus 71. *RNA Biology*, *10*(7), 1136–1145. doi:10.4161/rna.25107
- Y., Zhou, Y., Cheng, Y., Wu, P., Zhou, C., Cui, P., & Yu, H. (2019). Effectiveness of EV-A71 vaccination in prevention of pediatric hand, foot, and mouth disease associated with EV-A71 virus infection requiring hospitalization in Henan, China, 2017-18: a test-negative case-control study. *The Lancet Child & Adolescent Health*, *3*(10), 697-704. doi:10.1016/S2352-4642(19)30185-3
- Li, B., Cao, Y., Westhof, E., & Miao, Z. (2020). Advances in RNA 3D Structure Modeling Using Experimental Data. *Frontiers in genetics*, *11*, 574485. doi:10.3389/fgene.2020.574485
- Li, G., Gao, Q., Yuan, S., Wang, L., Altmeyer, R., Lan, K., & Zou, G. (2017). Characterization of three small molecule inhibitors of enterovirus 71 identified from screening of a library of natural products. *Antiviral Research*, *143*, 85-96. doi:10.1016/j.antiviral.2017.04.006
- Li, H., Li, W., Zhang, S., Qiu, M., Li, Z., Lin, Y., & Qiao, W. (2022). Enterovirus 71 Activates GADD34 via Precursor 3CD to Promote IRES-Mediated Viral

- Translation. *Microbiology spectrum*, 10(1), pp.e01388-21. doi:10.1128/spectrum.01388-21
- Li, H., Zhu, D., Zhang, C., Han, H., & Crandall, K. (2014). Characteristics and Prediction of RNA Structure. *BioMed research international*. doi: 10.1155/2014/690340
- Li, K., Liang, Y., Cheng, A., Wang, Q., Li, Y., Wei, H., & Wan, X. (2021). Antiviral Properties of Baicalin: a Concise Review. *Revista Brasileira de Farmacognosia*, 31(4), 408-419. doi:10.1007/s43450-021-00182-1
- Li, P., Bustamante, C., & Jr., I. (2006). Unusual mechanical stability of a minimal RNA kissing complex. *Proceedings of the National Academy of Sciences*, 103(43), 15847-15852. doi:10.1073/pnas.060720210
- Li, Q., Zheng, Z., Liu, Y., Zhang, Z., Liu, Q., Meng, J., & Wang, H. (2016). 2C Proteins of Enteroviruses Suppress IKK $\beta$  Phosphorylation by Recruiting Protein Phosphatase 1. *Journal of Virology*, 90(10), 5141-5151. doi:10.1128/JVI.03021-15
- Li, X., Liu, Y., Wu, T., Jin, Y., Cheng, J., Wan, C., & Shi, W. (2015). The Antiviral Effect of Baicalin on Enterovirus 71 In Vitro. *Viruses*, 7(8), 4756–4771. doi:10.3390/v7082841
- Li, X., Wang, M., Cheng, A., Wen, X., Ou, X., Mao, S., & Chen, X. (2020). Enterovirus Replication Organelles and Inhibitors of Their Formation. *Frontiers in Microbiology*, 11, 1817. doi:10.3389/fmicb.2020.01817
- Li, Z., Wu, Y., Li, H., Li, W., Tan, J., & Qiao, W. (2021). 3C protease of enterovirus 71 cleaves promyelocytic leukemia protein and impairs PML-NBs production. *Virology Journal*, 18(255). doi:10.1186/s12985-021-01725-7
- Li, Z., Zou, Z., Jiang, Z., Huang, X., & Liu, Q. (2019). Biological Function and Application of Picornaviral 2B Protein: A New Target for Antiviral Drug Development. *Viruses*, 11(6), 510. doi:10.3390/v11060510
- Lisi, V., & Major, F. (2007). A comparative analysis of the triloops in all high-resolution RNA structures reveals sequence–structure relationships. *RNA*, 13(9), 1537–1545. doi:10.1261/rna.597507
- Liu, M.-L., Lee, Y.-P., Wang, Y.-F., Lei, H.-Y., Liu, C.-C., Wang, S.-M., & Yu, C.-K. (2005). Type 1 interferons protect mice against enterovirus 71 infection. *General Virology*, 86, 3263-3269. *Journal of General Virology*, 86(12), 3263-3269. doi:10.1099/vir.0.81195-0
- Liu, Y., Zheng, Z., Shu, B., Meng, J., Zhang, Y., Zheng, C., & Wang, H. (2016). SUMO Modification Stabilizes Enterovirus 71 Polymerase 3D To Facilitate Viral Replication. *Journal of Virology*, 90(23), 10472–10485. doi:10.1128/JVI.01756-16
- Lloyd, R. (2016). Enterovirus Control of Translation and RNA Granule Stress Responses. *Viruses*, 8(4), 93. doi:10.3390/v8040093
- Lu, J.-Y., Brewer, G., Li, M.-L., Lin, K.-Z., Huang, C.-C., Yen, L.-C., & Lin, J.-Y. (2021). Secretory Carrier Membrane Protein 3 Interacts with 3A Viral Protein of Enterovirus and Participates in Viral Replication. *Microbiology Spectrum*, 9(1), e00475-21. doi:10.1128/Spectrum.00475-21
- Luchs, A., de Azevedo, L., de Souza, E., Medeiros, R., de Souza, Y., Teixeira, D., & da Costa, A. (2022). Coxsackievirus A6 strains causing an outbreak of hand-foot-

- and-mouth disease in Northeastern Brazil in 2018. *Revista do Instituto de Medicina Tropical de São Paulo*, 64. doi:10.1590/S1678-9946202264016
- Magnus, M., Kappel, K., Das, R., & Bujnicki, J. (2019). RNA 3D structure prediction guided by independent folding of homologous sequences. *BMC Bioinformatics*, 20(1), 1-15. doi:10.1186/s12859-019-3120-y
- Mahmud, B., Horn, C., & Tapprich, W. (2019). Structure of the 5' Untranslated Region of Enteroviral Genomic RNA. *Journal of Virology*, 93(23), e01288-19. doi:10.1128/JVI.01288-19
- Martinez-Salas, E., Francisco-Velilla, R., Fernandez-Chamorro, J., & Embarek, A. (2018). Insights into Structural and Mechanistic Features of Viral IRES Elements. *Frontiers in Microbiology*, 8, 2629. doi:10.3389/fmicb.2017.02629
- Martínez-Salas, E., Francisco-Velilla, R., Fernandez-Chamorro, J., Lozano, G., & Diaz-Toledano, R. (2015). Picornavirus IRES elements: RNA structure and host protein interactions. *Virus Research*, 206, 62-73. doi:10.1016/j.virusres.2015.01.012
- Mathews, D. (2019). How to Benchmark RNA Secondary Structure Prediction Accuracy. *Methods*, 162, 60-67. doi:10.1016/j.ymeth.2019.04.003
- Matsui, M., & Corey, D. (2017). Non-coding RNAs as drug targets. *Nature Reviews Drug Discovery*, 16(3), 167-179.
- Merkle, I., van Ooij, M. J. M., van Kuppeveld, F. J. M., Glaudemans, D. H. R. F., Galama, J. M. D., Henke, A., Zell, R., & Melchers, W. J. G. (2002). Biological Significance of a Human Enterovirus B-Specific RNA Element in the 3' Nontranslated Region. *Journal of Virology*, 76(19), 9900-9909. <https://doi.org/10.1128/JVI.76.19.9900-9909.2002>
- McKnight, K., & Lemon, S. (2018). Hepatitis A Virus Genome Organization and Replication Strategy. *Cold Spring Harbor Perspectives in Medicine*, 8(12), a033480. doi:10.1101/cshperspect.a033480
- Mirmomeni, M., Hughes, P., & Stanway, G. (1997). An RNA tertiary structure in the 3' untranslated region of enteroviruses is necessary for efficient replication. *Journal of Virology*, 71(3), 2363-2370. doi:10.1128/JVI.71.3.2363-2370.1997
- Moore, C., Guthrie, E., Huang, M.-H., & Taxman, D. (2013). Short Hairpin RNA (shRNA): Design, Delivery, and Assessment of Gene Knockdown. *Methods in Molecular Biology*, 629, 141-158. doi:10.1007/978-1-60761-657-3\_10
- Mu, Z., Wang, B., Zhang, X., Gao, X., Qin, B., Zhao, Z., & Cui, S. (2013). Crystal Structure of 2A Proteinase from Hand, Foot, and Mouth Disease Virus. *Journal of Molecular Biology*, 4530-4543. doi:10.1016/j.jmb.2013.08.016
- Nikonov, O., Chernykh, E., Garber, M., & Nikonova, E. (2017). Enteroviruses: Classification, Diseases They Cause, and Approaches to Development of Antiviral Drugs. *Biochemistry (Moscow)*, 57, 119-152. doi:10.1134/S0006297917130041
- Nisar, T., Sutherland-Foggio, H., & Husar, W. (2019). Antiviral amantadine. *The Lancet Neurology*, 18(12), 1080. doi:10.1016/S1474-4422(19)30361-8
- Norambuena, T., Cares, J., Capriotti, E., & Melo, F. (2013). WebRASP: a server for computing energy scores to assess the accuracy and stability of RNA 3D structures. *Bioinformatics*, 29(20), 2649-2650. doi:10.1093/bioinformatics/btt441

- Norder, H., Bjerregaard, L., Magnius, L., Lina, B., Aymard, M., & Chomel, J.-J. (2003). Sequencing of ‘untypable’ enteroviruses reveals two new types, EV-77 and EV-78, within human enterovirus type B and substitutions in the BC loop of the VP1 protein for known types. *Journal of General Virology*, *84*, 827-836. doi:10.1099/vir.0.18647-0
- Oberste, M., Maher, K., Kilpatrick, D., & Pallansch, M. (1999). Molecular Evolution of the Human Enteroviruses: Correlation of Serotype with VP1 Sequence and Application to Picornavirus Classification. *Journal of Virology*, *73*(3), 1941–1948. doi:10.1128/jvi.73.3.1941-1948.1999
- Olsthoorn, R., & Bol, J. (2002). Role of an essential triloop hairpin and flanking structures in the 3' untranslated region of Alfalfa mosaic virus RNA in vitro transcription. *Journal of Virology*, *76*(17), 8747-8756. doi:10.1128/jvi.76.17.8747-8756.2002
- Ooi, M., Solomon, T., Podin, Y., Mohan, A., Akin, W., Yusuf, M., & Cardoso, J. (2007). Evaluation of different clinical sample types in diagnosis of human enterovirus 71-associated hand-foot-and-mouth disease. *Journal of Clinical Microbiology*, *45*(6), 1858-1866. doi:10.1128/JCM.01394-06
- Opanda, S., Wamunyokoli, F., Khamadi, S., Coldren, R., & Bulimo, W. (2016). Genotyping of enteroviruses isolated in Kenya from pediatric patients using partial VP1 region. *SpringerPlus*, *5*(158), 1-12. doi:10.1186/s40064-016-1834-0
- Owens, R., & Baumstark, T. (2007). Structural differences within the loop E motif imply alternative mechanisms of viroid processing. *RNA*, *13*(6), 824–834. doi:10.1261/rna.452307
- Pascal, S., Garimella, R., Warden, M., & Ponniah, K. (2020). Structural Biology of the Enterovirus Replication-Linked 5'-Cloverleaf RNA and Associated Virus Proteins. *Microbiology and Molecular Biology Reviews*, *84*(2), e00062-19. doi:10.1128/MMBR.00062-19
- Peselis, A., & Serganov, A. (2014). Structure and function of pseudoknots involved in gene expression control. *Wiley Interdisciplinary Reviews: RNA*, *5*(6), 803-822. doi:10.1002/wrna.1247
- Plevka, P., Perera, R., Cardoso, J., Kuhn, R., & Rossmann, M. (2012). Crystal Structure of Human Enterovirus 71. *Science*, *8*(336(6086)), 1274. doi:10.1126/science.1218713
- Ponce-Salvatierra, A., Astha, Merdas, K., Nithin, C., Ghosh, P., Mukherjee, S., & Bujnicki, J. (2019). Computational modeling of RNA 3D structure based on experimental data. *Bioscience Reports*, *39*(2). doi:10.1042/BSR20180430
- Puenpa, J., Wanlapakorn, N., Vongpunsawad, S., & Poovorawan, Y. (2019). The History of Enterovirus A71 Outbreaks and Molecular Epidemiology in the Asia-Pacific Region. *Journal of Biomedical Science*, *26*(1), 1-11. doi:10.1186/s12929-019-0573-2
- Raj, S., Sasidharan, S., Dubey, V., & Saudagar, P. (2019). Identification of lead molecules against potential drug target protein MAPK4 from *L. donovani*: An in-silico approach using docking, molecular dynamics, and binding free energy calculation. *PloS one*, *14*(8), e0221331. doi:10.1371/journal.pone.0221331
- Réblová, K., Špačková, N., Štefl, R., Csaszar, K., Koča, J., Leontis, N., & Šponer, J. (2003). Non-Watson-Crick Basepairing and Hydration in RNA Motifs:

- Molecular Dynamics of 5S rRNA Loop E. *Biophysical journal*, 84(6), 3564-3582. doi:10.1016/S0006-3495(03)75089-9
- Reimann, B.-Y., Zell, R., & Kandolf, R. (1991). Mapping of a Neutralizing Antigenic Site of Coxsackievirus B4 by Construction of an Antigen Chimera. *Journal of Virology*, 65(7), 3475-3480.
- Rother, K., Rother, M., Boniecki, M., Puton, T., & Bujnicki, J. (2011). RNA and protein 3D structure modeling: Similarities and differences. *Journal of Molecular Modeling*, 17(9), 2325-2336. doi:10.1007/s00894-010-0951-x
- Rother, M., Rother, K., Puton, T., & Bujnicki, J. (2011). ModeRNA: a tool for comparative modeling of RNA 3D structure. *Nucleic Acids Research*, 39(10), 4007-4022. doi:10.1093/nar/gkq1320
- Sachse, M., de Castro, I., Tenorio, R., & Risco, C. (2019). Chapter One - The viral replication organelles within cells studied by electron microscopy. *Advances in Virus Research*, 105, 1-33. doi:10.1016/bs.aivir.2019.07.005
- Schlick, T., & Pyle, A. (2017). Opportunities and Challenges in RNA Structural Modeling and Design. *Biophysical Journal*, 113(2), 225-234. doi:10.1016/j.bpj.2016.12.037
- Schneidman-Duhovny, D., Inbar, Y., Nussinov, R., & Wolfson, H. (2005). PatchDock and SymmDock: servers for rigid and symmetric docking. *Nucleic acids research*, 33(suppl\_2), W363-W367.
- Schroeder, S. (2018). Challenges and approaches to predicting RNA with multiple functional structures. *RNA*, 24(12), 1615-1624. doi:10.1261/rna.067827.118
- Sharma, N., Ogram, S., Morasco, B., Spear, A., Chapman, N., & Flanagan, J. (2009). Functional role of the 5' terminal cloverleaf in Coxsackievirus RNA replication. *Virology*, 393(2), 238-249. doi:10.1016/j.virol.2009.07.039
- Sheehy, J., Davis, A., & Znosko, B. (2010). Thermodynamic characterization of naturally occurring RNA tetraloops. *RNA*, 16(2), 417-429. doi:10.1261/rna.1773110
- Sheridan, C. (2021). First small-molecule drug targeting RNA gains momentum. *Nature Biotechnology*, 39(1), 6-9.
- Shih, S.-R., Chiang, C., Chen, T.-C., Wu, C.-N., Hsu, J.-A., Lee, J.-C., & Ho, M.-S. (2004). Mutations at KFRDI and VGK domains of enterovirus 71 3C protease affect its RNA binding and proteolytic activities. *Journal of Biomedical Science*, 11(2), 239-248. doi:10.1007/BF02256567
- Shingler, K., Yoder, J., Carnegie, M., Ashley, R., Makhov, A., Conway, J., & Hafenstein, S. (2013). The Enterovirus 71 A-particle Forms a Gateway to Allow Genome Release: A CryoEM Study of Picornavirus Uncoating. *PLoS Pathogens*, 9(3), e1003240. doi:10.1371/journal.ppat.1003240
- Shorter, J., & Houry, W. (2018). Editorial: The Role of AAA+ Proteins in Protein Repair and Degradation. *Frontiers in Molecular Biosciences*, 5, 85. doi:10.3389/fmolb.2018.00085/full
- Simmonds, P., Gorbalenya, A., Harvala, H., Hovi, T., Knowles, N., Lindberg, A., & Zell, R. (2020). Recommendations for the nomenclature of enteroviruses and rhinoviruses. *Archives of Virology*, 165(3), 793-797. doi:10.1007/s00705-019-04520-6
- Sliva, K., & Schnierle, B. (2010). Selective gene silencing by viral delivery of short hairpin RNA. *Virology Journal*, 7(1), 1-11. doi:10.1186/1743-422X-7-248

- Smyth, M., & Martin, J. (2002). Picornavirus uncoating. *Molecular Pathology*, 55(4), 214–219. doi:10.1136/mp.55.4.214
- Spear, A., Ogram, S., Morasco, B., Smerage, L., & Flanagan, J. (2015). Viral Precursor Protein P3 and its Processed Products Perform Discrete and Essential Functions in the Poliovirus RNA Replication Complex. *Virology*, 485, 492–501. doi:10.1016/j.virol.2015.07.018
- Sperschneider, J., Datta, A., & Wise, M. (2011). Heuristic RNA pseudoknot prediction, including intramolecular kissing hairpins. *RNA*, 17(1), 27–38. doi:10.1261/rna.2394511
- Su, Y.-S., Tsai, A.-H., Ho, Y.-F., Huang, S.-Y., Liu, Y.-C., & Hwang, L.-H. (2018). Stimulation of the Internal Ribosome Entry Site (IRES)-Dependent Translation of Enterovirus 71 by DDX3X RNA Helicase and Viral 2A and 3C Proteases. *Frontiers in Microbiology*, 9, 1324. doi:10.3389/fmicb.2018.01324
- Supasorn, O., Tongtawe, P., Srimanote, P., Rattanakomol, P., & Thanongsaksrikul, J. (2020). A nonstructural 2B protein of enterovirus A71 increases cytosolic Ca<sup>2+</sup> and induces apoptosis in human neuroblastoma SH-SY5Y cells. *Journal of NeuroVirology*, 26(2), 201-213. doi:10.1007/s13365-019-00824-0
- Svitkin, Y., & Sonenberg, N. (2007). A highly efficient and robust in vitro translation system for expression of picornavirus and hepatitis C virus RNA genomes. *Methods in enzymology*, 429, 53-82. doi:10.1016/S0076-6879(07)29004-4.
- Svoboda, P., & Cara, A. (2006). Hairpin RNA: a secondary structure of primary importance. *Cellular and Molecular Life Sciences CMLS*, 63(7-8), 901-908. doi:10.1007/s00018-005-5558-5
- Sweeney, T., Abaeva, I., Pestova, T., & Hellen, C. (2014). The mechanism of translation initiation on Type 1 picornavirus IRESs. *The EMBO journal*, 33(1), 76-92. doi:10.1002/embj.201386124
- Tamura, M., & Holbrook, S. (2002). Sequence and Structural Conservation in RNA Ribose Zippers. *Journal of Molecular Biology*, 320(3), 455-474. doi:10.1016/S0022-2836(02)00515-6
- Thulasi, P., Pandya, L., & Znosko, B. (2010). Thermodynamic Characterization of RNA Triloops. *Biochemistry*, 49(42), 9058-9062. doi:10.1021/bi101164s
- Tolbert, M., Morgan, C., Pollum, M., Crespo-Hernández, C., Li, M.-L., Brewer, G., & Tolbert, B. (2017). HnRNP A1 Alters the Structure of a Conserved Enterovirus IRES Domain to Stimulate Viral Translation. *Journal of Molecular Biology*, 429(19), 2841–2858. doi:10.1016/j.jmb.2017.06.007
- Tsai, F.-J., Wen, C.-L., Lai, C.-C., Lan, Y.-C., Lai, C.-H., Hung, C.-H., & Lin, Y.-J. (2011). Kaempferol inhibits enterovirus 71 replication and internal ribosome entry site (IRES) activity through FUBP and HNRP proteins. *Food Chemistry*, 128(2), 312-322. doi:10.1016/j.foodchem.2011.03.022
- van der Linden, L., Wolthers, K., & van Kuppeveld, r. (2015). Replication and Inhibitors of Enteroviruses and Parechoviruses. *Viruses*, 7(8), 4529–4562. doi:10.3390/v7082832
- Vogt, D., & Andino, R. (2010). An RNA Element at the 5'-End of the Poliovirus Genome Functions as a General Promoter for RNA Synthesis. *PLoS pathogens*, 6(6), e1000936. doi:10.1371/journal.ppat.1000936
- Wang, X., An, Z., Huo, D., Jia, L., Li, J., Yang, Y., Liang, Z., Wang, Q., & Wang, H. (2019). Enterovirus A71 vaccine effectiveness in preventing enterovirus A71



- infection among medically-attended hand, foot, and mouth disease cases, Beijing, China. *Human Vaccines & Immunotherapeutics*, 15(5), 1183–1190. <https://doi.org/10.1080/21645515.2019.1581539>
- Wang, H., Zhang, D., Ge, M., Li, Z., Jiang, J., & Li, Y. (2015). Formononetin inhibits enterovirus 71 replication by regulating COX-2/PGE2 expression. *Virology Journal*, 12(1), 1-10. doi:10.1186/s12985-015-0264-x.
- Wang, H.-Q., Meng, S., Li, Z.-R., Peng, Z.-G., Han, Y.-X., Guo, S.-S., & Jiang, J.-D. (2013). The antiviral effect of 7-hydroxyisoflavone against Enterovirus 71 in vitro. *Journal of Asian Natural Products Research*, 15(4), 382-389. doi:10.1080/10286020.2013.770737
- Wang, S.-H., Wang, K., Zhao, K., Hua, S.-C., & Du, J. (2020). The Structure, Function, and Mechanisms of Action of Enterovirus Non-structural Protein 2C. *Frontiers in Microbiology*, 11, 615965. doi:10.3389/fmicb.2020.615965
- Warner, K., Hajdin, C., & Weeks, K. (2018). Principles for targeting RNA with drug-like small molecules. *Nature Reviews Drug Discovery*, 17(8), 547–558.
- Westhof, E., & Auffinger, P. (2000). RNA Tertiary Structure. *Encyclopedia of analytical chemistry*, 5222-5232. doi:10.1002/9780470027318.a1428
- Westhof, E., Masquida, B., & Jossinet, F. (2011). Predicting and Modeling RNA Architecture. *Cold Spring Harbor Perspectives in Biology*, 3(2), a003632. doi:10.1101/cshperspect.a003632
- Winkle, M., El-Daly, S., Fabbri, M., & Calin, G. (2021). Noncoding RNA therapeutics — challenges and potential solutions. *Nature Reviews Drug discovery*, 20(8), 629-651.
- World Health Organization & Centre for Disease Control and Prevention (2015). *Enterovirus surveillance guidelines: guidelines for enterovirus surveillance in support of the Polio Eradication Initiative*.
- Wu, K., Ng, M.-L., & Chu, J. (2010). Developments towards antiviral therapies against enterovirus 71. *Drug Discovery Today*, 15(23/24), ``. doi:10.1016/j.drudis.2010.10.008
- Xi, J., Ma, C., Wei, Z., Yin, B., Zhao, S., Quan, W., & Peng, X. (2021). A single mutation in the cis-acting replication element identified within the EV-A71 2C-coding region causes defects in virus production in cell culture. *Emerging Microbes & Infections*, 10(1), 1988-1999. doi:10.1080/22221751.2021.1977590
- Xi, J., Ye, F., Wang, G., Han, W., Wei, Z., Yin, B., & Peng, X. (2019). Polypyrimidine Tract-Binding Protein Regulates Enterovirus 71 Translation Through Interaction with the Internal Ribosomal Entry Site. *Virologica Sinica*, 34(1), 66-77. doi:10.1007/s12250-019-00089-1
- Xiao, X., Lei, X., Zhang, Z., Ma, Y., Qi, J., Wu, C., & Wang, J. (2017). Enterovirus 3A Facilitates Viral Replication by Promoting Phosphatidylinositol 4-Kinase IIIβ-ACBD3 Interaction. *Journal of Virology*, 91(19), e00791-17. doi:10.1128/JVI.00791-17
- Xie, L., Lu, B., Zheng, Z., Miao, Y., Liu, Y., Zhang, Y., & Wang, H. (2018). The 3C protease of enterovirus A71 counteracts the activity of host zinc-finger antiviral protein (ZAP). *Journal of General Virology*, 99(1), 73-85. doi:10.1099/jgv.0.000982
- Yadav, S., Pandey, S., Singh, V., Goel, Y., Kumar, A., & Singh, S. (2017). Molecular docking studies of 3-bromopyruvate and its derivatives to metabolic regulatory

- enzymes: Implication in designing of novel anticancer therapeutic strategies. *PloS one*, *12*(5), e0176403. doi:10.1371/journal.pone.0176403
- Yang, Y., & Wang, Z. (2019). IRES-mediated cap-independent translation, a path leading to hidden proteome. *Journal of molecular cell biology*, *11*(10), 911-919. doi:10.1093/jmcb/mjz091
- Yu, Y., Sweeney, T., Kafasla, P., Jackson, R., Pestova, T., & Hellena, C. (2011). The mechanism of translation initiation on Aichivirus RNA mediated by a novel type of picornavirus IRES. *The EMBO journal*, *30*(21), 4423-4436. doi:10.1038/emboj.2011.306
- Yuan, J., Shen, L., Wu, J., Zou, X., Gu, J., Chen, J., & Mao, L. (2018). Enterovirus A71 Proteins: Structure and Function. *Frontiers in Microbiology*, *9*(286). doi:10.3389/fmicb.2018.00286
- Zhang, C., Vasmatazis, G., Cornette, J., & DeLisi, C. (1997). Determination of atomic desolvation energies from the structures of crystallized proteins. *Journal of molecular biology*, *267*(3), 707-726. doi:10.1006/jmbi.1996.0859
- Zhou, Y., Jiang, Y., & Chen, S. (2022). RNA –ligand molecular docking: Advances and challenges. *WIREs Computational Molecular Science*, *12*(3), e1571. doi:10.1002/wcms.1571
- Zoll, J., Heus, H., van Kuppeveld, F., & Melchers, W. (2009). The structure–function relationship of the enterovirus 3. *Virus Research*, *139*(2), 209-216. doi:10.1016/j.virusres.2008.07.014

## APPENDICES

### Appendix A: EV-A71 strain 306A UTR sequences

>KJ746493.1 Enterovirus A71 strain 306A (5'UTR)

```
1 UAAAAACAGC CUGUGGGUUG CACCCACUCA CAGGGCCCAC
  UGGGCGCAAG CACUCUGGUA
 61 CUUCGGUACC UUUGUGCGCC UGUUUUACAC CCCCCCCCCA
  GUGAAACUUA GAAGCAGCAA
121 ACCACGAUCA AUAGCAGGCA UAACGCUCCA GUUAUGUCUU
  GAUCAAGCAC UUCUGUUUCC
181 CCGGACCGAG UAUCAAUAGA CUGC UUACGC GGUUGAAGGA
  GAAAACGUUC GUUAUCCGGC
241 UAGCUACUUC GGGAAACCUA GUAACACCAU GAAAGUUGCG
  GAGAGCUUCG UUCAGCACUC
301 CCCAGUGUA GAUCAGGUCG AUGAGUCACC GCAUUCCTCA
  CGGGUGACCG UGGCGGUGGC
361 UGCGUUGGCG GCCUGCCCAU GGGGUAACCC AUGGGGCGCU
  CUAUACGGA CAUGGUGUGA
421 AGAGUCUACU GAGCUAGUUA GUAGUCCUCC GGCCCCUGAA
  UGCGGCUAAU CCUAAUCGCG
481 GAGCACACGC CCACAAGCCA GCGGGUAGUG UGUCGUAACG
  GGUAACUCUG CAGCGGAACC
541 GACUACUUUG GGUGUCCGUG UUUCCUUUUA UCUUCAUAUU
  GGCUGCUUUA GGUGACAAUU
601 AAAGAAUUGU UACCAUAUAG CUAUUGGAUU GGCCAUCCGG
  UGUGCAACAG AGCAAUUGUU
661 UACCUAUUUA UUGGUUUUGU ACCAUUAACC UUGAAGUCUG
  UGACCACCCU UAAUUUAUUC
721 UUGAUCCUUA ACACAGCUAA AC
```

>KJ746493.1 Enterovirus A71 strain 306A (3' UTR)

```
1 AGGCCAUACA CACCUCAACC CCACCAGAAA UCUGGUCGUG
  AAUGUGACUG GUGGGGGUAA
61 AUUUGUUUAU ACCAGAAUAG CAAAAAAAAA AAAAAAAAAA
```

**Appendix B:** Details of the MEME suite motif standard RNA alphabet format.

ALPHABET "RNA" RNA-LIKE

# This alphabet will accept "T" in place of "U."

# in input sequences, but logos will use "U."

# Core symbols

A "Adenine" CC0000

C "Cytosine" 0000CC

U "Uracil" 008000

G "Guanine" FFB300

# Ambiguous symbols

T = U # (permit T in input sequences)

R = AG

Y = CU

K = GU

M = AC

S = CG

W = AU

B = CGU

D = GAU

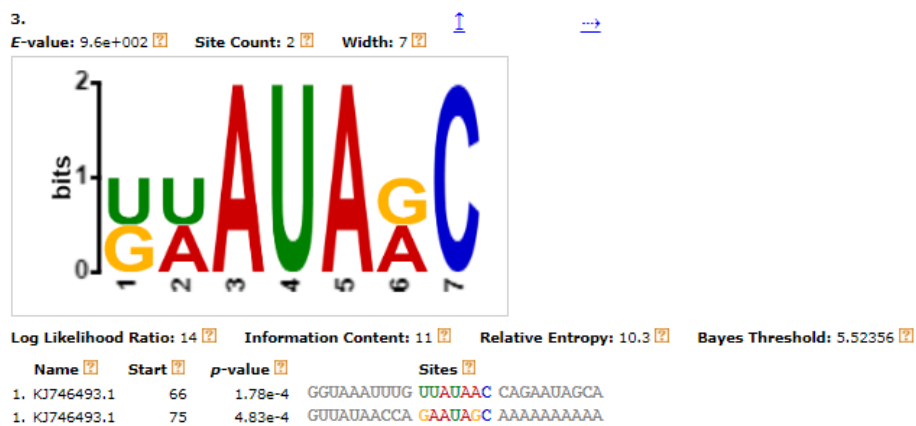
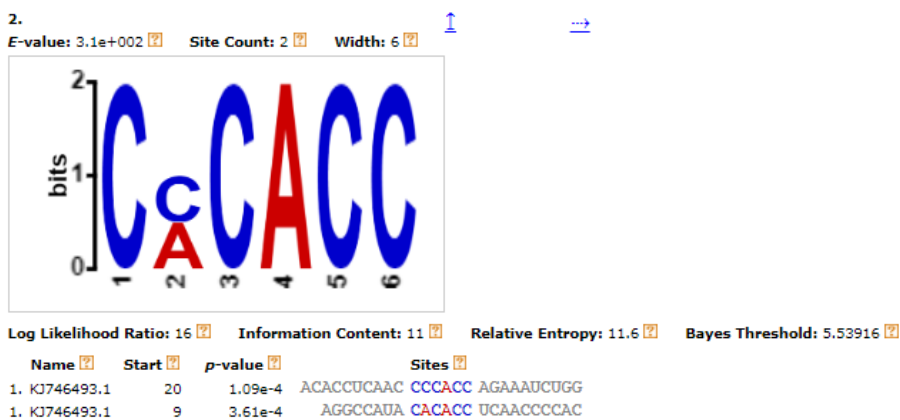
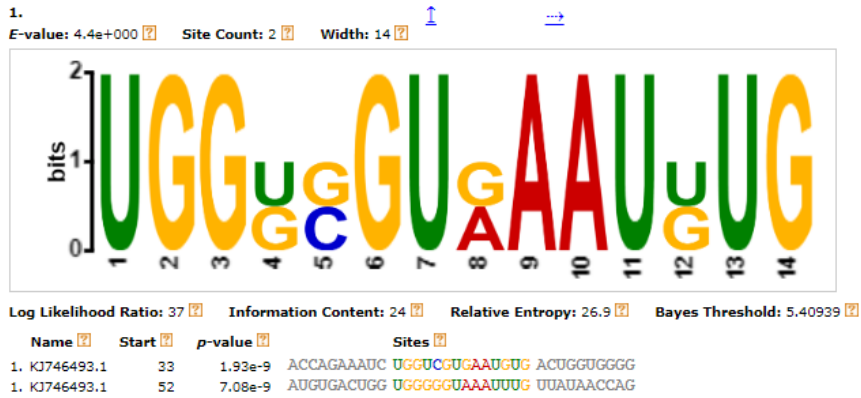
H = ACU

V = ACG

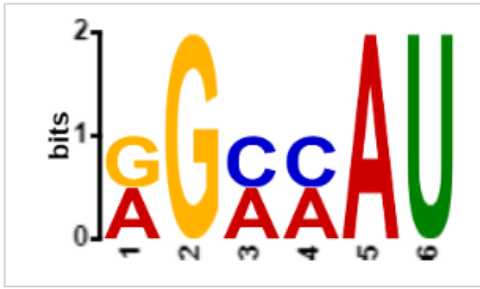
N = ACGU # wildcard symbol

**Appendix C:** Details of the predicted 3' UTR motifs of EV-A71 showing the log-likelihood ratio, information content, relative entropy, Bayes threshold, and sites where the motif appears.

### 3' UTR motifs



4. [E-value: 1.7e+003](#) [Site Count: 2](#) [Width: 6](#) [↑](#) [→](#)



[Log Likelihood Ratio: 12](#) [Information Content: 9](#) [Relative Entropy: 8.4](#) [Bayes Threshold: 5.53916](#)

| Name          | Start | p-value | Sites                        |
|---------------|-------|---------|------------------------------|
| 1. KJ746493.1 | 2     | 1.03e-4 | A GGCCAU ACACACCUCA          |
| 1. KJ746493.1 | 26    | 3.76e-3 | CAACCCACCC AGAAAU CUGGUCGUGA |

5. [E-value: 3.5e+003](#) [Site Count: 2](#) [Width: 6](#) [↑](#) [→](#)

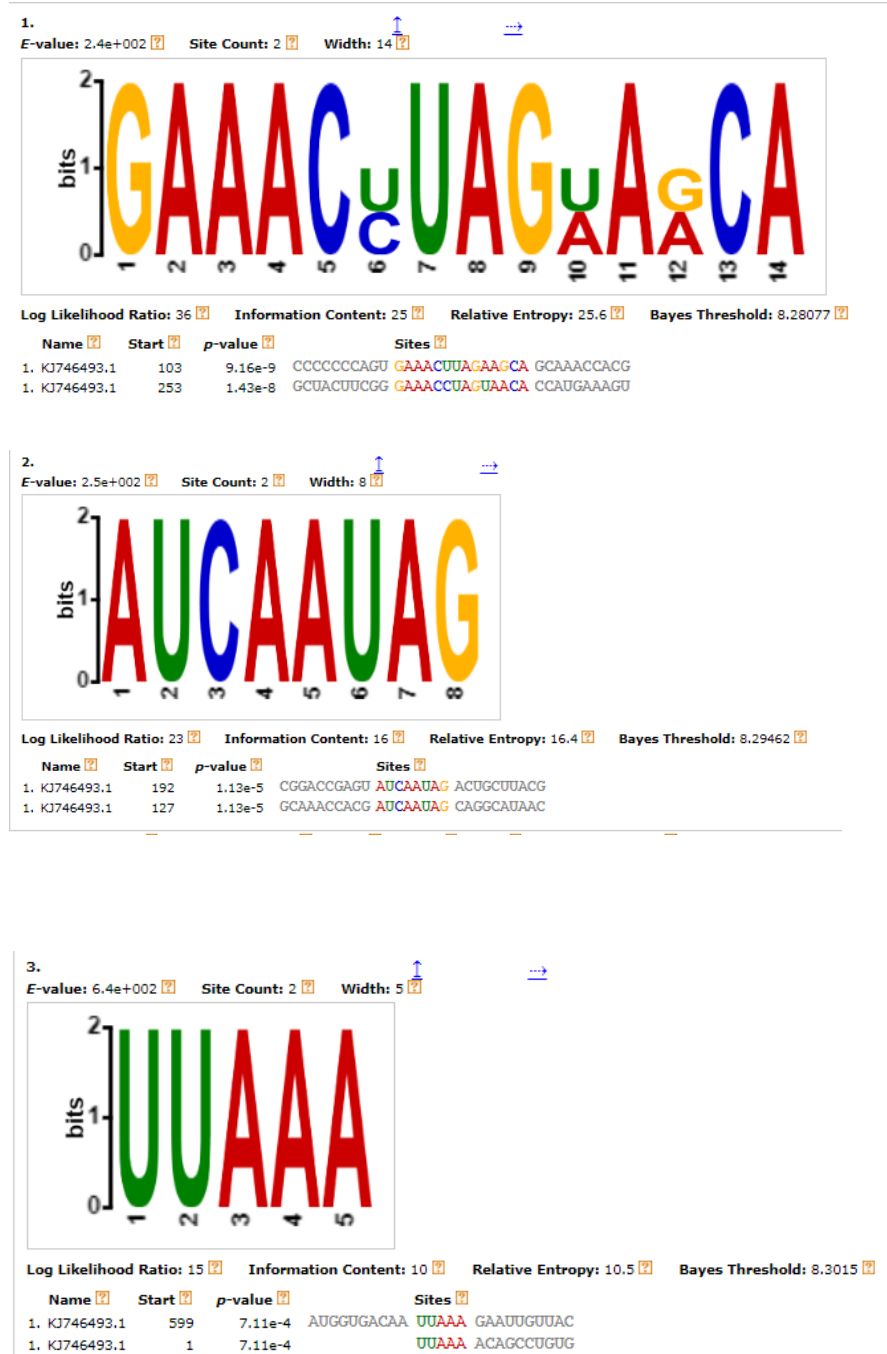


[Log Likelihood Ratio: 10](#) [Information Content: 12](#) [Relative Entropy: 7.1](#) [Bayes Threshold: 5.53916](#)

| Name          | Start | p-value | Sites                        |
|---------------|-------|---------|------------------------------|
| 1. KJ746493.1 | 93    | 7.26e-3 | AAAAAAAAAA AAAAAA AA         |
| 1. KJ746493.1 | 82    | 7.26e-3 | CCAGAAUAGC AAAAAA AAAAAAAAAA |

**Appendix D:** Details of the predicted 5' UTR motifs of EV-A71 showing the log-likelihood ratio, information content, relative entropy, Bayes threshold, and sites where the motif appears.

### 5' UTR motifs



4. E-value: 9.6e+002 Site Count: 3 Width: 8



Log Likelihood Ratio: 31 Information Content: 15.1 Relative Entropy: 15 Bayes Threshold: 7.36448

| Name          | Start | p-value | Sites                          |
|---------------|-------|---------|--------------------------------|
| 1. KJ746493.1 | 245   | 1.63e-5 | UCCGGCUAGC UACUUcGG GAAACCUAGU |
| 1. KJ746493.1 | 59    | 1.63e-5 | AGCACUCUGG UACUUcGG UACCUUUGUG |
| 1. KJ746493.1 | 544   | 3.10e-5 | CGGAACCGAC UACUUcGG GUGUCCGUGU |

5. E-value: 4.9e+002 Site Count: 4 Width: 13



Log Likelihood Ratio: 53 Information Content: 19.1 Relative Entropy: 19.2 Bayes Threshold: 7.27845

| Name          | Start | p-value | Sites                               |
|---------------|-------|---------|-------------------------------------|
| 1. KJ746493.1 | 496   | 3.96e-7 | CAGCCCCACA AGCCAGCGGUAG UGUGUCGUAA  |
| 1. KJ746493.1 | 8     | 3.96e-7 | UUAAAAC AGCCUGUGGUUG CACCCACUCA     |
| 1. KJ746493.1 | 432   | 4.83e-7 | GAGUCUACUG AGCUAGUUAGUAG UCCUCCGGCC |
| 1. KJ746493.1 | 619   | 5.84e-7 | GUUACCAUAI ACUAUUGGAUUG GCCAUC      |

6. E-value: 1.1e+003 Site Count: 2 Width: 7



Log Likelihood Ratio: 20 Information Content: 14 Relative Entropy: 14.2 Bayes Threshold: 8.29692

| Name          | Start | p-value | Sites                         |
|---------------|-------|---------|-------------------------------|
| 1. KJ746493.1 | 165   | 5.46e-5 | UGUCUUGAUC AAGCACU UCUGUUUCCC |
| 1. KJ746493.1 | 48    | 5.46e-5 | CACUGGGCGC AAGCACU CUGGUACUUC |



7.

E-value: 1.3e+003 Site Count: 2 Width: 10

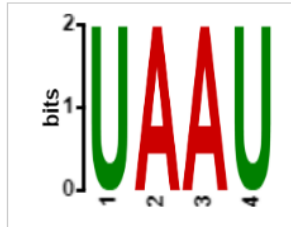


Log Likelihood Ratio: 24 Information Content: 17 Relative Entropy: 17.6 Bayes Threshold: 8.29002

| Name          | Start | p-value | Sites                           |
|---------------|-------|---------|---------------------------------|
| 1. KJ746493.1 | 216   | 5.50e-7 | UACGCGGUUG AAGGAGAAA CGUUCGUUU  |
| 1. KJ746493.1 | 589   | 5.17e-6 | UUGGUCUCUU AUGGUGACAA UAAAAGAAU |

8.

E-value: 1.7e+003 Site Count: 2 Width: 4



Log Likelihood Ratio: 12 Information Content: 8 Relative Entropy: 8.3 Bayes Threshold: 8.30378

| Name          | Start | p-value | Sites                      |
|---------------|-------|---------|----------------------------|
| 1. KJ746493.1 | 467   | 3.12e-3 | UGAADGCGGC UAAU CCUACUCGCG |
| 1. KJ746493.1 | 402   | 3.12e-3 | UGGGCGCUC UAAU ACGGACAUUG  |

9.

E-value: 1.8e+003 Site Count: 2 Width: 6



Log Likelihood Ratio: 17 Information Content: 12 Relative Entropy: 12.2 Bayes Threshold: 8.29921

| Name          | Start | p-value | Sites                        |
|---------------|-------|---------|------------------------------|
| 1. KJ746493.1 | 520   | 2.19e-4 | GUGUCGUUAC GGGUAA CUCUGCAGCG |
| 1. KJ746493.1 | 382   | 2.19e-4 | CCUGCCCAUG GGGUAA CCCAUGGGGC |

10.

E-value: 2.4e+003 Site Count: 2 Width: 7



Log Likelihood Ratio: 18 Information Content: 13 Relative Entropy: 13.3 Bayes Threshold: 8.29692

| Name          | Start | p-value | Sites                         |
|---------------|-------|---------|-------------------------------|
| 1. KJ746493.1 | 419   | 4.99e-5 | GACAUGGUGU GAAGAGU CUACUGAGCU |
| 1. KJ746493.1 | 320   | 1.03e-4 | AGAUCAGGUC GAUGAGU CACCGCAUUC |

11.

E-value: 2.2e+003 Site Count: 2 Width: 12

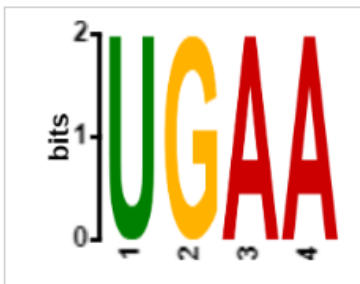


Log Likelihood Ratio: 30 Information Content: 21 Relative Entropy: 21.3 Bayes Threshold: 8.2854

| Name          | Start | p-value | Sites                              |
|---------------|-------|---------|------------------------------------|
| 1. KJ746493.1 | 566   | 2.35e-7 | CCGUGUUUCC UUUUAUCUUCAU AUUGGCUGCU |
| 1. KJ746493.1 | 152   | 2.35e-7 | AACGCUCAG UUAUGUCUUGAU CAAGCACUUC  |

12.

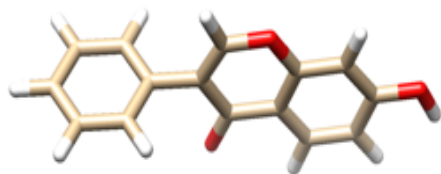
E-value: 2.4e+003 Site Count: 2 Width: 4



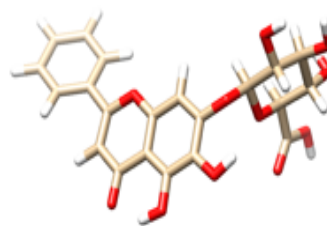
Log Likelihood Ratio: 11 Information Content: 8 Relative Entropy: 8.3 Bayes Threshold: 8.30378

| Name          | Start | p-value | Sites                      |
|---------------|-------|---------|----------------------------|
| 1. KJ746493.1 | 457   | 3.29e-3 | CUCCGGCCCC UGAA UGCGGCUAAU |
| 1. KJ746493.1 | 270   | 3.29e-3 | AGUAACACCA UGAA AGUUGCGGAG |

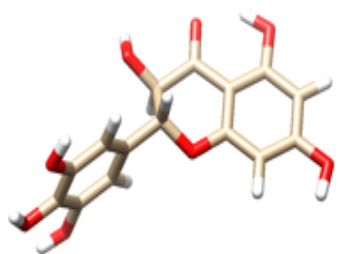
**Appendix E:** 3D structures of the 13 docked molecules in pdb format



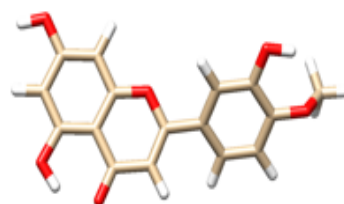
7-hydroxyisoflavone



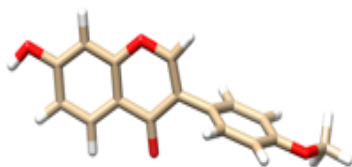
Baicalin



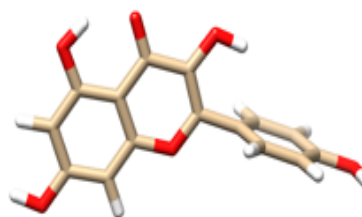
Dihromyricetin



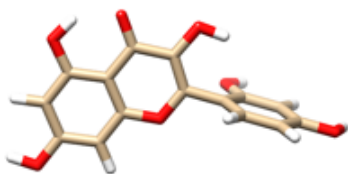
Diosmentin



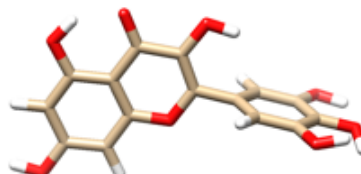
Formononetin



Kaempferol

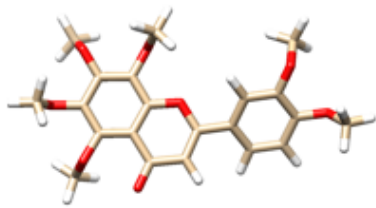


Morin hydrate

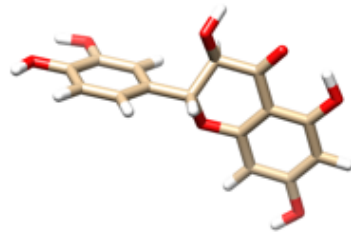


Myricetin

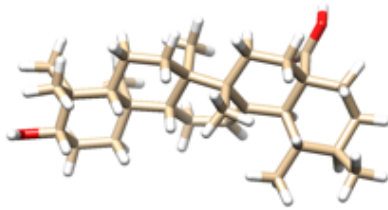




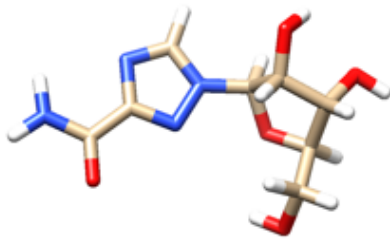
Nobiletin



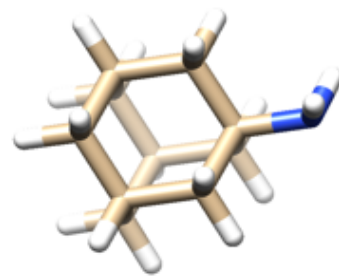
Taxifolin



Urisolic acid



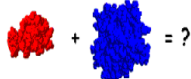
Ribavirin



Amantadine

**Appendix F:** A summary of tables containing the top 20 docking scores, ACE, and transformations for molecules bound on the 5' UTR (dihydromyricetin, myricetin, morin hydrate, nobiletin, taxifolin, and diosmetin).

Patchdock results: 5' UTR

**PATCHDOCK**  = ?

Molecular Docking Algorithm Based on Shape Complementarity Principles  
[\[About PatchDock\]](#) [\[Web Server\]](#) [\[Download\]](#) [\[Help\]](#) [\[FAQ\]](#) [\[References\]](#)

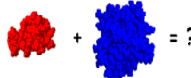
| Receptor                 | Ligand                               | Complex Type | Clustering RMSD | User e-mail           | Receptor Site | Ligand Site | Distance Constraints |
|--------------------------|--------------------------------------|--------------|-----------------|-----------------------|---------------|-------------|----------------------|
| <a href="#">d1tt.pdb</a> | <a href="#">dihydromyricetin.pdb</a> | drug         | 2.0             | shamimosata@gmail.com | -             | -           | -                    |

| Solution No | Score | Area   | ACE     | Transformation                      | PDB file of the complex       |
|-------------|-------|--------|---------|-------------------------------------|-------------------------------|
| 1           | 4004  | 488.20 | -270.08 | 1.91 -0.18 1.28 4.55 95.19 27.66    | <a href="#">result_1.pdb</a>  |
| 2           | 3982  | 464.90 | -250.84 | -1.38 0.10 1.15 4.58 94.39 27.75    | <a href="#">result_2.pdb</a>  |
| 3           | 3970  | 472.50 | -213.44 | 1.43 0.31 1.00 4.09 94.92 29.70     | <a href="#">result_3.pdb</a>  |
| 4           | 3904  | 467.10 | -198.76 | -1.71 0.40 0.91 3.32 94.13 29.37    | <a href="#">result_4.pdb</a>  |
| 5           | 3898  | 454.90 | -262.38 | 0.35 -0.68 -1.03 33.88 -3.34 24.06  | <a href="#">result_5.pdb</a>  |
| 6           | 3872  | 468.50 | -189.77 | 1.78 0.29 0.81 5.04 97.00 31.13     | <a href="#">result_6.pdb</a>  |
| 7           | 3862  | 487.40 | -257.88 | 1.70 -0.29 0.72 5.24 97.17 29.37    | <a href="#">result_7.pdb</a>  |
| 8           | 3848  | 464.00 | -291.03 | 2.53 1.16 0.22 7.21 99.57 29.94     | <a href="#">result_8.pdb</a>  |
| 9           | 3844  | 457.30 | -258.66 | -0.23 0.92 2.48 34.60 -3.49 23.83   | <a href="#">result_9.pdb</a>  |
| 10          | 3804  | 461.10 | -245.85 | 1.89 -0.91 0.54 5.18 97.93 30.29    | <a href="#">result_10.pdb</a> |
| 11          | 3774  | 453.80 | -190.38 | 1.27 0.90 1.31 4.75 94.78 28.08     | <a href="#">result_11.pdb</a> |
| 12          | 3758  | 487.70 | -280.51 | 1.16 1.51 1.12 6.12 97.84 29.69     | <a href="#">result_12.pdb</a> |
| 13          | 3758  | 489.80 | -313.37 | -1.54 1.21 -2.14 5.64 97.71 27.96   | <a href="#">result_13.pdb</a> |
| 14          | 3756  | 436.40 | -254.52 | -3.06 -0.67 -0.94 32.90 -2.52 25.20 | <a href="#">result_14.pdb</a> |
| 15          | 3754  | 436.30 | -201.07 | -0.82 -0.83 -1.91 6.02 97.96 30.61  | <a href="#">result_15.pdb</a> |
| 16          | 3750  | 447.90 | -212.55 | -2.84 -0.28 -2.02 4.35 94.31 28.12  | <a href="#">result_16.pdb</a> |
| 17          | 3728  | 453.30 | -198.16 | 1.53 0.65 0.83 4.89 96.36 29.36     | <a href="#">result_17.pdb</a> |
| 18          | 3726  | 428.30 | -234.81 | 0.52 -0.51 -1.61 4.31 90.74 26.46   | <a href="#">result_18.pdb</a> |
| 19          | 3722  | 471.40 | -227.69 | 1.99 0.59 0.64 5.98 98.15 30.40     | <a href="#">result_19.pdb</a> |
| 20          | 3720  | 447.00 | -166.85 | 1.52 0.13 0.54 3.18 95.95 31.04     | <a href="#">result_20.pdb</a> |

[show next 20 >>](#)

Dihydromyricetin

**PATCHDOCK**  = ?

Molecular Docking Algorithm Based on Shape Complementarity Principles  
[\[About PatchDock\]](#) [\[Web Server\]](#) [\[Download\]](#) [\[Help\]](#) [\[FAQ\]](#) [\[References\]](#)

| Receptor                   | Ligand                        | Complex Type | Clustering RMSD | User e-mail           | Receptor Site | Ligand Site | Distance Constraints |
|----------------------------|-------------------------------|--------------|-----------------|-----------------------|---------------|-------------|----------------------|
| <a href="#">dom4fs.pdb</a> | <a href="#">myricetin.pdb</a> | drug         | 2.0             | shamimosata@gmail.com | -             | -           | -                    |

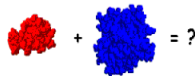
  

| Solution No | Score | Area   | ACE     | Transformation                       | PDB file of the complex       |
|-------------|-------|--------|---------|--------------------------------------|-------------------------------|
| 1           | 4304  | 518.10 | -348.11 | 2.57 -0.19 1.91 2.15 36.80 17.17     | <a href="#">result_1.pdb</a>  |
| 2           | 4214  | 478.20 | -301.38 | 2.86 -0.27 2.46 -25.01 46.84 -54.98  | <a href="#">result_2.pdb</a>  |
| 3           | 4150  | 435.10 | -233.78 | -0.97 -1.16 -3.05 -14.49 52.84 10.70 | <a href="#">result_3.pdb</a>  |
| 4           | 4000  | 449.80 | -282.20 | -1.99 0.90 -0.46 -25.32 48.50 -54.05 | <a href="#">result_4.pdb</a>  |
| 5           | 3996  | 437.80 | -287.95 | 1.39 -0.33 -0.09 -1.73 46.24 -4.04   | <a href="#">result_5.pdb</a>  |
| 6           | 3988  | 437.20 | -302.55 | -2.55 0.72 -0.54 -24.28 46.27 -54.85 | <a href="#">result_6.pdb</a>  |
| 7           | 3970  | 425.70 | -292.63 | -0.44 0.74 2.07 -13.10 52.26 12.17   | <a href="#">result_7.pdb</a>  |
| 8           | 3968  | 474.70 | -300.72 | 2.85 0.80 -2.12 -22.81 30.02 -36.89  | <a href="#">result_8.pdb</a>  |
| 9           | 3962  | 427.80 | -279.66 | -0.65 1.11 1.84 -12.79 53.21 13.70   | <a href="#">result_9.pdb</a>  |
| 10          | 3958  | 462.20 | -335.00 | -0.03 0.42 3.08 0.90 45.83 -5.68     | <a href="#">result_10.pdb</a> |
| 11          | 3954  | 427.80 | -282.46 | -1.20 -0.81 -1.17 -12.55 51.98 11.85 | <a href="#">result_11.pdb</a> |
| 12          | 3944  | 463.20 | -317.78 | 1.95 -0.28 -0.14 -0.18 46.03 -4.89   | <a href="#">result_12.pdb</a> |
| 13          | 3936  | 424.10 | -232.49 | 2.23 0.77 0.66 -26.79 22.54 -49.38   | <a href="#">result_13.pdb</a> |
| 14          | 3930  | 450.10 | -310.55 | -0.68 0.23 -0.54 -25.66 48.55 -54.97 | <a href="#">result_14.pdb</a> |
| 15          | 3916  | 424.20 | -237.79 | -1.56 0.47 -1.59 -12.09 39.62 7.42   | <a href="#">result_15.pdb</a> |
| 16          | 3914  | 443.10 | -312.12 | -2.75 1.03 -0.10 -24.48 43.45 -54.44 | <a href="#">result_16.pdb</a> |
| 17          | 3898  | 524.00 | -362.84 | 0.60 -0.43 2.16 1.67 38.37 17.01     | <a href="#">result_17.pdb</a> |
| 18          | 3882  | 437.40 | -302.60 | -1.76 -0.42 -0.16 -0.98 46.11 -4.13  | <a href="#">result_18.pdb</a> |
| 19          | 3868  | 427.30 | -316.29 | 0.03 1.31 1.03 -12.53 53.52 15.76    | <a href="#">result_19.pdb</a> |
| 20          | 3858  | 456.50 | -309.56 | 0.61 -0.91 -3.06 -24.07 44.31 -54.97 | <a href="#">result_20.pdb</a> |

[show next 20 >>](#)

Myricetin

# PATCHDOCK



Molecular Docking Algorithm Based on Shape Complementarity Principles

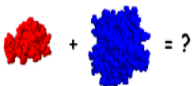
[\[About PatchDock\]](#) [\[Web Server\]](#) [\[Download\]](#) [\[Help\]](#) [\[FAQ\]](#) [\[References\]](#)

| Receptor                   | Ligand                           | Complex Type | Clustering RMSD | User e-mail                           | Receptor Site                 | Ligand Site | Distance Constraints |
|----------------------------|----------------------------------|--------------|-----------------|---------------------------------------|-------------------------------|-------------|----------------------|
| <a href="#">dom4fs.pdb</a> | <a href="#">morinhydrate.pdb</a> | drug         | 2.0             | shamimosata@gmail.com                 | -                             | -           | -                    |
| Solution No                | Score                            | Area         | ACE             | Transformation                        | PDB file of the complex       |             |                      |
| 1                          | 4072                             | 479.10       | -292.56         | 2.99 -0.30 2.21 -24.86 45.90 -54.68   | <a href="#">result_1.pdb</a>  |             |                      |
| 2                          | 4002                             | 443.30       | -288.05         | -2.50 0.54 -0.70 -25.55 47.32 -55.30  | <a href="#">result_2.pdb</a>  |             |                      |
| 3                          | 3982                             | 446.50       | -323.65         | -0.04 0.29 -3.09 0.72 45.51 -4.78     | <a href="#">result_3.pdb</a>  |             |                      |
| 4                          | 3972                             | 522.80       | -339.64         | 0.61 -0.40 2.04 1.12 38.65 17.09      | <a href="#">result_4.pdb</a>  |             |                      |
| 5                          | 3960                             | 429.80       | -257.74         | -0.15 -1.16 -2.31 -14.10 53.11 12.20  | <a href="#">result_5.pdb</a>  |             |                      |
| 6                          | 3912                             | 456.80       | -278.72         | -0.39 0.11 -0.54 -26.43 48.14 -55.32  | <a href="#">result_6.pdb</a>  |             |                      |
| 7                          | 3908                             | 451.90       | -277.72         | -2.51 -0.30 2.37 -25.52 47.59 -54.44  | <a href="#">result_7.pdb</a>  |             |                      |
| 8                          | 3896                             | 446.90       | -321.50         | -3.06 0.45 3.06 -0.13 45.80 -4.38     | <a href="#">result_8.pdb</a>  |             |                      |
| 9                          | 3884                             | 437.60       | -275.02         | 0.47 -0.80 -0.62 -14.46 54.67 15.78   | <a href="#">result_9.pdb</a>  |             |                      |
| 10                         | 3878                             | 438.30       | -305.96         | 0.74 0.62 -0.61 -24.60 47.25 -54.91   | <a href="#">result_10.pdb</a> |             |                      |
| 11                         | 3876                             | 450.20       | -306.31         | -0.48 -0.59 2.64 -23.69 46.94 -54.58  | <a href="#">result_11.pdb</a> |             |                      |
| 12                         | 3872                             | 430.20       | -285.12         | -0.39 0.75 1.90 -12.94 52.81 12.03    | <a href="#">result_12.pdb</a> |             |                      |
| 13                         | 3866                             | 433.60       | -216.10         | 2.36 1.34 0.05 -14.15 53.09 9.39      | <a href="#">result_13.pdb</a> |             |                      |
| 14                         | 3858                             | 446.40       | -350.21         | -2.19 0.16 1.80 0.09 -29.39 -34.45    | <a href="#">result_14.pdb</a> |             |                      |
| 15                         | 3838                             | 425.90       | -305.03         | -1.89 -0.98 -2.99 -23.90 44.00 -54.00 | <a href="#">result_15.pdb</a> |             |                      |
| 16                         | 3832                             | 434.90       | -251.20         | 1.49 1.03 2.44 -14.32 54.54 15.66     | <a href="#">result_16.pdb</a> |             |                      |
| 17                         | 3822                             | 500.90       | -319.87         | -0.40 -0.11 2.06 1.82 36.77 17.40     | <a href="#">result_17.pdb</a> |             |                      |
| 18                         | 3822                             | 418.70       | -237.68         | 2.46 0.73 0.69 -27.38 21.83 -50.72    | <a href="#">result_18.pdb</a> |             |                      |
| 19                         | 3816                             | 421.30       | -241.86         | -0.19 -1.09 -2.88 -14.07 52.64 9.98   | <a href="#">result_19.pdb</a> |             |                      |
| 20                         | 3816                             | 417.40       | -294.17         | -0.23 1.20 1.26 -12.53 53.06 13.99    | <a href="#">result_20.pdb</a> |             |                      |

[show next 20 >>](#)

## Morin hydrate

# PATCHDOCK



Molecular Docking Algorithm Based on Shape Complementarity Principles

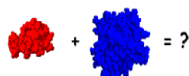
[\[About PatchDock\]](#) [\[Web Server\]](#) [\[Download\]](#) [\[Help\]](#) [\[FAQ\]](#) [\[References\]](#)

| Receptor                   | Ligand                        | Complex Type | Clustering RMSD | User e-mail                           | Receptor Site                 | Ligand Site | Distance Constraints |
|----------------------------|-------------------------------|--------------|-----------------|---------------------------------------|-------------------------------|-------------|----------------------|
| <a href="#">dom4fs.pdb</a> | <a href="#">nobiletin.pdb</a> | drug         | 2.0             | shamimosata@gmail.com                 | -                             | -           | -                    |
| Solution No                | Score                         | Area         | ACE             | Transformation                        | PDB file of the complex       |             |                      |
| 1                          | 5780                          | 636.80       | -348.49         | -2.53 -0.04 -2.38 -24.20 44.31 -53.50 | <a href="#">result_1.pdb</a>  |             |                      |
| 2                          | 5506                          | 612.20       | -317.77         | 2.37 1.12 1.65 -13.52 52.19 11.61     | <a href="#">result_2.pdb</a>  |             |                      |
| 3                          | 5420                          | 610.60       | -305.01         | -2.73 -0.63 0.77 -3.34 45.25 19.56    | <a href="#">result_3.pdb</a>  |             |                      |
| 4                          | 5400                          | 602.30       | -349.25         | 0.75 -0.39 -1.84 -25.01 43.83 -55.74  | <a href="#">result_4.pdb</a>  |             |                      |
| 5                          | 5382                          | 668.50       | -323.22         | -1.04 -0.32 -1.63 -2.27 45.59 17.70   | <a href="#">result_5.pdb</a>  |             |                      |
| 6                          | 5346                          | 621.30       | -303.47         | -1.92 -1.18 -0.90 -13.88 53.89 16.80  | <a href="#">result_6.pdb</a>  |             |                      |
| 7                          | 5342                          | 625.70       | -353.57         | 3.03 -0.98 3.14 -24.04 45.24 -53.68   | <a href="#">result_7.pdb</a>  |             |                      |
| 8                          | 5326                          | 575.60       | -268.41         | 1.86 1.33 1.51 -23.42 46.38 -49.51    | <a href="#">result_8.pdb</a>  |             |                      |
| 9                          | 5294                          | 642.80       | -277.44         | 0.05 -0.83 -0.92 -4.55 43.30 19.45    | <a href="#">result_9.pdb</a>  |             |                      |
| 10                         | 5246                          | 615.40       | -382.82         | -2.27 -0.88 -2.57 -25.25 43.40 -56.10 | <a href="#">result_10.pdb</a> |             |                      |
| 11                         | 5244                          | 617.50       | -232.14         | 3.13 0.83 0.01 -8.99 39.69 10.91      | <a href="#">result_11.pdb</a> |             |                      |
| 12                         | 5230                          | 675.60       | -358.76         | -0.74 -0.18 2.33 1.40 35.85 16.37     | <a href="#">result_12.pdb</a> |             |                      |
| 13                         | 5228                          | 569.10       | -264.75         | -0.67 1.43 1.47 -13.48 52.65 10.43    | <a href="#">result_13.pdb</a> |             |                      |
| 14                         | 5212                          | 622.40       | -343.91         | 0.90 -0.59 1.22 -2.52 47.35 18.10     | <a href="#">result_14.pdb</a> |             |                      |
| 15                         | 5206                          | 632.00       | -365.30         | -3.07 0.77 0.28 -24.07 45.67 -54.70   | <a href="#">result_15.pdb</a> |             |                      |
| 16                         | 5202                          | 668.20       | -382.71         | 0.45 0.63 -0.20 -24.41 47.13 -54.67   | <a href="#">result_16.pdb</a> |             |                      |
| 17                         | 5154                          | 645.40       | -496.03         | -1.83 -0.02 1.80 -0.01 -30.61 -33.60  | <a href="#">result_17.pdb</a> |             |                      |
| 18                         | 5154                          | 593.80       | -346.44         | 0.31 -0.97 -2.60 -25.27 44.11 -55.48  | <a href="#">result_18.pdb</a> |             |                      |
| 19                         | 5138                          | 702.20       | -319.06         | 0.78 0.18 -0.78 -1.06 38.14 16.28     | <a href="#">result_19.pdb</a> |             |                      |
| 20                         | 5134                          | 580.80       | -276.65         | 0.58 -1.29 -2.20 -23.30 46.02 -50.33  | <a href="#">result_20.pdb</a> |             |                      |

[show next 20 >>](#)

## Nobiletin

# PATCHDOCK



Molecular Docking Algorithm Based on Shape Complementarity Principles

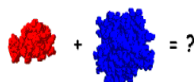
[\[About PatchDock\]](#) [\[Web Server\]](#) [\[Download\]](#) [\[Help\]](#) [\[FAQ\]](#) [\[References\]](#)

| Receptor                 | Ligand                        | Complex Type | Clustering RMSD | User e-mail                         | Receptor Site                 | Ligand Site | Distance Constraints |
|--------------------------|-------------------------------|--------------|-----------------|-------------------------------------|-------------------------------|-------------|----------------------|
| <a href="#">d1tt.pdb</a> | <a href="#">taxifolin.pdb</a> | drug         | 2.0             | shamimosata@gmail.com               | -                             | -           | -                    |
| Solution No              | Score                         | Area         | ACE             | Transformation                      | PDB file of the complex       |             |                      |
| 1                        | 3956                          | 463.60       | -251.71         | -0.47 0.83 2.90 34.71 -3.83 22.73   | <a href="#">result_1.pdb</a>  |             |                      |
| 2                        | 3940                          | 487.40       | -250.77         | 1.67 -0.34 0.78 4.93 96.84 29.01    | <a href="#">result_2.pdb</a>  |             |                      |
| 3                        | 3936                          | 472.40       | -191.57         | -1.75 0.46 1.03 4.37 95.07 28.89    | <a href="#">result_3.pdb</a>  |             |                      |
| 4                        | 3908                          | 481.30       | -263.92         | 2.32 -0.15 1.19 4.92 96.59 27.77    | <a href="#">result_4.pdb</a>  |             |                      |
| 5                        | 3878                          | 459.80       | -200.79         | 1.95 -0.20 -2.29 5.80 97.50 31.04   | <a href="#">result_5.pdb</a>  |             |                      |
| 6                        | 3848                          | 437.50       | -244.01         | -2.49 -0.87 -1.11 32.67 -3.37 24.35 | <a href="#">result_6.pdb</a>  |             |                      |
| 7                        | 3848                          | 466.20       | -294.87         | 2.51 1.15 0.10 6.71 98.82 29.95     | <a href="#">result_7.pdb</a>  |             |                      |
| 8                        | 3808                          | 466.30       | -244.31         | 2.72 -1.00 -0.38 35.00 -3.15 23.41  | <a href="#">result_8.pdb</a>  |             |                      |
| 9                        | 3792                          | 461.90       | -209.11         | -1.43 0.20 0.72 5.37 97.15 31.32    | <a href="#">result_9.pdb</a>  |             |                      |
| 10                       | 3792                          | 450.40       | -209.74         | 1.22 0.91 1.07 5.09 95.88 29.55     | <a href="#">result_10.pdb</a> |             |                      |
| 11                       | 3788                          | 482.00       | -293.79         | -1.08 0.98 -2.32 5.67 97.22 28.82   | <a href="#">result_11.pdb</a> |             |                      |
| 12                       | 3784                          | 453.50       | -203.19         | 1.49 0.33 0.94 4.35 94.91 28.82     | <a href="#">result_12.pdb</a> |             |                      |
| 13                       | 3758                          | 446.30       | -173.13         | 1.79 0.38 0.49 4.57 97.19 31.92     | <a href="#">result_13.pdb</a> |             |                      |
| 14                       | 3744                          | 391.30       | -245.28         | -2.61 0.73 -2.75 10.46 108.69 27.50 | <a href="#">result_14.pdb</a> |             |                      |
| 15                       | 3738                          | 431.30       | -148.25         | 1.14 0.64 1.21 3.44 92.29 26.22     | <a href="#">result_15.pdb</a> |             |                      |
| 16                       | 3736                          | 440.60       | -196.46         | -1.05 -0.04 -2.21 6.04 98.47 31.19  | <a href="#">result_16.pdb</a> |             |                      |
| 17                       | 3734                          | 441.60       | -243.58         | 1.29 0.80 0.98 6.91 98.75 30.10     | <a href="#">result_17.pdb</a> |             |                      |
| 18                       | 3728                          | 442.20       | -210.33         | -1.18 -0.88 -0.69 5.01 93.23 27.31  | <a href="#">result_18.pdb</a> |             |                      |
| 19                       | 3716                          | 422.10       | -210.46         | -0.48 0.59 2.87 4.24 91.90 27.33    | <a href="#">result_19.pdb</a> |             |                      |
| 20                       | 3706                          | 463.90       | -244.23         | -1.27 0.26 1.06 5.62 96.32 29.52    | <a href="#">result_20.pdb</a> |             |                      |

[show next 20 >>](#)

## Taxifolin

# PATCHDOCK



Molecular Docking Algorithm Based on Shape Complementarity Principles

[\[About PatchDock\]](#) [\[Web Server\]](#) [\[Download\]](#) [\[Help\]](#) [\[FAQ\]](#) [\[References\]](#)

| Receptor                   | Ligand                        | Complex Type | Clustering RMSD | User e-mail                           | Receptor Site                 | Ligand Site | Distance Constraints |
|----------------------------|-------------------------------|--------------|-----------------|---------------------------------------|-------------------------------|-------------|----------------------|
| <a href="#">dom4fs.pdb</a> | <a href="#">diosmetin.pdb</a> | drug         | 2.0             | shamimosata@gmail.com                 | -                             | -           | -                    |
| Solution No                | Score                         | Area         | ACE             | Transformation                        | PDB file of the complex       |             |                      |
| 1                          | 4346                          | 473.60       | -324.28         | 2.76 -0.49 2.50 -24.34 46.79 -54.99   | <a href="#">result_1.pdb</a>  |             |                      |
| 2                          | 4242                          | 475.30       | -284.93         | -2.86 0.79 0.70 -26.99 22.29 -51.00   | <a href="#">result_2.pdb</a>  |             |                      |
| 3                          | 4226                          | 495.10       | -394.16         | 1.51 -0.19 -1.16 -0.06 -30.26 -34.09  | <a href="#">result_3.pdb</a>  |             |                      |
| 4                          | 4170                          | 492.40       | -290.85         | 3.00 0.05 -0.60 -26.48 47.74 -55.25   | <a href="#">result_4.pdb</a>  |             |                      |
| 5                          | 4160                          | 497.20       | -299.25         | 1.98 -0.18 2.68 -25.83 48.34 -54.89   | <a href="#">result_5.pdb</a>  |             |                      |
| 6                          | 4156                          | 474.70       | -324.82         | 2.06 -0.50 2.04 -24.28 45.65 -54.43   | <a href="#">result_6.pdb</a>  |             |                      |
| 7                          | 4154                          | 504.50       | -277.68         | -0.27 0.31 -0.60 -0.58 37.88 17.00    | <a href="#">result_7.pdb</a>  |             |                      |
| 8                          | 4152                          | 492.90       | -307.12         | -2.28 -1.02 -3.09 -23.86 44.09 -53.99 | <a href="#">result_8.pdb</a>  |             |                      |
| 9                          | 4138                          | 476.70       | -251.85         | -2.60 -0.86 -0.67 -15.13 54.91 16.60  | <a href="#">result_9.pdb</a>  |             |                      |
| 10                         | 4136                          | 524.10       | -297.21         | -0.45 -0.11 2.12 0.73 36.77 16.81     | <a href="#">result_10.pdb</a> |             |                      |
| 11                         | 4132                          | 449.70       | -250.30         | -2.95 -1.26 -2.19 -14.21 52.90 11.97  | <a href="#">result_11.pdb</a> |             |                      |
| 12                         | 4114                          | 478.50       | -278.78         | -2.32 0.72 -0.31 -24.30 47.88 -54.39  | <a href="#">result_12.pdb</a> |             |                      |
| 13                         | 4100                          | 468.60       | -337.92         | -2.83 0.40 -3.11 0.30 45.86 -5.27     | <a href="#">result_13.pdb</a> |             |                      |
| 14                         | 4096                          | 451.90       | -254.20         | 2.10 -0.76 2.79 -24.16 48.10 -53.37   | <a href="#">result_14.pdb</a> |             |                      |
| 15                         | 4094                          | 546.70       | -293.74         | -2.30 0.26 -0.83 0.39 38.83 16.40     | <a href="#">result_15.pdb</a> |             |                      |
| 16                         | 4092                          | 440.20       | -256.35         | 3.09 -0.24 -0.23 4.26 45.40 -6.24     | <a href="#">result_16.pdb</a> |             |                      |
| 17                         | 4092                          | 449.60       | -253.01         | -2.71 -1.14 -1.28 -13.99 54.79 15.67  | <a href="#">result_17.pdb</a> |             |                      |
| 18                         | 4088                          | 459.40       | -238.92         | 0.64 0.79 -0.14 -24.21 47.84 -53.60   | <a href="#">result_18.pdb</a> |             |                      |
| 19                         | 4076                          | 499.60       | -265.00         | 2.60 0.47 -0.77 -26.08 46.99 -54.47   | <a href="#">result_19.pdb</a> |             |                      |
| 20                         | 4054                          | 442.90       | -237.57         | -0.95 -0.95 0.00 -14.53 54.09 17.50   | <a href="#">result_20.pdb</a> |             |                      |

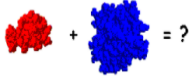
[show next 20 >>](#)

## Diosmetin



**Appendix G:** A summary of tables containing the top 20 docking scores, ACE, and transformations for molecules bound on the 3' UTR (formononetin, kaempferol, ursolic acid, 7-hydroxyisoflavone).

Patchdock results: 3' UTR

**PATCHDOCK** 

Molecular Docking Algorithm Based on Shape Complementarity Principles  
[\[About PatchDock\]](#) [\[Web Server\]](#) [\[Download\]](#) [\[Help\]](#) [\[FAQ\]](#) [\[References\]](#)

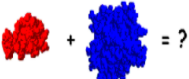
| Receptor                       | Ligand                           | Complex Type | Clustering RMSD | User e-mail           | Receptor Site | Ligand Site | Distance Constraints |
|--------------------------------|----------------------------------|--------------|-----------------|-----------------------|---------------|-------------|----------------------|
| <a href="#">threeprime.pdb</a> | <a href="#">formononetin.pdb</a> | drug         | 2.0             | shamimosata@gmail.com | -             | -           | -                    |

| Solution No | Score | Area   | ACE     | Transformation                         | PDB file of the complex       |
|-------------|-------|--------|---------|--|-------------------------------|
| 1           | 4256  | 471.00 | -236.89 | 3.02 -0.89 -1.73 -25.33 -81.26 -13.77  | <a href="#">result_1.pdb</a>  |
| 2           | 4126  | 466.60 | -190.53 | 0.07 -1.10 -1.79 -25.73 -80.68 -12.24  | <a href="#">result_2.pdb</a>  |
| 3           | 4118  | 468.10 | -263.49 | 1.27 0.94 1.45 -24.84 -80.91 -13.55    | <a href="#">result_3.pdb</a>  |
| 4           | 3976  | 453.10 | -182.97 | -2.04 -0.88 -1.18 -26.66 -80.56 -13.39 | <a href="#">result_4.pdb</a>  |
| 5           | 3944  | 458.90 | -221.21 | 3.11 -1.00 -2.01 -24.66 -79.49 -11.52  | <a href="#">result_5.pdb</a>  |
| 6           | 3934  | 436.30 | -231.96 | 0.92 -0.97 -1.93 -24.28 -79.95 -11.07  | <a href="#">result_6.pdb</a>  |
| 7           | 3924  | 477.70 | -169.59 | 2.14 0.09 3.06 -28.48 -78.02 -9.14     | <a href="#">result_7.pdb</a>  |
| 8           | 3910  | 440.40 | -210.26 | 0.78 0.82 1.04 -24.97 -79.28 -10.05    | <a href="#">result_8.pdb</a>  |
| 9           | 3882  | 441.10 | -218.34 | -2.52 1.07 0.85 -25.27 -81.14 -12.71   | <a href="#">result_9.pdb</a>  |
| 10          | 3878  | 447.70 | -222.79 | -0.93 -0.97 -2.16 -26.29 -82.03 -14.87 | <a href="#">result_10.pdb</a> |
| 11          | 3868  | 445.10 | -216.78 | 1.58 1.05 1.20 -24.72 -80.00 -11.87    | <a href="#">result_11.pdb</a> |
| 12          | 3856  | 464.80 | -210.39 | -1.67 0.92 0.92 -26.28 -81.71 -14.80   | <a href="#">result_12.pdb</a> |
| 13          | 3844  | 459.20 | -277.07 | 0.65 0.75 0.94 -25.20 -80.92 -12.45    | <a href="#">result_13.pdb</a> |
| 14          | 3828  | 427.90 | -221.49 | -1.26 1.00 1.57 -25.23 -82.13 -16.03   | <a href="#">result_14.pdb</a> |
| 15          | 3824  | 426.80 | -174.64 | 0.32 -0.51 -0.90 -27.82 -81.11 -16.53  | <a href="#">result_15.pdb</a> |
| 16          | 3818  | 433.50 | -210.86 | 1.16 0.94 1.78 -26.00 -82.46 -15.63    | <a href="#">result_16.pdb</a> |
| 17          | 3798  | 443.90 | -252.38 | -1.54 1.02 1.51 -24.67 -81.21 -13.58   | <a href="#">result_17.pdb</a> |
| 18          | 3788  | 429.00 | -204.88 | 2.54 1.11 1.45 -24.14 -78.48 -9.40     | <a href="#">result_18.pdb</a> |
| 19          | 3786  | 439.50 | -271.25 | 0.85 -1.01 -1.63 -24.54 -81.05 -13.62  | <a href="#">result_19.pdb</a> |
| 20          | 3776  | 446.50 | -204.30 | 1.21 -0.96 -0.96 -26.79 -80.88 -12.84  | <a href="#">result_20.pdb</a> |

[show next 20 >>](#)

Formononetin

**PATCHDOCK** 

Molecular Docking Algorithm Based on Shape Complementarity Principles  
[\[About PatchDock\]](#) [\[Web Server\]](#) [\[Download\]](#) [\[Help\]](#) [\[FAQ\]](#) [\[References\]](#)

| Receptor                       | Ligand                         | Complex Type | Clustering RMSD | User e-mail           | Receptor Site | Ligand Site | Distance Constraints |
|--------------------------------|--------------------------------|--------------|-----------------|-----------------------|---------------|-------------|----------------------|
| <a href="#">threeprime.pdb</a> | <a href="#">kaempferol.pdb</a> | drug         | 2.0             | shamimosata@gmail.com | -             | -           | -                    |

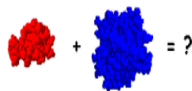
  

| Solution No | Score | Area   | ACE     | Transformation                         | PDB file of the complex       |
|-------------|-------|--------|---------|--|-------------------------------|
| 1           | 3972  | 433.60 | -229.41 | 0.28 -1.00 -1.50 -24.68 -80.37 -11.62  | <a href="#">result_1.pdb</a>  |
| 2           | 3816  | 423.80 | -278.05 | 0.51 1.07 1.00 -25.05 -82.31 -15.74    | <a href="#">result_2.pdb</a>  |
| 3           | 3808  | 437.40 | -201.45 | -2.60 0.99 1.94 -26.27 -80.47 -13.01   | <a href="#">result_3.pdb</a>  |
| 4           | 3790  | 424.60 | -227.58 | -1.32 1.14 1.51 -25.77 -82.62 -15.60   | <a href="#">result_4.pdb</a>  |
| 5           | 3782  | 433.00 | -148.95 | 0.55 -1.03 -1.18 -26.41 -79.24 -11.04  | <a href="#">result_5.pdb</a>  |
| 6           | 3756  | 446.70 | -199.79 | 1.51 -0.53 -1.25 -26.88 -80.04 -13.21  | <a href="#">result_6.pdb</a>  |
| 7           | 3746  | 415.50 | -213.94 | -2.54 -0.92 -1.83 -25.45 -81.83 -15.20 | <a href="#">result_7.pdb</a>  |
| 8           | 3738  | 417.30 | -171.94 | -0.52 -0.50 -2.85 -23.91 -77.49 -7.78  | <a href="#">result_8.pdb</a>  |
| 9           | 3710  | 433.40 | -202.91 | -0.98 -1.00 -1.16 -25.96 -80.34 -12.07 | <a href="#">result_9.pdb</a>  |
| 10          | 3704  | 405.20 | -199.64 | -2.93 -0.72 -1.40 -26.40 -81.97 -15.90 | <a href="#">result_10.pdb</a> |
| 11          | 3702  | 401.10 | -257.46 | 2.55 -1.18 -1.80 -25.62 -83.05 -15.87  | <a href="#">result_11.pdb</a> |
| 12          | 3656  | 420.60 | -160.83 | -2.64 -0.94 -1.24 -26.55 -79.12 -10.17 | <a href="#">result_12.pdb</a> |
| 13          | 3630  | 413.90 | -224.97 | 2.86 -0.85 -1.52 -24.42 -78.18 -8.94   | <a href="#">result_13.pdb</a> |
| 14          | 3624  | 423.30 | -294.26 | -2.46 -0.76 -2.08 -24.39 -80.91 -13.09 | <a href="#">result_14.pdb</a> |
| 15          | 3624  | 439.90 | -232.76 | 2.82 -0.99 -1.61 -24.78 -80.00 -12.44  | <a href="#">result_15.pdb</a> |
| 16          | 3614  | 414.30 | -191.68 | -0.26 -0.94 -2.09 -25.10 -78.46 -9.97  | <a href="#">result_16.pdb</a> |
| 17          | 3610  | 388.60 | -224.94 | -3.11 1.07 0.78 -25.73 -81.64 -15.25   | <a href="#">result_17.pdb</a> |
| 18          | 3596  | 424.80 | -194.60 | 2.99 -1.06 -2.55 -24.95 -79.99 -11.57  | <a href="#">result_18.pdb</a> |
| 19          | 3576  | 411.10 | -156.72 | -1.68 0.15 0.02 -25.55 -78.28 -8.59    | <a href="#">result_19.pdb</a> |
| 20          | 3556  | 400.50 | -216.31 | 0.73 0.57 -0.13 -27.82 -80.74 -14.76   | <a href="#">result_20.pdb</a> |

[show next 20 >>](#)

Kaempferol

# PATCHDOCK



Molecular Docking Algorithm Based on Shape Complementarity Principles

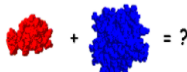
[\[About PatchDock\]](#) [\[Web Server\]](#) [\[Download\]](#) [\[Help\]](#) [\[FAQ\]](#) [\[References\]](#)

| Receptor                       | Ligand                           | Complex Type | Clustering RMSD | User e-mail                            | Receptor Site                 | Ligand Site | Distance Constraints |
|--------------------------------|----------------------------------|--------------|-----------------|--|-------------------------------|-------------|----------------------|
| <a href="#">threeprime.pdb</a> | <a href="#">ursolic_acid.pdb</a> | drug         | 2.0             | shamimosata@gmail.com                  | -                             | -           | -                    |
| Solution No                    | Score                            | Area         | ACE             | Transformation                         | PDB file of the complex       |             |                      |
| 1                              | 5860                             | 720.90       | -387.79         | -2.74 1.03 1.12 -26.23 -80.73 -13.46   | <a href="#">result_1.pdb</a>  |             |                      |
| 2                              | 5848                             | 744.00       | -359.03         | -0.45 -1.10 -1.87 -26.22 -81.12 -14.29 | <a href="#">result_2.pdb</a>  |             |                      |
| 3                              | 5736                             | 715.90       | -358.87         | 0.36 -1.08 -1.01 -26.18 -80.06 -12.35  | <a href="#">result_3.pdb</a>  |             |                      |
| 4                              | 5612                             | 702.10       | -387.14         | 1.80 -1.11 -1.35 -25.97 -80.81 -14.11  | <a href="#">result_4.pdb</a>  |             |                      |
| 5                              | 5606                             | 694.50       | -375.49         | 3.06 -1.14 -2.39 -25.63 -80.50 -13.00  | <a href="#">result_5.pdb</a>  |             |                      |
| 6                              | 5580                             | 691.50       | -388.46         | -0.96 1.05 1.05 -25.33 -80.01 -11.83   | <a href="#">result_6.pdb</a>  |             |                      |
| 7                              | 5542                             | 734.00       | -382.98         | 1.17 -0.37 -0.43 -29.32 -79.66 -12.81  | <a href="#">result_7.pdb</a>  |             |                      |
| 8                              | 5506                             | 686.40       | -395.85         | 2.69 -0.76 -2.49 -24.36 -79.23 -10.28  | <a href="#">result_8.pdb</a>  |             |                      |
| 9                              | 5496                             | 695.90       | -398.56         | 2.23 1.18 1.00 -25.37 -80.45 -12.80    | <a href="#">result_9.pdb</a>  |             |                      |
| 10                             | 5490                             | 706.40       | -348.80         | -3.04 1.13 1.17 -26.07 -79.99 -11.20   | <a href="#">result_10.pdb</a> |             |                      |
| 11                             | 5482                             | 706.50       | -445.52         | -0.71 0.79 1.52 -25.68 -80.98 -13.49   | <a href="#">result_11.pdb</a> |             |                      |
| 12                             | 5474                             | 706.60       | -346.98         | -1.35 -1.24 -1.75 -25.93 -80.65 -13.35 | <a href="#">result_12.pdb</a> |             |                      |
| 13                             | 5454                             | 669.70       | -381.41         | 2.27 -1.01 -2.47 -26.66 -81.42 -15.56  | <a href="#">result_13.pdb</a> |             |                      |
| 14                             | 5450                             | 655.20       | -356.88         | 0.35 -1.27 -1.88 -25.34 -80.23 -12.04  | <a href="#">result_14.pdb</a> |             |                      |
| 15                             | 5446                             | 667.70       | -301.35         | -2.77 -1.14 -2.45 -26.05 -79.65 -11.31 | <a href="#">result_15.pdb</a> |             |                      |
| 16                             | 5424                             | 669.60       | -401.00         | -2.59 0.96 0.37 -26.77 -81.00 -14.86   | <a href="#">result_16.pdb</a> |             |                      |
| 17                             | 5412                             | 684.50       | -427.11         | -0.07 -0.83 -2.27 -26.95 -82.21 -15.44 | <a href="#">result_17.pdb</a> |             |                      |
| 18                             | 5410                             | 687.40       | -350.50         | -2.55 1.11 1.73 -26.76 -80.21 -12.24   | <a href="#">result_18.pdb</a> |             |                      |
| 19                             | 5386                             | 695.60       | -358.92         | -0.32 0.83 1.18 -26.87 -81.23 -15.05   | <a href="#">result_19.pdb</a> |             |                      |
| 20                             | 5344                             | 688.30       | -358.32         | -2.95 1.18 1.31 -26.67 -81.78 -15.51   | <a href="#">result_20.pdb</a> |             |                      |

[show next 20 >>](#)

## Ursolic acid

# PATCHDOCK



Molecular Docking Algorithm Based on Shape Complementarity Principles

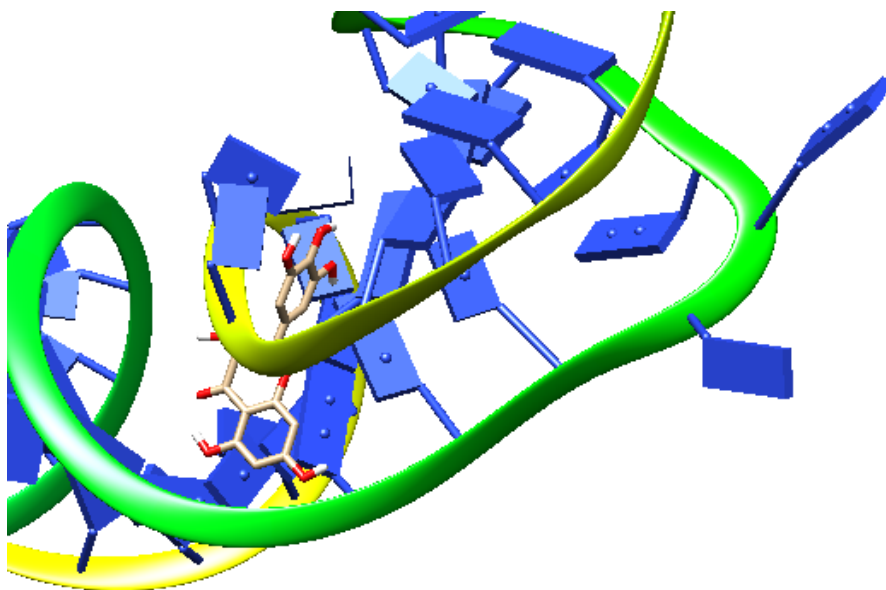
[\[About PatchDock\]](#) [\[Web Server\]](#) [\[Download\]](#) [\[Help\]](#) [\[FAQ\]](#) [\[References\]](#)

| Receptor                       | Ligand                                 | Complex Type | Clustering RMSD | User e-mail                            | Receptor Site                 | Ligand Site | Distance Constraints |
|--------------------------------|--|--------------|-----------------|--|-------------------------------|-------------|----------------------|
| <a href="#">threeprime.pdb</a> | <a href="#">7hydroxyisoflavone.pdb</a> | drug         | 2.0             | shamimosata@gmail.com                  | -                             | -           | -                    |
| Solution No                    | Score                                  | Area         | ACE             | Transformation                         | PDB file of the complex       |             |                      |
| 1                              | 3706                                   | 436.70       | -206.52         | 2.73 0.85 1.90 -25.53 -80.71 -12.95    | <a href="#">result_1.pdb</a>  |             |                      |
| 2                              | 3640                                   | 408.20       | -212.68         | 0.23 -0.95 -1.82 -25.38 -80.87 -12.20  | <a href="#">result_2.pdb</a>  |             |                      |
| 3                              | 3622                                   | 409.30       | -221.59         | -0.07 1.13 1.58 -25.03 -81.33 -13.62   | <a href="#">result_3.pdb</a>  |             |                      |
| 4                              | 3620                                   | 421.40       | -227.81         | 2.31 0.80 1.46 -25.33 -79.86 -11.57    | <a href="#">result_4.pdb</a>  |             |                      |
| 5                              | 3574                                   | 403.70       | -174.18         | -2.52 -1.02 -1.92 -26.56 -80.73 -13.10 | <a href="#">result_5.pdb</a>  |             |                      |
| 6                              | 3556                                   | 412.10       | -160.09         | -1.58 0.95 2.12 -26.63 -80.01 -11.10   | <a href="#">result_6.pdb</a>  |             |                      |
| 7                              | 3510                                   | 393.00       | -216.87         | 1.13 -0.94 -1.51 -25.10 -82.52 -16.33  | <a href="#">result_7.pdb</a>  |             |                      |
| 8                              | 3510                                   | 409.60       | -238.45         | -1.00 -0.96 -1.91 -25.48 -81.86 -13.79 | <a href="#">result_8.pdb</a>  |             |                      |
| 9                              | 3490                                   | 411.50       | -266.51         | 2.33 -0.79 -2.02 -25.42 -81.74 -13.20  | <a href="#">result_9.pdb</a>  |             |                      |
| 10                             | 3486                                   | 391.10       | -253.87         | 1.77 0.95 1.14 -24.85 -81.96 -15.00    | <a href="#">result_10.pdb</a> |             |                      |
| 11                             | 3484                                   | 387.50       | -158.10         | 1.81 -0.16 2.62 -28.50 -78.99 -13.72   | <a href="#">result_11.pdb</a> |             |                      |
| 12                             | 3484                                   | 395.40       | -251.46         | -1.72 -0.96 -1.73 -24.17 -80.35 -12.02 | <a href="#">result_12.pdb</a> |             |                      |
| 13                             | 3466                                   | 387.20       | -164.65         | -3.00 -1.06 -2.13 -24.95 -78.40 -9.77  | <a href="#">result_13.pdb</a> |             |                      |
| 14                             | 3462                                   | 416.20       | -169.50         | 1.36 -0.50 -3.01 -25.82 -77.85 -9.23   | <a href="#">result_14.pdb</a> |             |                      |
| 15                             | 3454                                   | 401.40       | -232.66         | 2.89 0.89 1.73 -24.56 -78.52 -9.85     | <a href="#">result_15.pdb</a> |             |                      |
| 16                             | 3444                                   | 404.60       | -239.12         | -0.07 0.91 1.51 -24.40 -79.81 -12.17   | <a href="#">result_16.pdb</a> |             |                      |
| 17                             | 3414                                   | 396.50       | -227.16         | -1.41 -0.80 -1.52 -25.64 -83.16 -15.87 | <a href="#">result_17.pdb</a> |             |                      |
| 18                             | 3410                                   | 401.20       | -195.37         | 0.68 -0.89 -0.85 -25.93 -80.63 -11.33  | <a href="#">result_18.pdb</a> |             |                      |
| 19                             | 3406                                   | 405.70       | -170.58         | 0.15 0.98 1.52 -25.79 -78.60 -10.67    | <a href="#">result_19.pdb</a> |             |                      |
| 20                             | 3394                                   | 366.40       | -219.42         | 1.84 1.25 0.85 -25.46 -82.88 -16.57    | <a href="#">result_20.pdb</a> |             |                      |

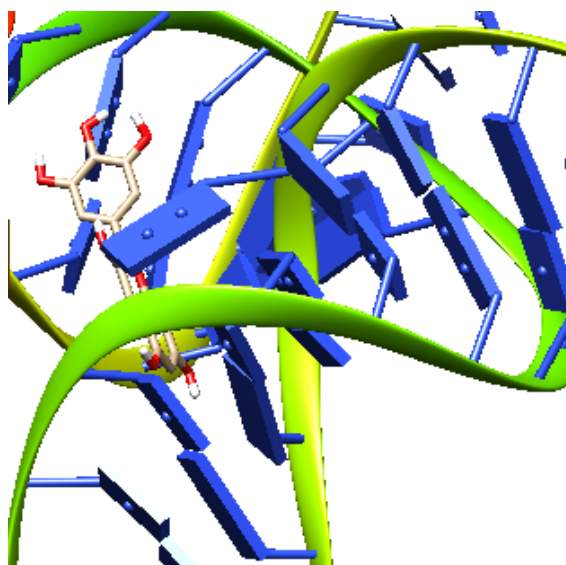
## 7-hydroxyisoflavone

**Appendix H:** 3D docked complexes of the 5' UTR of EV-A71 with different molecules.

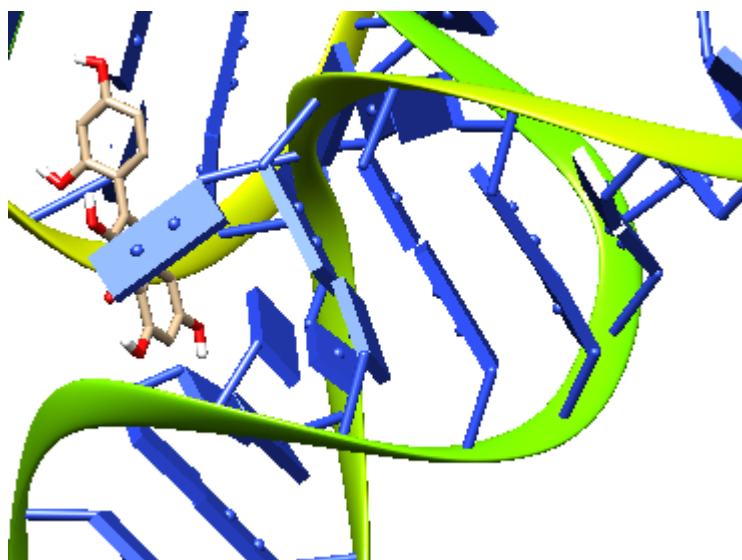
Molecular docking results



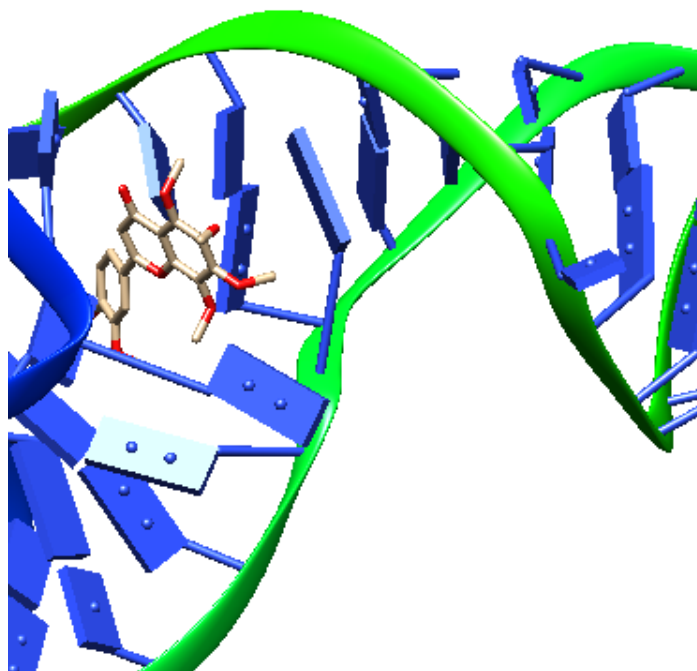
Dihydromyricetin bound on motif 1, domain II of the IRES (5' UTR) with an ACE of -317.37 kcal/mol



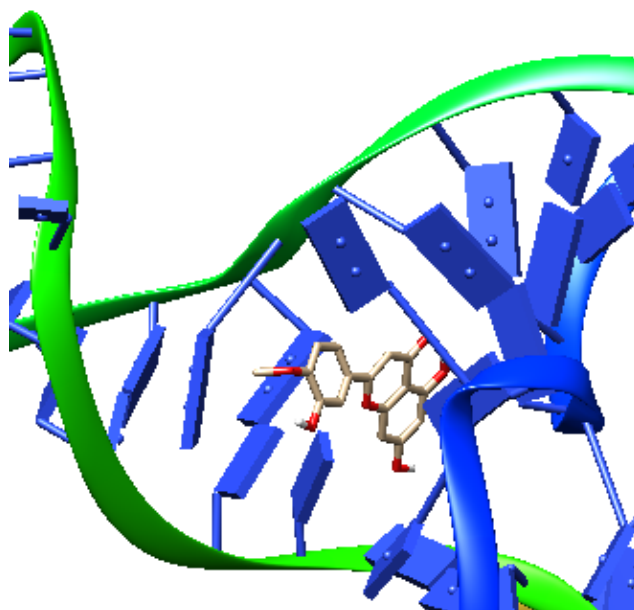
Myricetin bound on motif 5, domain V of the IRES with an ACE of  $-362.84$  kcal/mol



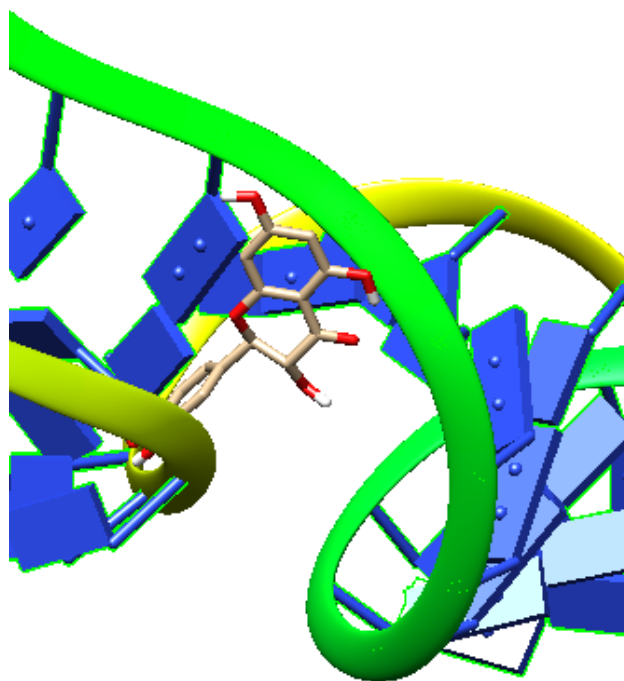
Morin hydrate bound on motif 5, domain V of the IRES with an ACE of  $-339.64$  kcal/mol



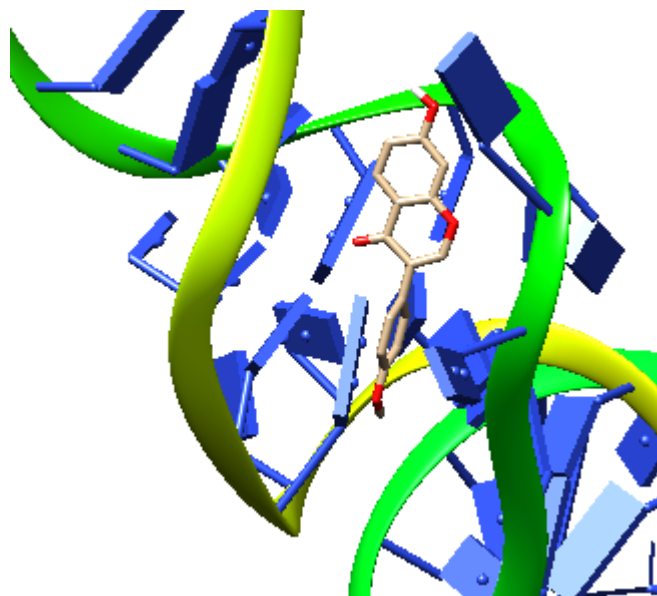
Nobiletin bound on domain IV of the IRES with an ACE of  $-496.04$  kcal/mol



Diosmetin bound on domain IV of the IRES with an ACE of -394.16 kcal/mol

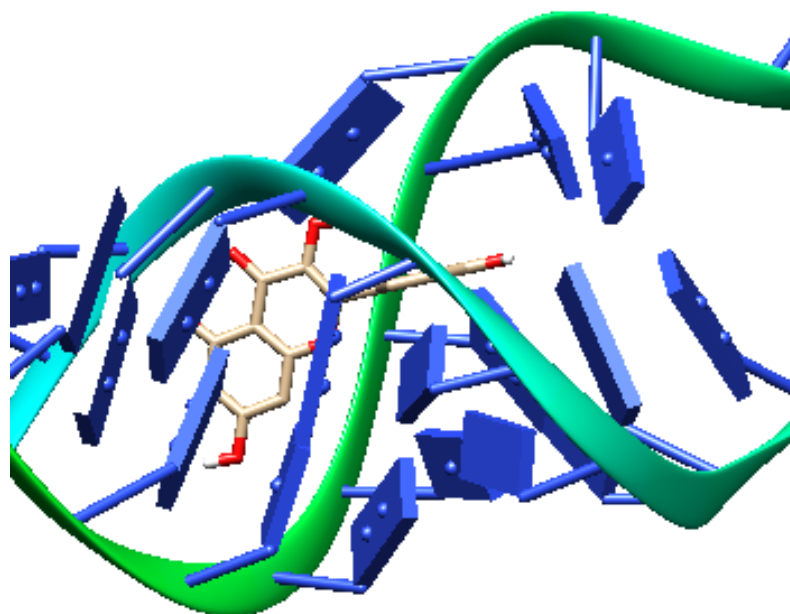


Taxifolin bound on domain II of the IRES with an ACE of -263.92 kcal/mol

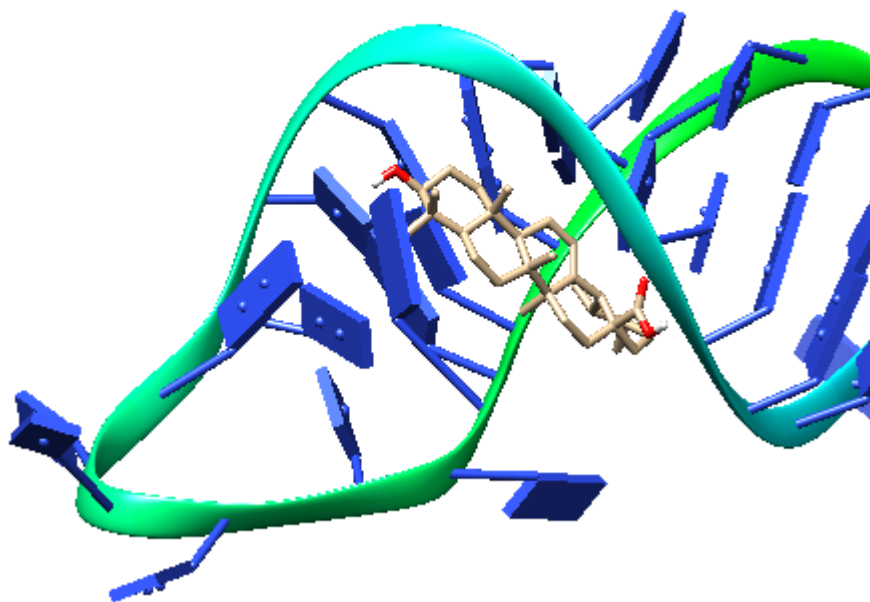


Formononetin bound on domain II of the IRES with an ACE of -273.30 kcal/mol

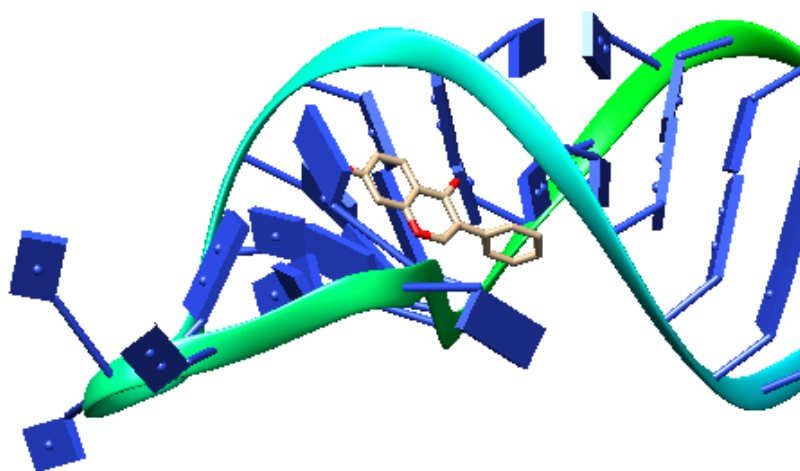
**Appendix I:** 3D docked complexes of the 3' UTR of EV-A71 with different molecules.



Kaempferol bound on domain Y of the 3'UTR with an ACE of -294.26 kcal/mol



Urisolic acid bound on domain Y of the 3' UTR with an ACE of -445.52 kcal/mol



7-hydroxyisoflavone bound on domain Y of the 3' UTR with an ACE of -266.51 kcal/mol